2017

Manipulation of Latex Particle Surfaces and Morphology During Emulsion Polymerization and Some Potential Applications

Yuanyuan Wang
Lehigh University

Manipulation of Latex Particle Surfaces and Morphology During Emulsion Polymerization and Some Potential Applications

by

Yuanyuan Wang

A Dissertation

Presented to the Graduate and Research Committee

of Lehigh University

in Candidacy for the Degree of

Doctor of Philosophy

in

Chemical Engineering

Lehigh University

May 2017

CERTIFICATE OF APPROVAL

Approved and recommended for acceptance as a dissertation in partial fulfillment of the requirements for the degree of Doctor of Philosophy.

Yuanyuan Wang

"Manipulation of Latex Particle Surfaces and Morphology during Emulsion Polymerization and Some Potential Applications"

Date

Accepted Date

Dr. Raymond A. Pearson
Dissertation Director
Co-Chairman and Advisor

Committee members:

Dr. Mohamed S. El-Aasser
Co-Chariman and Advisor

Dr. James F. Gilchrist

Dr. Eric S. Daniels

Dr. Peerapan Dittanet

ACKNOWLEDGEMENTS

I would like to thank my advisors, Prof. Ray Pearson for his kind support and patient, Prof. Mohamed El-Aasser for his warm encouragement and support. Their guidance and mentorship is essential to my completion of this dissertation research.

Thanks to my doctoral committee members, Prof. James Gilchrist, Dr. Eric Daniels and Dr. Peerapan Dittanet for their advice and support.

I would like to thank every student and scholar who had been in EPI with me, Shi Wang, Funian Zhao, Taewook Kwon, Erjun Tang, Cheng Fang, Shulin Sun, Sandeep Magdum, and Hao Huang. I will always appreciate your companionship and friendship in my three years at EPI.

Many thanks to previous EPI students Lili Liu, Yuzhen Yang and Megan Casey, and Prof. Kemal Tuzla, Prof. Mayuresh Kothare and Prof. Manoj Chaudhury in ChemE department. Your advice and encouragement game me confidence to complete my PhD study.

Many thanks to previous and current students and scholars in Prof. Pearson's lab, Binay Patel, Yilin Chen, Amelia Labak, Gabby Esposito, Osama Khayat, Karan Dixit and Steve Antalics. I could not imagine three years of PhD study without your help, companionship and fun.

I would also like to acknowledge many personnel in EPI, ChemE and MatSci department, Prof. Daniel Ou-Yang, Eric Daniels, Debra Nyby, Barbara Kessler, Tracey Lopez, Janine Jekels, Paul Bader, Robert Keyse, William Mushock, Michael Rex, Laura Moyer, Lisa Arechiga, Sue Stetler, Katrina Kraft, Janie Carlin and Mary Anne Lynch. Without your help my PhD research and process would not be so smooth.

Lastly, I would like to express my love to my family and friends for their constant love, understanding and support. My husband Zhou and my daughter Beibei are light of my life.

Most special thanks and appreciation to Ginny Klein and late Prof. Andy Klein, without whom I simply would not be a better me as of now.

TABLE OF CONTENTS

LIST OF TABLES

Chapter 2

Chapter 3

Chapter 4

LIST OF FIGURES

Chapter 1

Chapter 2

Chapter 3

Chapter 4

ABSTRACT

This dissertation contains two portions: modification of latex particle surfaces with polymerizable surfactants during emulsion polymerization for latex and coating application; synthesis of latex particles of multilayer morphology for epoxy toughening applications.

The main focus of first portion of this dissertation research is to evaluate improvements in poly (*n*-butyl methacrylate) – PBMA - latex and film properties resulting from the use of a polymerizable surfactant HITENOL KH-10 compared with its non-polymerizable control LA-12 during the latex synthesis via emulsion polymerization, and to investigate the underlying mechanism of those improvements. Latexes prepared with KH-10 exhibited 240% higher stability against $CaCl_2$ addition, and resulted in films with suppressed water-sensitivity and surfactant migration. Mechanism accounting for these improvements of the PBMA latex and film properties is a significant difference in surfactant distribution/incorporation into different loci in latex system (including in aqueous phase, on latex particle surfaces and inside latex particles) between KH-10 and LA-12. 66% of KH-10 was anchored on latex particles surfaces compared with only 21% for LA-12. Further study found the increase of surface-anchored polymerizable surfactants causes a 300% increase of particle coalescence enthalpy during film formation, increasing the energy barrier for dried particles to heal and form a coherent film.

The second portion of this dissertation research focuses on development of a novel emulsion polymerization technique for synthesizing silica/PBA/PMMA multilayer core-shell composite latex particles with single cores of silica nanoparticles (avg. diam. 22 nm), because these multilayer particles were proposed to be promising toughening agents for epoxy. Colloidal silica nanoparticles were surface-treated with silane (3-methacryloxypropyl trimethoxysilane) before sequential emulsion polymerization of *n*-butyl acrylate (BA) and methyl methacrylate (MMA). Precise control of a series of parameters including surfactant concentration and monomer feed rate is critical for successful synthesis of multilayer particles with single silica cores. Synthesized multilayer nanoparticles were extracted from latex and utilized as epoxy toughening agents for diglycidyl ether of bisphenol A (DGEBA) compared with two other toughening agents—commercial core-shell poly(styrene-butadiene) rubber (CSR) particles and hybrid toughening agents containing mixture of CSR and silica nanoparticles. Multilayer particles exceeded the other two in toughening ability at low volume fractions in epoxy (<2.5%) but exhibited a decreasing toughening ability as volume fraction increased, a trend contrary to the other two. Particle dispersion morphology and fracture surface morphology were investigated by transmission electron microscopy (TEM) and scanning electron microscopy (SEM). It was observed that multilayer particles formed small clusters throughout the matrix for all volume fractions studied (1.25% - 7.5%), while CSR and silica nanoparticles were uniformly and individually dispersed inside epoxy matrix. SEM images of fracture surfaces showed that matrix void growth might be the primary toughening mechanism for multilayer-particle-toughened epoxy but void growth became less prominent as volume fraction of particles

increased, corresponding to the trend that epoxy toughness decreased as volume fraction of multilayer particles increased.

CHAPTER 1

INTRODUCTION

1.1. Polymerizable Surfactant in Emulsion Polymerization

1.1.1. Motivation

A surfactant is a key ingredient in emulsion polymerization. It forms micelles above the critical micellar concentration (CMC), which swollen with monomer become the main locus of radical polymerization leading to latex particle nucleation and growth. . Resulting latex particles are also stabilized by surfactants adsorbed at their surcfaces. Colloidal latex polymer particles synthesized via emulsion polymerization are thermodynamically unstable. They range from approximately 70 to hundreds of nanometer diameter and engage in constant Brownian motion and tend to aggregate upon collision due to attractive forces. [1] DLVO theory is widely used to explain and predict colloidal stability of latex system. [2, 3] In order to increase repulsive forces for better latex stability, two major aspects are considered: enhance electrostatic stabilization effect by increasing particle surface charge density; enhance steric stabilization effect by adsorption or grafting of long chain molecules. The former is usually achieved by adsorption of anionic or cationic surfactants, and/or copolymerization with hydrophilic monomers like acrylic/methacrylic acids and sulfonate monomers. [4, 5] The latter can be achieved by adsorption of nonionic surfactants [6] and/or polymeric stabilizers [7]. Use of conventional surfactants can take advantage of these two stabilization mechanisms.

There are some issues with use of conventional surfactants. These surfactant molecules are mostly physically adsorbed on latex particle surfaces. When physical equilibrium between adsorbed surfactants on surface of latex particles and free surfactant molecules in the aqueous phase shifts under various condition changes, adsorbed surfactants might become more mobile and desorb from particle surfaces and cause particle aggregation due to lack of sufficient stabilization. These condition changes include but not limit to: change of pH, increase of electrolyte concentration, pigment addition, freeze-thaw cycle and high shear processes. For latex film formation, films prepared from latexes with conventional surfactants often encounter surfactant migration issues because they are only physically trapped inside the film. In a moisture-rich environment, surfactant concentration gradient throughout the film will drive surfactant molecules to migrate to film/air or film/substrate interfaces and to form tiny hydrophilic aggregations and defects inside the film. This thermodynamically favored surfactant migration might impair film tackiness, gloss, clarity, adhesion to substrate and mechanical strength. Surfactant migration will also increase film permeability to moisture and oxygen, thus decrease corrosion resistance of coatings.

To mitigate surfactant migration in both latexes and films, polymerizable surfactants can be utilized during emulsion polymerization instead of conventional surfactants. Polymerizable surfactant molecules are amphiphilic with a polymerizable site usually located in their hydrophobic ends. They might copolymerize into polymer chains near the end of emulsion polymerization process and incorporate into polymer at low concentrations without altering bulk polymer properties. Because they are covalently bound onto polymer particles, they give latexes better stability against change of

conditions than conventional surfactants. [8] Polymerizable surfactants not only provide enhanced latex stabilization, but may also offer property improvement of films cast from latexes. Use of polymerizable surfactants can suppress surfactant migration to some extent because most of them are chemically anchored inside latex films. [9]

To gain a deep understanding of polymerizable surfactants, not only possible improvements in latex and film properties by polymerizable surfactants should be quantified and compared with non-polymerizable surfactants, but also the underlying surfactant incorporation mechanism where those improvements stem from should be investigated. In this work both aspects were studied.

1.1.2. Emulsion Polymerization

Emulsion polymerization is a type of radical polymerization. Radicals are generated from decomposed water-soluble initiator for starting growing polymer chains. In the presence of surfactants typically used in emulsion polymerization at a concentration above the CMC, surfactant micelles are formed and become swollen with monomers. The monomer-swollen micelles by capturing radicles become the main locus for particle nucleation because of their small size and high number (~10 nm in diameter; 10^{17}-10^{19} per dl). Under constant stirring or agitation, monomers (oil phase) are emulsified by surfactants to form an oil/water emulsion with relatively larger droplet size (~ 1 – 10 micron in diameter) and their number on the order of $10^{-9\text{-}12}$; which makes them less competitive for capturing radicals compared to the monomer-swollen micelles. The emulsification of monomer into oil-in-water droplets, however, facilitates the transport of their monomer to the site of polymerization by diffusion through the aqueous phase. . Many polymers are synthesized via emulsion polymerization in industry: polybutadiene,

styrene-butadiene rubber, poly (vinyl acetate), acrylics, poly (vinyl chloride), etc. Emulsion polymerization process is widely adopted in industry because it has the following advantages. Polymerization is an exothermic reaction and water in emulsion is a great medium for heat transfer. Emulsion polymerization can give both high rate of reaction and high molecular weight due to radical segregation within the growing particle swollen with monomers. Resulting latexes may be used directly for end products like paints, coatings and adhesives.

Mechanism of emulsion polymerization is a form of free radical polymerization mechanism with some unique features. Surfactants or emulsifiers are key ingredients in emulsion polymerization. A surfactant molecule has both hydrophilic and hydrophobic ends. At low concentration surfactants dissolve in water as single molecules. When concentration reaches or above a critical micelle concentration (CMC), surfactant molecules aggregate to form micelles with their hydrophobic ends inside away from aqueous phase. For monomers sparingly soluble in water (concentration range of 0.34 ~ 15 mM), the reaction mechanism was well established by Harkins' model [10, 11] and Smith-Ewart theory. [12]

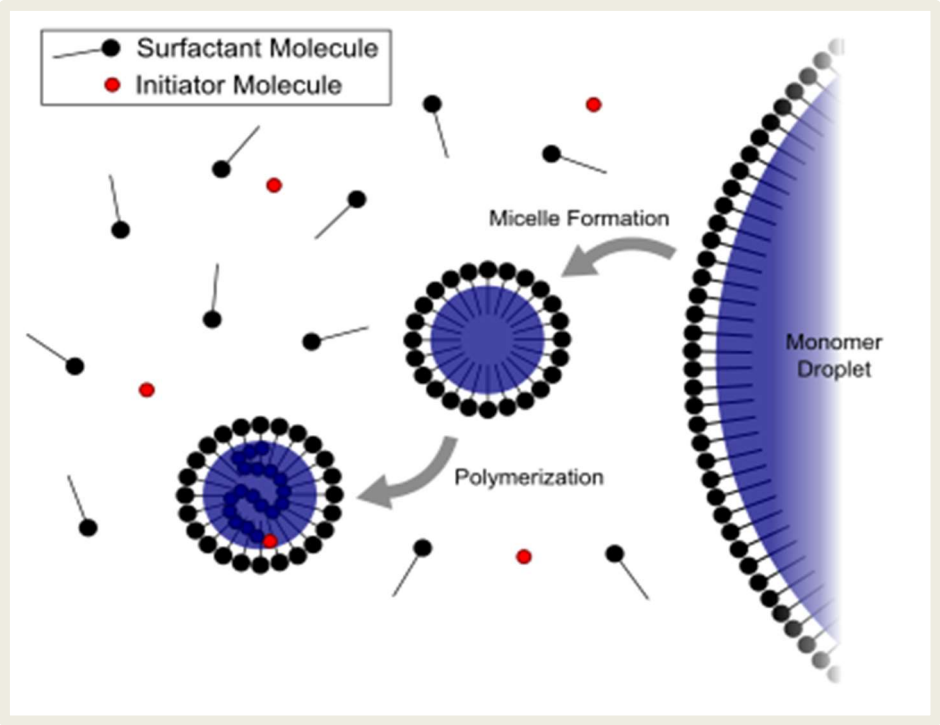

Figure 1-1. Emulsion polymerization system. (Source: wikipedia).

Main loci of polymerization reaction is monomer-swollen micelles because they contribute to ~95% interface area for capturing primary radicals. (Figure 1-1) Theoretical average radical number in a micelle swollen with styrene monomer is 0.5. Emulsion polymerization rate and degree of polymerization are highly affected by total number of polymer particles formed, which directly relates to surfactant concentration in the emulsion. The dependency according to Smith-Ewart theory [12] for emulsion polymerization of styrene can be expressed as following:

$$\begin{aligned} N &\propto [I]^{0.4}[S]^{0.6} \\ R_p &\propto [M][I]^{0.4}[S]^{0.6} \\ X_n &\propto [M][I]^{-0.4}[S]^{0.6} \end{aligned} \tag{1}$$

where N is total latex particle number, I is initiator concentration in the emulsion, S is surfactant concentration, M is monomer concentration, R_p is rate of polymerization. From these expressions we can see that, in emulsion polymerization, effect of monomer and initiator concentrations on rate and degree of polymerization are similar with radical polymerization. Besides, surfactant concentration plays an important role in emulsion polymerization. Increase of surfactant concentration can simultaneously increase rate and degree of polymerization. This is the main characteristic of emulsion polymerization.

Among several types of emulsion polymerization, miniemulsion polymerization and seeded emulsion polymerization have distinct characteristics from conventional emulsion polymerization. In conventional emulsion polymerization, monomer droplets contribute too little surface area to efficiently capture free radicals so they are not considered to be main loci for particle nucleation. But in miniemulsion polymerization, under high energy input like sonication and microfluidization, monomer phase can be broken down to 100 - 500 nm droplets (in the presence of surfactant and co-surfactant – a compound which has must have low water-solubility (~ $10^{-5\text{-}6}$ and low molecular weight 200 – 2000 g/mol) having sufficiently large area to become principal loci for capturing radicals and nucleating polymer particles. [13] Seeded emulsion polymerization is a process in which pre-formed latex particles are the main loci for polymerization. Because surfactant amount is well controlled below the CMC in the aqueous phase so that new latex particles can hardly be generated while the majority of added monomer polymerize within pre-formed latex particles. This process typically leads to larger latex particles and well controls particle size distribution. [14]

1.1.3. Conventional Surfactants in Emulsion Polymerization and Latex Film Formation

As mentioned above, surfactants play an essential role in emulsion polymerization. They emulsify monomer to form emulsions. Emulsified monomer phase (either monomer-swollen micelles or sub-micron monomer droplets) becomes the main location for polymer particle nucleation. Surfactants also stabilize growing monomer-swollen particles as well as final latex particles. The driving force for surfactants to stabilize particles is their adsorption onto particle surface which in turn decreases polymer/water interfacial free energy ΔG_I due to decrease of interfacial tension γ:

$$\Delta G_I = \gamma A_I, \text{ where } A_I \text{ is interfacial area} \quad (2)$$

Surfactants are amphiphilic molecules in nature in order to be able to adsorb on interfaces and thus stabilize oil droplets or polymer particles in aqueous phase. Besides, polymeric stabilizers such as amphiphilic polymers or block copolymers are widely used to stabilize latexes. [15] Surfactant molecules form small aggregates of 50-100 molecules in aqueous phase. These aggregates are called “micelles”. In latex system above critical micelle concentration of a surfactant, the surfactant molecules exist in a dynamic equilibrium among three main locations:

$$\text{Micellar surfactant} \xleftrightarrow{k_1} \text{Solute surfactant} \xleftrightarrow{k_2} \text{Adsorbed surfactant}$$

Addition of large area of hydrophobic interfaces (e.g. hydrophobized inorganic particles, organic pigments, etc.) into latex system may cause it to destabilize. Existing surfactant molecules are driven to adsorb onto new interfaces thus the original equilibrium of surfactants is shifted. A decrease of adsorbed surfactants on polymer particle surface results in insufficient electrostatic or steric repulsion among particles so

they might aggregate upon collision. DLVO theory accounts for colloidal stability from electrostatic repulsion between particles (see Figure 1-2). [16-18] The theory explains colloidal stability by considering energy change when particles are approaching each other. Two major forces contribute to the energy change: London - Van der Waals attractive forces and electrostatic repulsive forces. Fischer's solvency theory is generally accepted for accounting for steric repulsion. [19] The theory was developed based on Flory polymer solution theory. [20]

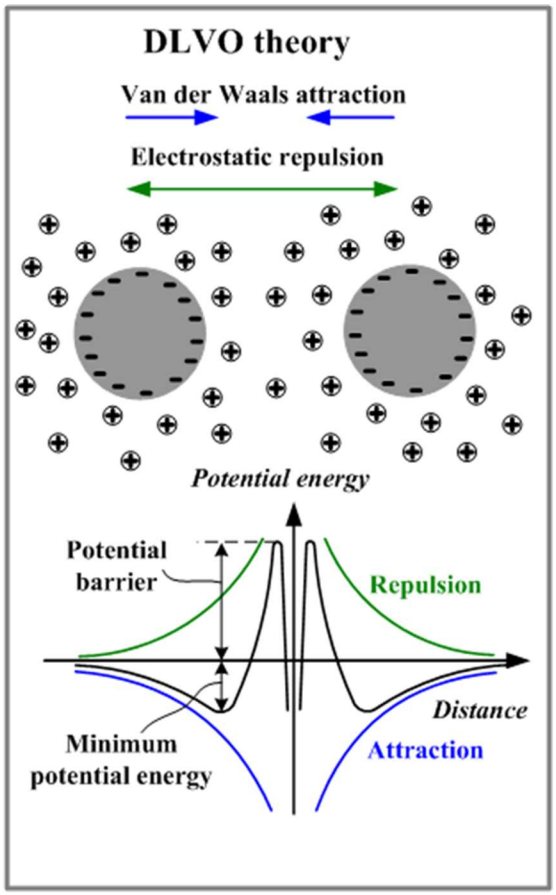

Figure 1-2. DLVO theory. (Source: SEAS Soft Matter wiki).

Change of latex pH or electrolyte concentration changes particle surface charge density and electrical double layer thickness (characterized by Debye length) around it. A

shorter Debye length means weaker electrostatic repulsion force and tendency for particles to aggregate and destabilize the latex. Thus upon these changes, electrostatic repulsive forces are changed while steric repulsive forces are generally not affected. Steric repulsion can be sensitive to temperature change. But electrolyte is inevitably coexisting within latexes. Latexes typically contain some electrolyte or organic acid after synthesis. For industrial purposes, salts are often post-added into latexes for specific latex application and film properties. Thus good colloidal stability of latexes against electrolyte addition is important.

Other than electrolyte addition, high shear processing/transportation and freeze-thaw cycle may easily destabilize latexes. Under high shear conditions, both collision frequency and violence increase, raising probability of particle aggregation after repulsion is overcome by kinetic energy from violent collision. During freezing of latexes, ice crystals form and result in interstices between them, where higher pressure, higher electrolyte concentration and higher collision frequency work together to destabilize latexes. [21]

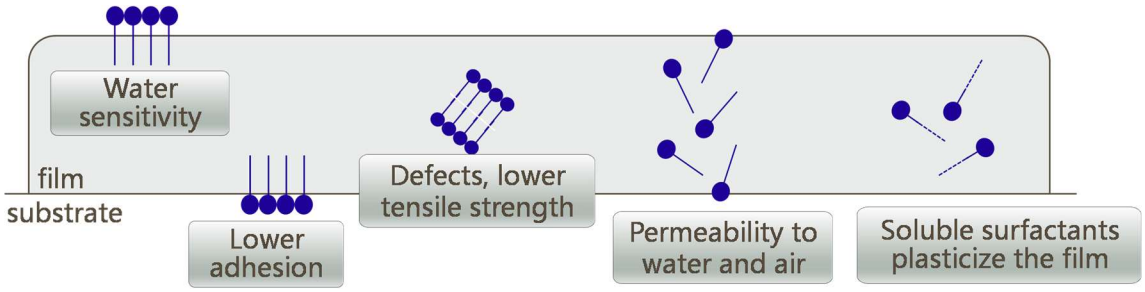

Figure 1-3. Surfactant migration inside latex film.

Regarding to above-mentioned destabilization mechanisms of latexes, conventional anionic surfactants have limited benefits for preventing them. Nonionic

surfactants help with post-polymerization latex stability against electrolyte addition because they provide stabilization mainly due to steric repulsion thus are less sensitive to changes of pH and electrolyte concentration. Besides, although conventional surfactants are essential during emulsion polymerization, after latex film formation, they might have negative effects on film properties. As illustrated in Figure 1-3, due to their amphiphilic nature, surfactant molecules tend to migrate inside the film and form small aggregates, which can cause hydrophilic pockets and defects [22] leading to an increase in film permeability and sensitivity to moisture. Surfactant molecules might migrate to either film-air interface or film-substrate interface. This phenomenon is called "surfactant exudation". Surfactant exudation at film-air interface can adversely affect film tackiness, gloss and water-resistance. Surfactant exudation at film-substrate can decrease adhesion and corrosion-resistance in combination with film permeability to air and moisture. [23-26] Last but not least, surfactants often have a plasticizing effect on latex films, lowering glass transition temperature of film and thus mechanical properties.

Several solutions were proposed to address issues of conventional surfactant regarding to latex and film properties. Nonionic surfactants are less sensitive to pH and electrolyte concentration changes of latexes so they can be employed to enhance latex stability. [27] However, nonionic surfactants often have lower efficiency in aiding particle nucleation during the initial stage of emulsion polymerization than anionic ones. Thus usually nonionic surfactants still have to be used in combination with anionic ones. To minimize adverse effect of conventional surfactants, surfactant-free emulsion polymerization was also studied. [28] Instead of surfactants, hydrophilic/charged groups of initiator molecules on surface of latex particles provide colloidal stability. But this

method often requires low solid content and high initiator concentration. It is hard to apply this method for industrial productions. Another solution is introduction of hydrophilic group into emulsion polymers. For example, carboxylic, amine or sulfonated monomers can be copolymerized into polymer particles and their hydrophilic groups on latex particle surfaces increase colloidal stability. [28] However, polymerization of hydrophilic monomers will generate more water-soluble oligomers. Latex viscosity and latex film hydrophilicity often increases, not desirable in many cases.

1.1.4. Polymerizable Surfactants

Polymerizable surfactants are surfactants having a group that can participate in polymerization reaction and incorporate into latex polymer particles during emulsion polymerization. Because they can copolymerize as a monomer they are also called "surfmers". They have a potential to address issues of conventional surfactant described in last section. Because they can chemically be incorporated into latex particles and on particle surfaces, they do not easily desorb from particle surface and thus decrease latex colloidal stability like conventional surfactants do under certain conditions such as high shear, pigment addition, free-thaw cycle. Due to the same reason, for film-forming latexes, the use of polymerizable surfactant might mitigate surfactant migration effect and its adverse consequences.

A cooperative project consisting of 25 publications on "Reactive surfactants in heterophase polymerization" sponsored by the European Union were published. [29] Various polymerizable surfactants and their role in emulsion polymerization were studied. For example, polymerizable surfactants were synthesized from maleic derivatives and they increased water resistance of resultant latex films due to surfactant

grafting during polymerization. Polymerizable surfactants derived from isophthalic acid improved latex stability of storage and against $CaCl_2$ addition. [30] Previous students at the Emulsion Polymers Institute did a series of studies on polymerizable surfactants in emulsion polymerization including kinetics of emulsion and seeded polymerization of vinyl acetate [31], styrene [32] using TREM LF-40, kinetics of emulsion and miniemulsion polymerization of HITENOL surfactants and incorporation mechanism. [33, 34] As depicted in Figure 1-4, the incorporation of TREM LF-40 was found more complex due to the presence of a polymerizable site (2) as well as another site (1) which actively engaged in chain transfer reactions during emulsion polymerization. .

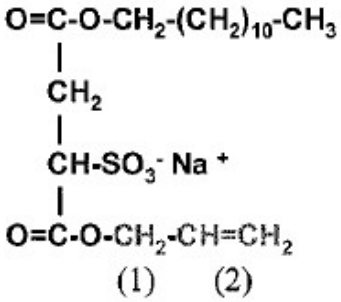

Figure 1-4. Molecular structure of TREM LF-40.

Studies of polymerizable surfactants mainly focused on synthesis of novel reactive surfactants, their effects in emulsion polymerization and resulting latex and film properties. [35-41] They were often compared with commonly-used surfactants like sodium dodecyl sulfate (SDS), sodium laureth sulfate (SLES) and sodium dodecylbenzenesulfonate (SDBS) to prove their superiority in improving latex stability and water-resistance of film. But one thing to take into account is, these polymerizable surfactants often have very different molecular structures from common control

surfactants while molecular structure of surfactants determines practically all the surfactant characteristics in applications. Thus, a pair of polymerizable surfactant and non-polymerizable surfactant with similar molecular structure would be a better approche to investigate the sole effect of polymerizable site within the surfactant. Based on this consideration, in Chapter 2, a pair of commercially available surfactants were studied to elucidate their role in emulsion polymerization and resulting latex and film properties, along with the underlying mechanism.

1.2. Multilayer Particles for Toughening Epoxy

1.2.1. Motivation

Epoxy resins are widely used in everyday consumer products and industrial applications, e.g. coatings, adhesives, composite materials, underfill for electronic packaging, etc. However, despite high performance of modulus and thermal stability, in some cases their application is limited due to inherent brittleness of thermosetting polymers. Thus, improving toughness of epoxy especially by introducing a second phase has been studied extensively. This second dispersed phase could be silica particles, rubber particles, thermoplastics, block copolymers and even intentionally formed microvoids. [42] Compared to conventional micron-sized particles, silica nanoparticles have been proved to effectively increase modulus and toughness of epoxy without increasing viscosity of filled resins. [43, 44]

Rubbery polymers (elastomers) have been studied and applied as a major epoxy toughening method since McGarry and Willner [45] and Sultan [46, 47]. Liquid rubbers (e.g. carboxyl-terminated butadiene acrylonitrile copolymers) soluble in epoxy resins are extensively used as epoxy-toughening agents. Upon curing of epoxy, rubbers are forced

to phase separate to form small rubbery domains within epoxy matrix. [48] However, use of liquid rubber as epoxy toughening agent has two disadvantages, which could be improved by two routes respectively: (1) rubber toughened epoxy often has compromised modulus, stiffness, thermal stability and convenience for processing. Thus, thermoplastics or inorganic fillers like silica particles can be introduced into rubber toughened epoxy to compensate for those adverse effects. [49-51] Block copolymers comprised of rubbery blocks and high T_g epoxy-miscible blocks [52, 53], rubber particles encapsulated by glassy polymer shells [54], and silica-nanoparticle-included rubber-toughened epoxy were all proposed and studied [55]; (2) rubber domains and particles are formed during curing of epoxy resins. So their size/distribution and morphology are strongly affected by and dependent on curing chemistry and process, while size and morphology of rubber domains directly affect epoxy toughening efficiency and even toughening mechanism. [56] In order to gain more control over size and morphology of toughening agents, core-shell rubber particles with epoxy-miscible shell were proposed. These hybrid particles have rubber cores and thermoplastic polymer shells, efficiently toughening epoxy with less compromise of modulus than liquid rubbers only. [49, 57]

Interface between rubber phase and epoxy matrix is an important topic for study of rubber-toughened epoxy and toughening mechanism. Rubbers mainly toughen epoxy by particle cavitation induced shear banding and plastic void growth of epoxy matrix. [58] Thus it was pointed out that the adhesion between rubber particles and epoxy matrix plays only a minor role in fracture toughness. [59] Meanwhile, the dispersion of rubber particles in epoxy plays an important role. Hence, controlled rubber encapsulated core-shell particles should be employed for studying rubber interface effect. But one thing to

take into account is that, with outer shell of glassy polymer introduced most possibly the blend morphology and dispersion of particles will change [56, 60], directly affecting fracture toughness of the composites. In this work, novel core-shell structured particles were synthesized via emulsion polymerization for toughening epoxy. These particles have silica core, rubbery layer and epoxy-miscible outer shell. They were expected to have superior toughening effect while not compromise modulus and yield strength. They were also compared with hybrid toughening agents with the same composition but without structured core-shell morphology to prove a synergistic effect exists.

1.2.2. Epoxy Resins

Epoxy is a generally used name for both epoxy resins and cured form of them. They are among the mostly studied thermoset materials and have wide range of applications both in industry and everyday life. Epoxy has been extensively used in coatings, adhesives, composite materials, electronics components, underfill materials in microelectronic packaging, high-voltage electrical insulators, etc.

Epoxy resins are a group of pre-polymers containing two or more reactive epoxide groups. Content of epoxide groups is an important structural property of epoxy resins. This is often expressed as epoxy equivalent weight, which is the weight in grams of resin containing 1 mole equivalent of epoxide (g/eq.). Amount of curing agent is calculated based on epoxy equivalent weight close to stoichiometry for optimal properties. Below are two commonly used epoxy resins:

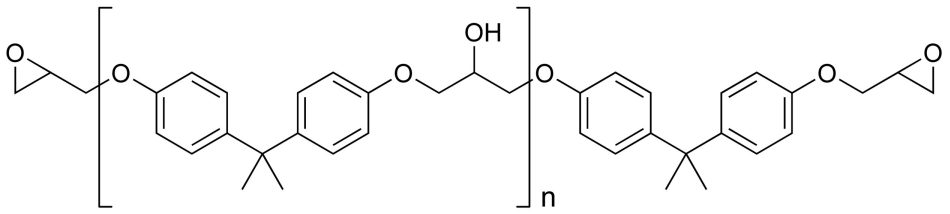

diglycidyl ether bisphenol A (DGEBA)

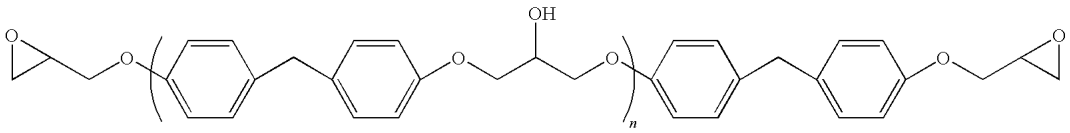

diglycidyl ether bisphenol F (DGEBF)

Figure 1-5. Two common epoxy resins.

From molecular structures of the above two typical epoxy resins, we can see the rigidity of epoxy materials is from bisphenol groups. Cured epoxy has good chemical and thermal resistance due to ether links. Use of epoxy in adhesives is based on hydroxyl groups forming polar interactions with glass, ceramic, wood and many other substrates. [61-63].

Curing of epoxy is to react with a compound containing a reactive hydrogen atom and to form a copolymer matrix. Various curing agents (hardeners) are used for this purpose such as amines, anhydrides, phenols and thiols. [64] Epoxies cured by different curing agents exhibited distinct mechanical and thermal properties. [65] The more active sites a curing agent has in its chemical structure, the higher crosslink extent cured epoxy matrix has and thus higher rigidity of epoxy. Highly-crosslinked epoxy is hard to be toughened because mobility of main polymer chains is largely lost and common toughening mechanism will not become effective. [66] Piperidine may be utilized as a

catalyzing curing agent in order to obtain a more “toughenable” epoxy matrix for study of toughening agents. Reaction stoichiometry is 1:1 piperidine to epoxide group.

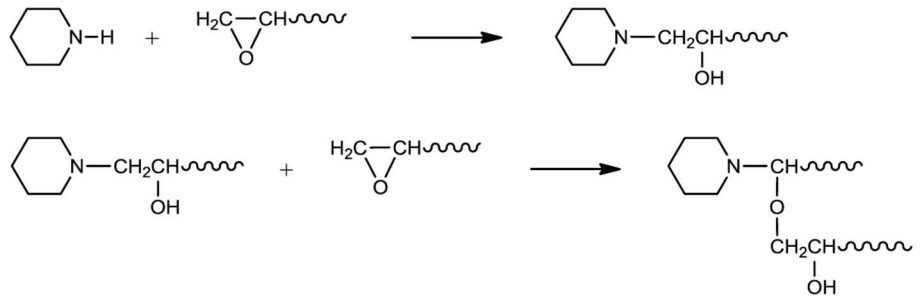

Figure 1-6. Reaction chemistry of piperidine cured epoxy. Reprinted. [63]

1.2.3. Deformation and Fracture Mechanism of Epoxy

Epoxies are generally considered to be inherently brittle materials, whose deformation and fracture mechanisms are usually studied using Linear Elastic Fracture Mechanics (LEFM). [67] Before introduction of basics of LEFM, three modes of loading for study of fracture toughness are illustrated in Figure 7. A crack might be loaded in one of these modes or in a combination of them.

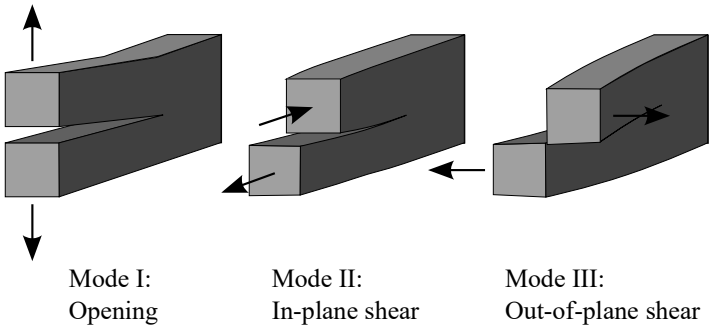

Figure 1-7. Three fracture modes. (Source: wikipedia).

Among the three types of fracture modes, mode I crack opening is mostly studied because it is common in cracks of engineering materials and with this mode of fracture materials often show their most prominent crack propagation.

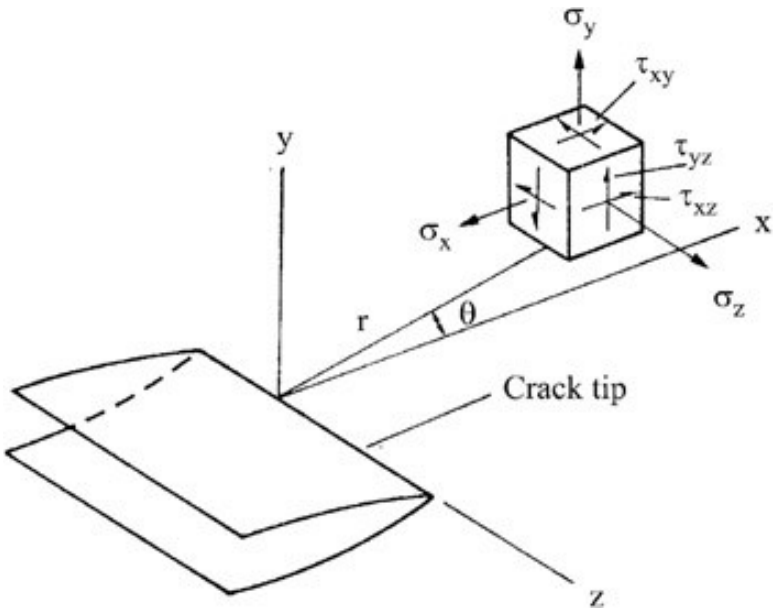

Figure 1-8. Stress field at crack tip. Reprinted. [68]

Under mode I (opening) of fracture, stress field at crack tip (depicted in Figure 1-8) was solved and expressed for elastic materials as following: [69]

$$\begin{aligned}\sigma_x &= \frac{K_I}{\sqrt{2\pi r}}\cos\frac{\theta}{2}\left(1-\sin\frac{\theta}{2}\sin\frac{3\theta}{2}\right)\\ \sigma_y &= \frac{K_I}{\sqrt{2\pi r}}\cos\frac{\theta}{2}\left(1+\sin\frac{\theta}{2}\sin\frac{3\theta}{2}\right)\\ \tau_{xy} &= \frac{K_I}{\sqrt{2\pi r}}\cos\frac{\theta}{2}\left(\sin\frac{\theta}{2}\cos\frac{3\theta}{2}\right)\end{aligned} \tag{3}$$

K_I is termed as stress intensity factor for mode I fracture, with which complete stress field at crack tip for elastic materials can be computed. There exists a critical value

of K_I for a given material: K_{IC}, at which crack propagation initiates and fracture occurs. Under plane strain condition, it is related to critical strain energy release rate G_{IC} as per the following relationship: [69]

$$G_{IC} = \frac{K_{IC}^2}{E(1-\nu^2)} \tag{4}$$

where E is modulus of elasticity and ν is Poisson's ratio of a material. G_{IC} is critical value of energy dissipated during fracture per unit of newly created fracture surface area during mode I fracture.

1.2.4. Epoxy Toughening

Epoxy is a stiff and brittle material, having low resistance to crack propagation. Thus it is often used as a matrix material encompassing a discontinuous phase—toughening agents to form a composite material. The addition of toughening agents increases ductility, toughness and resistance to crack propagation. Various materials are studied and utilized for their ability to toughen epoxy, such as inorganic particles/platelets/nanofibers, rubbers (reactive liquid elastomers), structured core-shell rubber particles, thermoplastics, block copolymers, etc. These materials aid to increase toughness of epoxy via different toughening mechanisms depending on their size/morphology, modulus and miscibility with epoxy matrix.

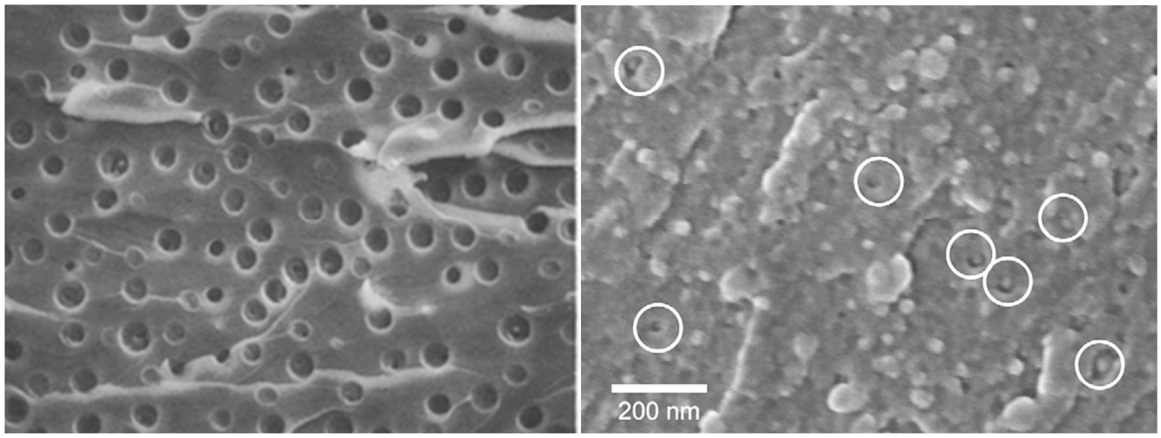

Figure 1-9. Major toughening mechanisms. Left: SEM image of fracture surface of a 3-point bend specimen of epoxy/piperidine/CTBN at stress-whitened zone. [70] Right: SEM image of fracture surface of epoxy toughened by 9.6 vol.% silica nanaoparticles (voids around nanoparticles were circled). [71]

Figure 1-9 illustrates two toughening mechanisms for different toughening agents. Left one is epoxy (D.E.R. 331) toughened by reactive liquid rubber (carboxyl-terminated butadiene-acrylonitrile, CTBN). Cavitation of rubber particles under stress induced shear yielding (shear banding) and plastic void growth, which were believed to be the two most contributing toughening mechanisms for rubber-toughened epoxy. [72-74]

Right image in Figure 1-9 is an epoxy toughened by silica nanoparticles (ca. 20 nm diameter). Similar to other rigid toughening agents like clay platelets [75] and carbon nanofibers [76], under stress, silica nanoparticles debonded from epoxy matrix and induced plastic void growth. Poor adhesion at particle/matrix interfaces has been shown to contribute to toughening. [71] Matrix shear banding also contributes to toughness of epoxies filled by silica nanoparticles. [77] It was found that only a fraction of total particles debonded, and that toughness was independent of particle size. [78, 79] Both finite-element modeling and experiments suggested a 10-20% fraction of total particles in

local stress field debonded. [80, 81] Use of rigid toughening agents can retain modulus, stiffness and glass transition temperature of composite materials while rubber-toughened epoxy often has reduced values of these properties.

Structured core-shell rubber particles are studied and utilized as epoxy toughening agents for their better-regulated size/morphology than liquid rubbers. These particles often have rubber cores and rigid shell of thermoplastics to facilitate dispersion in epoxy. Core-shell rubber particles with various shell compositions and thickness were also studied. [82] It was found that particle dispersion in the epoxy matrix rather than particle/matrix interface adhesion affected toughening. With well-controlled shell chemical composition thus tuning the shell/matrix interaction, it was found that shell/matrix interaction influenced toughening through particle dispersion and blend morphology. [83] In particular, microclusters of particles were found to enhance fracture toughness. Besides, if the shell polymer is miscible with epoxy and has strong adhesion to epoxy matrix, the cavitation of the rubbery core under stress facilitates toughness. [84]

The use of two or more toughening agents of different modulus or size to form toughened hybrid composites might induce multiple toughening mechanisms and provide a synergistic toughening effect. This synergistic toughening effect was found when low fraction (1.6-3.2%) of silica nanoparticles were added into rubber-toughened epoxy. [85] But further increase of silica content did not render this effect. A combination of large glass spheres and rubber was found to have synergistic toughening effect for hybrid epoxy composites. [86] Rubber-induced plastic deformation and crack-pinning by glass spheres were claimed to be underlying mechanisms accounting for this effect. A similar

system containing rubber particles and solid glass spheres was proved to have this toughening effect too. [87]

1.2.5. Novel multilayer particles for toughening epoxy

Core-shell particles with core materials like polybutadiene, acrylate polyurethane and siloxane are widely used for toughening epoxy. [88, 89] Multilayer core-shell particles were studied for this purpose too. [90-92] In these studies, two, three and four-layer polymer particles were prepared via sequential emulsion polymerization. Designed structures of particles were depicted in Figure 1-10.

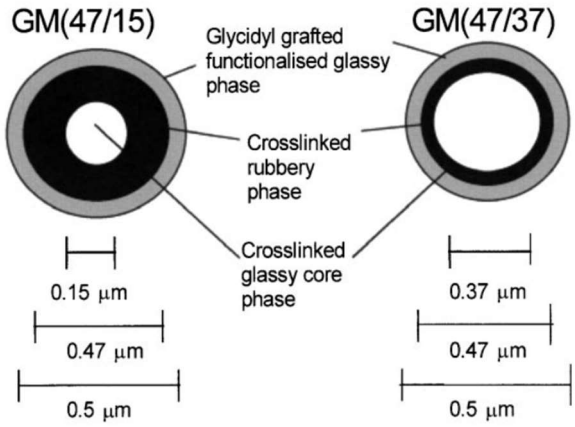

Figure 1-10. Multilayer polymer particles for toughening epoxy. Reprinted. [92]

These multilayer particles have rigid PMMA core, rubbery middle layer of cross-linked PBA and epoxy-miscible shell of poly[(methyl methacrylate)-co-(ethylacrylate)-co-(glycidyl methacrylate)] comprising 15 mol.% glycidyl methacrylate. These particles were coagulated, washed and dried for mixing with epoxy resin via resin transfer molding to make toughened laminates. Except for Young's modulus, tensile, compressive and

impact properties improved as modifier content increased. Both multilayer particles showed better toughening effect than CTBN at same modifier content.

Multilayer particles consisting of nano-sized silica core, rubbery poly(hexylmethacrylate) (PHMA) middle layer and epoxy-compatible poly(glycidylmethacrylate) (PGMA) shell were synthesized using reversible addition-fragmentation chain-transfer (RAFT) polymerization technique. [93] Molecular weight and graft density was varied for synthesizing multilayer particles. Their typical structure was depicted in Figure 1-11.

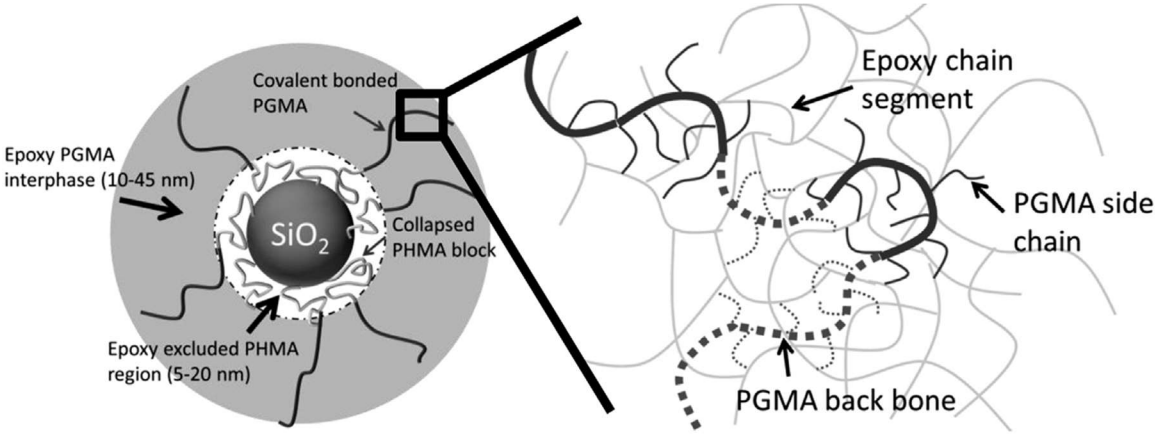

Figure 1-11. Chain configurations of grafted PHMA and PGMA in epoxy. Reprinted. [93]

Compared to neat epoxy, multilayer particles depicted in Figure 1-11 showed a high toughening efficiency, especially for those with lower graft density and/or higher molecular weight. Fracture toughness was tripled in the study. Main toughening mechanism was attributed to plastic void growth and shear banding.

Above studies investigated several multilayer particles for toughening epoxy. Although improved toughening efficiency was found, one link was missing for both: was the improvement of toughness by multilayer particles the result of the specific multilayer

structure or due to the practical combination of several polymer materials? To find the answer to this question, these structured multilayer particles should be compared with hybrid toughening agents containing the same polymer composition but without the multilayer structure. In Chapter 3 and 4, specifically designed multilayer particles were synthesized and compared with hybrid toughening system to elucidate the effect of multilayer structure.

1.3. References

[1] J. Theodoor, G. Overbeek. Adv. Colloid and Interface Sci., 16 (1982), 17.

[2] J.J. Valle-Delgado, J.A. Molina-Bolívar, F. Galisteo-González, M.J. Gálvez-Ruiz. Colloid Polym. Sci., 281 (2003), 708.

[3] S. García-García, S. Wold, M. Jonsson. J Colloid and Interface Sci., 315 (2007), 512.

[4] K. Sakota, T. Okaya. J. Appl. Polym. Sci., 21 (1977), 1025.

[5] D. Bastos and F. J. de 1as Nieves. Colloid Polym Sci., 272 (1994), 592.

[6] M. S. Romero-Cano, A. Martín-Rodríguez, G. Chauveteau, and F. J. de las Nieves. J. Colloid and Interface Sci., 198 (1998), 273.

[7] K. A. Vaynberg, N. J. Wagner, and R. Sharma. Biomacromolecules, 1 (2000), 466.

[8] A. Guyot, Adv. Colloid and Interface Sci., 108 (2004), 3.

[9] E. Aramendia, J. Mallégol, C. Jeynes,‖, M. J. Barandiaran, J. L. Keddie, and J. M. Asua. Langmuir, 19 (2003), 3212.

[10] W. D. Harkins. J. Am. Chem. Soc., 69 (1947), 1428.

[11] W. D. Harkins. J. Polym. Sci., 5 (1947), 217.

[12] W. V. Smith, R. H. Ewart. J. Chem. Phys., 16 (1948), 592.

[13] J. Ugelstad, M. S. El-Aasser, J. W. Vanderhoff. J. Polym. Sci., Poly. Lett., 111 (1973), 503.

[14] B.S. Hawkett, D. H. Napper, R. G. Gilbert. J. Chem. Soc., Faraday Trans. 1, 76 (1980), 1323.

[15] A. Guyot and K. Tauer. in Reactions and Synthesis in Surfactant Systems. ed. J. Texter, Marcel Dekker, New York, (2001), pp. 547-575.

[16] B. Derjaguin. Acta Phys. Chim., 10 (1939), 333.

[17] B. Derjaguin and L. D. Landau. Acta Phys. Chim., 14 (1941), 633.

[18] E. J. W. Verwey and J. T. G. Overbeek. Theory of Stability of Lyophobic Colloids. Elsevier, Amsterdam. (1948)

[19] E. W. Fischer. Kolloid-Z. u. z. Polymere, 160 (1958), 120.

[20] P. J. Flory. Principles of Polymer Chemistry, Cornell University Press, ch.12, (1953)

[21] D. C. Blackley, Polymer Latices-Science and Technology, 2nd ed., vol. 1, Chapman & Hall, (1997)

[22] B. J. Roulstone, M. J. Wilkinson, J. Hearn. Polym. Int. 27 (1992), 43.

[23] C. I. Zhao, Y. Holl, T. Pith and M. Lambla. Colloid Polym. Sci., 265 (1987), 823.

[24] K. W. Evanson, T. A. Thorstenson, M. W. Urban. J. Appl. Polym. Sci., 42 (1991), 2297.

[25] J. I. Amalvy, D. B. Soria. Prog. Org. Coatings, 28 (1996), 279.

[26] D. Juhuë, Y. Wang, J. Lang, O. -M. Leung, M. C. Goh and M. A. Winnik. Polym. Mater. Sci., 73 (1995), 86.

[27] M.S. Romero-Cano, A. Martín-Rodríguez, G. Chauveteau, F.J. de las Nieves. J. Colloid and Interface Sci. 198 (1998), 273.

[28] J. Eastoe and C. Ellis. Adv. Colloid and Interface Sci. 134-135 (2007), 89.

[29] A. Guyot, K. Tauer, J.M. Asua, S. Van Es, C. Gauthier, A.C. Hellgren, D.C. Sherrington, A. Montoya-Goni, M. Sjoberg, O. Sindt, F. Vidal, M. Unzue, H. Schoonbrood, E. Shipper and P. Lacroix-Desmazes. Acta Polym. 50 (1999), 57.

[30] P. Reb, K. Margarit-Puri, M. Klapper, K. Mullen. Macromolecules, 33 (2000), 7718.

[31] M. B. Urquiola. The Role of Polymerizable Surfactants in Emulsion Polymerization (Ph.D. diss.), 1992, Lehigh University

[32] X. Wang. Emulsion Polymerization of Styrene Using a Reactive Surfactant (Ph.D. diss.), 2000, Lehigh University

[33] Z. Lai. Role of Reactive Surfactants in Emulsion Polymerization (Ph.D. diss.), 2004, Lehigh University

[34] S. Braganza-Pugh. Role of Reactive Surfactants in Miniemulsion Polymerization (Ph.D. diss.), 2010, Lehigh University

[35] E. Ozdeger, E. D. Sudol, M. S. El-Aasser and A. Klein, J. Polym. Sci. Part A Polym. Chem., 35 (1997), 3837.

[36] J. I. Amalvy, M. J. Unzue, H. A. S. Schoonbrood, J. M. Asua. Macromolecules, 31 (1998), 5631.

[37] D. Colombié, E. D. Sudol and M. S. El-Aasser, Macromolecules, 33 (2000), 7283.

[38] X. Wang, B. Boya, E. D. Sudol and M. S. El-Aasser, Macromolecules, 34 (2001), 8907.

[39] S. Krishnan, A. Klein, M. S. El-Aasser, E. D. Sudol, Macromolecules, 36 (2003), 3152.

[40] E. Aramendia, M. J. Barandiaran, J. C. de La Cal, J. Grade, T. Blease, J. M. Asua. J. Polym. Sci. Part A: Polym. Chem., 42 (2004), 4202.

[41] C. Arnold, F. Thalmann, C. Marques, P. Marie, Y. Holl, J. Phys. Chem. B, 114 (2010), 9135.

[42] R. Bagheri, R. A. Pearson. Polymer, 36 (1995), 4883.

[43] A.J. Kinloch, R. D. Mohammed and A.C. Taylor. J Mater. Sci., 40 (2005), 5083.

[44] C. Chen, R. S. Justice, D. W. Schaefer, J. W. Baur. Polymer, 49 (2008), 3805.

[45] F. J. McGarry and A. M. Willner, Toughening of an Epoxy Resin by an Elastomer Second Phase, Research Report R68-8, MIT, Boston, 1968.

[46] J.N. Sultan, R.C. Liable, F.J. McGarry. Polym. Symp. 16 (1971), 127.

[47] R. Bagheri , B. T. Marouf and R. A. Pearson. Polym. Reviews, 49 (2009), 201.

[48] S. Sprenger. Polymer, 54 (2013), 4790.

[49] J. Kinloch, M. L. Yuen. J. Mater. Sci., 29 (1994), 3781.

[50] J. Kinloch, D. L. Maxwell and R. J. Young. J. Mater. Sci., 20 (1985), 4169.

[51] Y. L. Liang, R. A. Pearson. Polymer, 51 (2010), 4880.

[52] R. M. Hydro, R. A. Pearson, J. Polym. Sci. Part B: Polym. Physics, 45 (2007), 1470.

[53] H. M. Chong, A. C. Taylor, J Mater. Sci., 48 (2013), 6762.

[54] K. F. Lin, Y. D. Shieh, J. Appl. Polym. Sci., 70 (1998), 2313.

[55] J. Kinloch, R. D. Mohammed, A. C. Taylor, J Mater Sci., 40 (2005), 5083.

[56] J. Y. Qian. The Development of Core-Shell Latex Particles as Toughening Agents for Epoxies (Ph.D. diss.), 1994, Lehigh University

[57] C. K. Riew, A. R. Siebert, R. W. Smith, M. Fernando, and A. J. Kinloch. Abstracts of Papers of the American Chemical Society, 207 (1994), 3.

[58] R. Bagheri and R. A. Pearson, Polymer, 20 (1996), 4529.

[59] Y. Huang, A. J. Kinloch, R. J. Bertsch and A. R. Siebert. in Toughened Plastics I Adv. in Chem. Ser. 233, ACS, Washington, DC, 1993, pp. 189

[60] H. J. Sue, E. I. Garcia-Meitin, D. M. Pickelman, and P. C. Yang, in Toughened Plastics I Adv. in Chem. Ser. 233, ACS, Washington, DC, 1993, pp. 259.

[61] C.A. May, Epoxy Resins Chemistry and Technology, Marcel Dekker, Inc, New York, 1988, pp. 55

[62] F.J. McGarry. Polymer Toughening, Marcel Dekker, New York, 1996.

[63] P. Dittanet. Fracture Behavior of Silica Nanoparticle Filled Epoxy Resin (Ph.D. diss.), 2011, Lehigh University

[64] J. C. Salamone (ed.). Polymeric Materials Encyclopedia, CRC Press, Inc., 1996.

[65] J. S. Pulgisi and M. A. Chaudhari. Epoxies, Engineering Plastics, ASM International, Metals Park, OH, 1988.

[66] R. A. Pearson and A. F. Yee, J. Mater. Sci., 24 (1989), 2571.

[67] A. A. Griffith. Philosophical Transactions of the Royal Society of London, A, 221 (1921), 163-198

[68] N. E. Frost, K. J. Marsh, L. P. Pook. Metal Fatigue. Dover Publications, Inc. Mineola, New York, 1974

[69] G. R. Irwin, J. Appl. Mech., 24 (1957), 361.

[70] R. A. Pearson and A. F. Yee, J. Mater. Sci., 26 (1991), 3828.

[71] B. B. Johnsen, A. J. Kinloch, R. D. Mohammed, A. C. Taylor and S. Sprenger. Polymer, 48 (2007), 530.

[72] V. V. Kozii and B. A. Rozenberg. Polym. Sci., 34 (1992), 919.

[73] R. A. Pearson and A. F. Yee, J. Mater. Sci., 26 (1991), 3828.

[74] H. -J. Sue, Polym. Eng. Sci., 31 (1991), 275.

[75] A. S. Zerda, A. J. Lesser. J. Polym. Sci. Part B: Polymer Physics. 39 (2001), 1137.

[76] M. Arai, Y. Noro, K. Sugimoto, M. Endo. Composites Sci. and Technol., 68 (2008), 516.

[77] Y. L. Liang, R. A. Pearson. Polymer, 50 (2009), 4895.

[78] P. Dittanet, R. A. Pearson. Polymer, 53 (2012), 1890.

[79] P. Dittanet, R. A. Pearson. Polymer, 54 (2013), 1832.

[80] T.H. Hsieh, A.J. Kinloch, K. Masania, A.C. Taylor, S. Sprenger. Polymer, 51 (2010), 6284.

[81] D.J. Bray, P. Dittanet, F.J. Guild, A.J. Kinloch, K. Masania, R.A. Pearson, A.C. Taylor. Polymer, 54 (2013), 7022.

[82] H.-J. Sue, E. I. Garcia-Meitin, D. M. Pickelman, P. C. Yang. in Toughened Plastics I, ACS ser., 233 (1993), 259

[83] J. Y. Qian, The Development of Core-Shell Latex Particles as Toughening Agents for Epoxies (Ph.D. diss.), 1994, Lehigh University

[84] J. Chen, A. J. Kinloch, S. Sprenger, A. C. Taylor. Polymer 54 (2013), 4276.

[85] Y. -L. Liang. The Toughening Mechanisms in Epoxy-Silica Nanocomposites and Hybrid Epoxy-Silica-Rubber Nanocomposites (Ph.D. diss.), 2008, Lehigh University

[86] A. J. Kinloch, D. L. Maxwell, R. J. Young. J Mater. Sci., 20 (1985), 4169.

[87] H. R. Azimi, R. A. Pearson, R. W. Hertzberg. J Appl. Polym. Sci., 58 (1995), 449.

[88] J. Y. Qian, R. A. Pearson, V. L. Dimonie, M. S. El-Aasser. J Appl. Polym. Sci., 58 (1995), 439.

[89] J. Shen, Y. Zhang, J. Qiu, J. Kuang. J Mater. Sci., 39 (2004), 6383.

[90] R. J. Day, P. A. Lovell and D. Pierre. Polym. Int., 44 (1997), 288.

[91] P. A. Lovell, J. McDonald, D. E. J. Saunders and R. J. Young. Polymer, 34 (1993), 61.

[92] R.J. Day, P.A. Lovell and A.A. Wazzan. Composites Sci. and Technol., 61 (2001), 41.

[93] J. Gao, J. Li, S. Zhao, B. C. Benicewicz, H. Hillborg and L. S. Schadler. Polymer, 54 (2013), 3961.

CHAPTER 2

ROLE OF POLYMERIZABLE SURFACTANTS IN EMULSION POLYMERIZATION AND RESULTING LATEX/FILM PROPERTIES

2.1. Introduction

Surfactant is a key ingredient in emulsion polymerization. However, conventional surfactants brought in some issues in their use. Because surfactant molecules are mostly physically adsorbed on latex particle surfaces, upon change of pH, increase of electrolyte concentration, pigment addition, freeze-thaw cycle and high shear process, physically adsorbed surfactants might desorb from particle surfaces and cause particle aggregation due to lack of sufficient stabilization. For latex film formation, films prepared from latexes with conventional surfactants often encounter surfactant migration issues because they are only physically trapped inside the film. In a moisture-rich environment, surfactant concentration gradient throughout the film will drive surfactant molecules to migrate to film/air or film/substrate interfaces and form tiny hydrophilic aggregations and defects inside the film. This surfactant migration might impair film tackiness, gloss, clarity, adhesion to substrate and mechanical strength. Surfactant migration will also increase film permeability to moisture and oxygen, thus decrease corrosion resistance of coatings.

Use of polymerizable surfactants instead of conventional ones might address these issues. A polymerizable surfactant has a reactive group that can participate in polymerization reaction and incorporate into latex polymer particles during emulsion

polymerization. Because they can chemically incorporate onto particle surfaces, they do not easily desorb from particle surface. For film-forming latexes, use of polymerizable surfactant might mitigate surfactant migration and its adverse consequences.

Studies of polymerizable surfactants mainly focused on synthesis of novel reactive surfactants, their effects in emulsion polymerization and resulting latex and film properties. [1-7] They were often compared with common surfactants like sodium dodecyl sulfate (SDS) to prove they can enhance latex stability and water-resistance of film. But these polymerizable surfactants often have very different molecular structures from the control surfactants while molecular structure of surfactants determines practically all the surfactant characteristics in applications. Thus, a pair of polymerizable surfactant and non-polymerizable surfactant with similar molecular structures offers a more effective approach to investigate the sole effect of polymerizable site within the surfactant.

To gain a deep understanding of polymerizable surfactants, not only possible improvements in latex and film properties by polymerizable surfactants should be quantified and compared with non-polymerizable surfactants, but also the underlying surfactant incorporation mechanism where those improvements stem from should also be investigated. In this chapter both aspects were studied. A pair of commercially available surfactants was studied to elucidate their role in emulsion polymerization and resulting latex and film properties, along with the underlying mechanism. Based on previous research it was found that the chosen polymerizable surfactants for the this research do not favor homopolymerization. [8]

2.2. Experimental

2.2.1. Materials

Table 2-1. Materials for polymerization

Monomer	Initiator	Buffer	Costabilizer
n-butyl methacrylate	potassium persulfate	sodium bicarbonate	hexadecane
Acros	Sigma-Aldrich	Sigma-Aldrich	Sigma-Aldrich

Table 2-2. Surfactants

Surfactant	Type	Chemical structure
HITENOL KH-10	Anionic	Alkyl ethoxylate (ca.10) ether sulfuric ester salt
H-3527	Nonionic	Nonionic version of KH-10
HITENOL LA-12	Anionic	Lauryl ethoxylate (ca.6) ether ammonium sulfate

All three surfactants in Table 2-2 were donated by Daiichi Kogya Seiyaku Co. Ltd., Japan. KH-10 is an eco-friendly polymerizable surfactant without allyl phenol groups. LA-12 is non-polymerizable surfactants. LA-12 has a similar molecular structure to KH-10 but without a reactive double bond, so LA-12 was used as a control to compare with KH-10.

Table 2-3.Chemicals used during latex characterizations

Test	TEM	Ion exchange	Titration	Electrolyte stability	
Function	Staining agent	Ion exchange resin	Titrant	Electrolyte	
Name	Phosphotungstic acid	AG 501-X8 Resin	0.02N NaOH	NaCl	$CaCl_2$
MFR	Fisher	BioRad	J. T. Baker	Aldrich	Aldrich

2.2.2. Polymerization Procedure

Miniemulsion polymerization (see recipe in Table 2-6): aqueous phase containing surfactant and buffer was prepared first. The oil phase was then prepared by dissolving hexadecane into n-butyl methacrylate. The oil phase was slowly added into the aqueous phase with stirring at 500 rpm. After 10 min of mixing at 500 rpm, the crude emulsion

was sonicated for 10 minutes with the Branson Sonifier at duty cycle of 70% and an output power level of 7 while stirred at 200 rpm. The resulting miniemulsion was degassed by flowing nitrogen though the miniemulsion for 10 min and finally used for polymerization. Initiator solution was added by different methods in accordance with the experiments described below. The polymerization temperature was 70°C. This procedure was established through repeating and modifying Braganza-Pugh's miniemulsion polymerization procedure. [9]

Emulsion polymerization: aqueous phase containing surfactant and buffer was made first. Oil phase was *n*-butyl methacrylate (BMA) monomer. Oil phase was slowly added into aqueous phase while stirred at 500 rpm. After 10 min mixing at 500 rpm, the emulsion was poured into reaction bottle and degassed by nitrogen flow for 10 min. Potassium persulfate ($K_2S_2O_8$) initiator solution was added right before the bottle was sealed by cap and Teflon tape. Polymerization was at 70°C for 12 hours.

2.2.3. Instruments

A constant temperature end-to-end mixing polymerization unit (Atlas LP2 computer-controlled dyeing system) and an in-house setup of 250 mL four-necked glass reactor equipped with a reflux condenser, a half-moon shaped PTFE stirrer, a thermometer and nitrogen purge inlet with sampling outlet were used to carry out polymerization. A Branson Sonifier (Model 450) was used as homogenizing device to prepare miniemulsions. Fisher Automatic Tensiometer (6 cm Pt-Ir ring) was used to measure surface tension and determine CMCs, with measurements taken at 23±0.5°C. UV-vis spectrophotometer (Spectronic Genesys 2) with wavelength range 200-700 nm was used to generate calibration curves for surfactant concentration in BMA monomer.

Shimadzu UV-2101PC spectrophotometer was used for turbidity measurements (at 20°C) at wavelength of 450 nm. A Nicomp Submicron Particle Sizer (Model 370) was used to measure the latex particle size and size distribution. A DSC 2920 Differential Scanning Calorimeter was used to measure the glass transition temperature of polymer. A Rame-Hart NRL Model 100 Goniometer was used to measure the contact angle of latex films. JEOL JEM-1200EX TEM, Hitachi 4300SE/N SEM and Zeiss 1550 FESEM were used to image dried latex particles for sizing purpose and morphology observation. Solver NEXT NT-MDT fully automated atomic force microscopy was used for latex film morphology observation. Scienta ESCA-300 X-ray photoelectron spectroscope was used for qualitatively study of surfactant distribution in latex films. Pressured stirred filtration cell UHP-76 (Advantec, MFS, Inc.) together with 76 mm diameter 0.1 micron pore size polycarbonate filter paper (GE Water & Process Technologies) and in-house assembled conductometric titration unit (Figure 2-1) were used for latex cleaning and titration of surfactant end group.

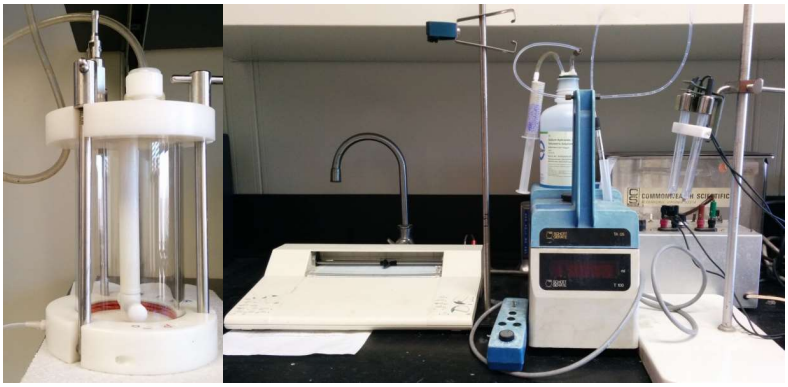

Figure 2-1: Pressured stirred filtration cell (left) and conductometric titration unit (right).

2.3. Results and Discussion

2.3.1. Surfactant Characterizations

Critical micelle concentration (CMC) was measured for each surfactant (Figure 2-2). Resulting surface tension – concentration curve can be utilized to quantify surfactant concentration in later experiments.

From measured critical micelle concentrations of three HITENOL surfactants (Table 2-4), it was found that they have very low CMCs comparing to 8.0 mM for sodium dodecyl sulfate (SDS). This means they can form micelles spontaneously at very low concentrations. When applied in miniemulsion polymerization, these surfactants have to be kept carefully under CMC concentrations in the aqueous phase to prevent micelle formation and micellar nucleation that are not desired in miniemulsion polymerization.

Table 2-4. Critical micelle concentrations of three surfactants.

Surfactant	Apparent CMC (g/L)	Molecular weight (g/mol)	CMC (mM)
KH-10	0.190	793	0.24
H-3527	0.0366	696	0.053
LA-12	0.0943	547	0.17

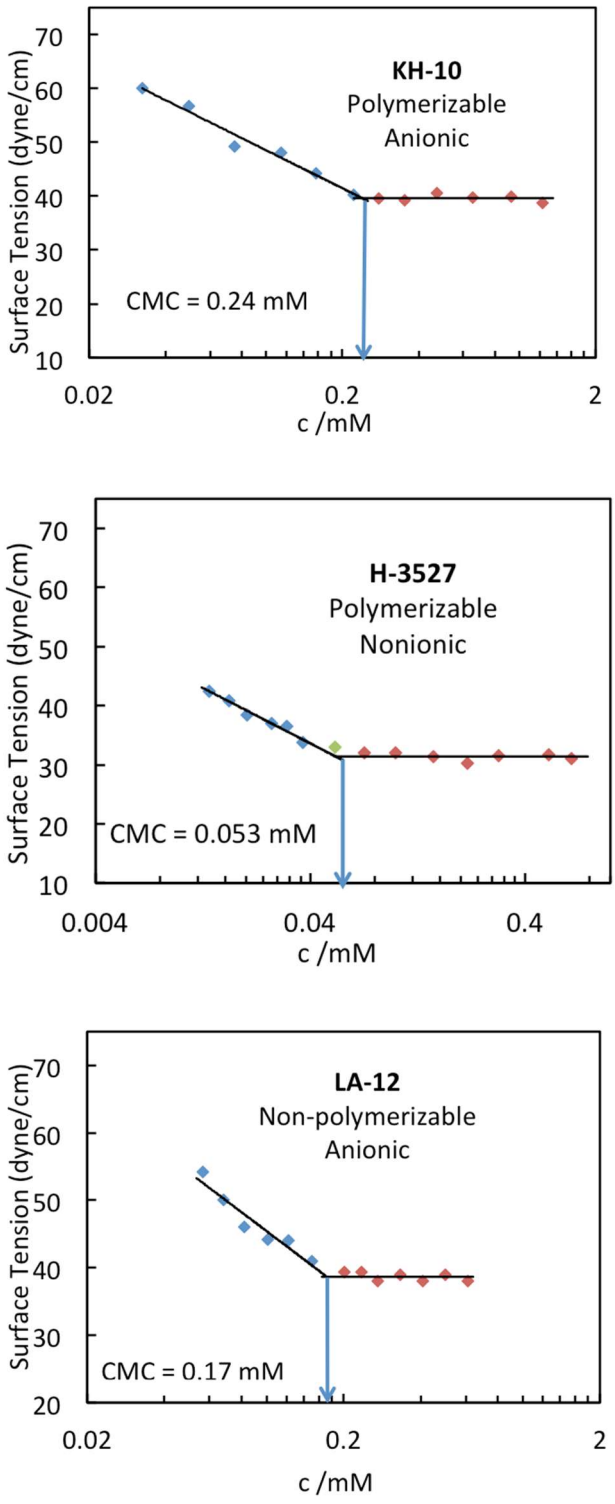

Figure 2-2. CMC of three surfactants.

UV absorbance calibration curves of surfactant concentration in BMA (Figure 2-3) were obtained by measuring absorbance of surfactant-in-BMA solution at maximum absorption wavelength (ethoxylate groups) at different surfactant concentrations (mole fractions). H-3527 the nonionic surfactant, though having similar structure with the other two anionic surfactants, exhibited low UV absorption even at its maximum absorption wavelength (see Table 2-5), which makes it harder to detect the amount of H-3527 in BMA solution than that of the other two surfactants.

Table 2-5. UV absorbance calibration curves of surfactants in BMA solution

Surfactant	Adsorption wavelength	Calibration curve	R^2
KH-10	304 nm	y = 131.71x	0.995
H-3527	301 nm	y = 5.8173x	0.979
LA-12	295 nm	y = 30.291x	0.968

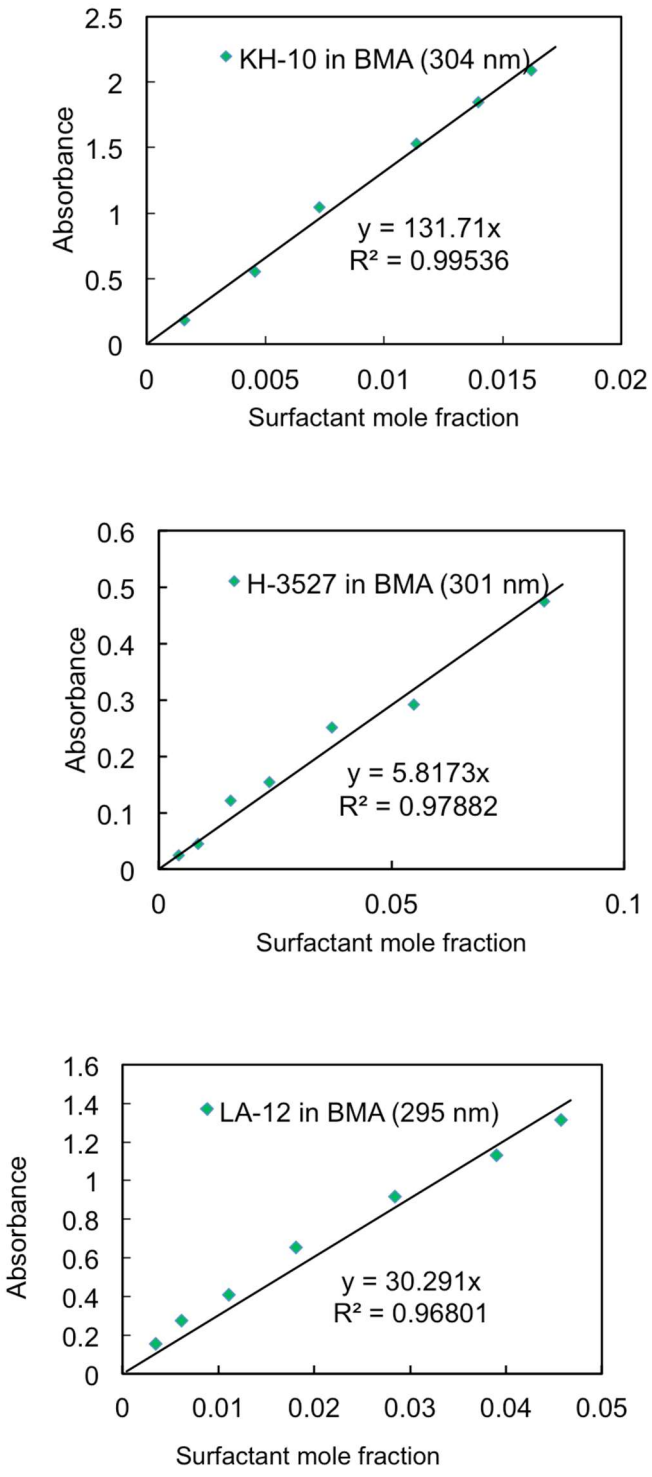

Figure 2-3. UV absorbance of surfactants in BMA solutions.

2.3.2. Miniemulsion Polymerization System

2.3.2.1. Effects of Experimental Variables on Latexes Prepared via Miniemulsion Polymerization

Several important experimental conditions were varied (at a fixed solids content 13%, 8 g BMA, 52 g water, 0.25 g hexadecane, 0.05 g KPS) to determine their effects on the resulting latex particle size and latex properties in order to establish a model emulsion system. Among these conditions, sonication time, if longer than ten minutes, had little effect on particle size and latex appearance. 10 mM of buffer concentration was suitable to prepare stable latexes. Then all three surfactants were used at the same concentration (12 mM) to further evaluate their effectiveness in stabilizing latexes (Figure 2-4).

Figure 2-4: Appearance of latexes with different surfactants. (From left: KH-10, H-3527, LA-12)

As expected, the nonionic surfactant H-3527, though polymerizable, appeared to be the least effective surfactant when used alone. Examination of latex particle size showed that the average particle size of latexes prepared with H-3527 was four to five times larger than the cases where KH-10 and LA-12 were used. There were little differences in the size of latex particles made with these two surfactants. Latexes prepared with two anionic surfactants (polymerizable KH-10 and non-polymerizable LA-

12) exhibited number-average particle diameters of ~ 70 nm, while the use of nonionic H-3527 resulted in particle diameters ~350 nm. In order to prepare small latex particles, nonionic H-3527 should not be used alone.

2.3.2.2. Kinetic Study of Miniemulsion Polymerization with Polymerizable Surfactants

After model miniemulsion polymerization conditions were established for larger scale experiments (see Table 2-6 for recipe), polymerization in a constant temperature stirred reactor was carried out with polymerizable surfactant KH-10 to examine the kinetics during the reaction. During polymerization process, 1~2 mL latex samples were drawn out at certain time intervals from a sampling tube and put into vials containing known amount of 1% hydroquinone solution to stop reaction. A typical conversion result is shown in Figure 2-5.

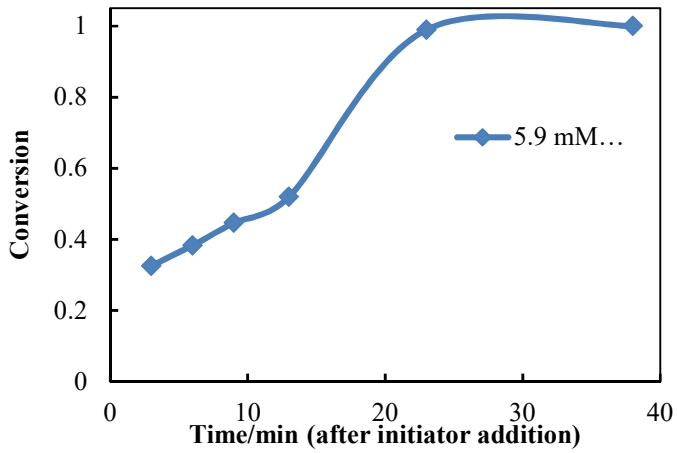

Figure 2-5. Conversion-time curve of miniemulsion polymerization of BMA w. KH-10.

Table 2-6. Recipe used for study of miniemulsion polymerization kinetics.

Ingredient	Amount	Comment
BMA	35 g	250 mL reactor
Hexadecane	1.26 g	3.6 wt.% of BMA
Water	110 g	25% solids
Surfactant (KH-10)	Various	5.9 - 23.6 mM
$NaHCO_3$	0.065 g	10 mM in water
KPS	0.2 g	6.7 mM in water

From Figure 2-5 we can observe typical miniemulsion polymerization kinetics. Comparing with Braganza-Pugh's miniemulsion polymerization kinetics obtained with a Mettler RC1 Reaction Calorimeter (Figure 4-3(a) in [9]), although her recipe had different monomer (styrene) and slightly different KH-10 surfactant concentration from this study, the shape of conversion-time curve and the exhibited stages of reaction were very similar except the reaction time in her study was almost twice of that in this study. However, the contribution of micellar nucleation to a steep increase of conversion at the very early reaction stage was not shown in Figure 2-5, because after initiator addition the 1st sample took 2-3 min to prepare and finish. A distinct reaction rate change occurred at around 13 min. With conversion near 60%, the point of inflection on the curve marked a maximum of polymerization reaction rate, which meant disappearance of monomer droplets according to miniemulsion polymerization mechanism. Then the reaction rate decreased continuously because the monomer concentration decreased inside of nucleated droplets, which could be observed from this part of conversion curve having a decreasing slope. Resulted particle size and size distribution was found to be similar to that when non-polymerizable LA-12 was used. This result of similar particle size distribution between comparable latexes prepared with polymerizable surfactant and non-

polymerizable surfactant corresponds well with previous studies in similar systems. Matahwa and coworkers [10] synthesized cationic and anionic amphiphilic monomers (surfmers) and used them to stabilize particles in RAFT miniemulsion polymerizations of styrene and MMA and compared results with conventional surfactants. They found reaction rate, particle size and molecular weight distribution when surfmers were used to be mostly the same as those with conventional surfactants [10]. Crespy and coworkers studied miniemulsion polymerization of vinyl monomers stabilized with polymerizable anionic surfactant Tego XP-1008 and polymerizable nonionic surfactant Tego XP-1007. Miniemulsions prepared were stable and latex particles had similar size and molecular weight distribution with that when non-polymerizable surfactants were used. [11]

2.3.2.3. Improvement in Latex Stability by Polymerizable Surfactant

Latexes prepared with reactive surfactants exhibited good shelf-life stability (more than four months) and great stability against dilution. Another important stability test for latexes is stability against electrolyte addition. Monovalent and divalent electrolytes were used to examine the stability of latexes prepared with polymerizable KH-10 and non-polymerizable control LA-12 surfactants in order to determine the extent of improvement introduced by particle surface modification by polymerizable surfactants. The recipe used (25% solids) to examine the latex stability against added electrolyte is: 50 g BMA, 17 mM surfactant, 1.8 g hexadecane (3.6 wt% based on BMA), 0.13 g sodium biocarbonate (10 mM, based on water), and 0.3 g KPS (7 mM based on water). Latexes made were diluted to 0.13% solids. 4 M NaCl or 2M $CaCl_2$ were added to diluted latexes to achieve different electrolyte concentrations. Then the turbidity change of the latex after electrolyte addition was recorded by UV-vis spectrophotometer (Figures 2-6

and 2-7). The initial slopes of the different turbidity-time curves were plotted to determine critical coagulation concentration (C.C.C.) (Figures 2-8 and 2-9).

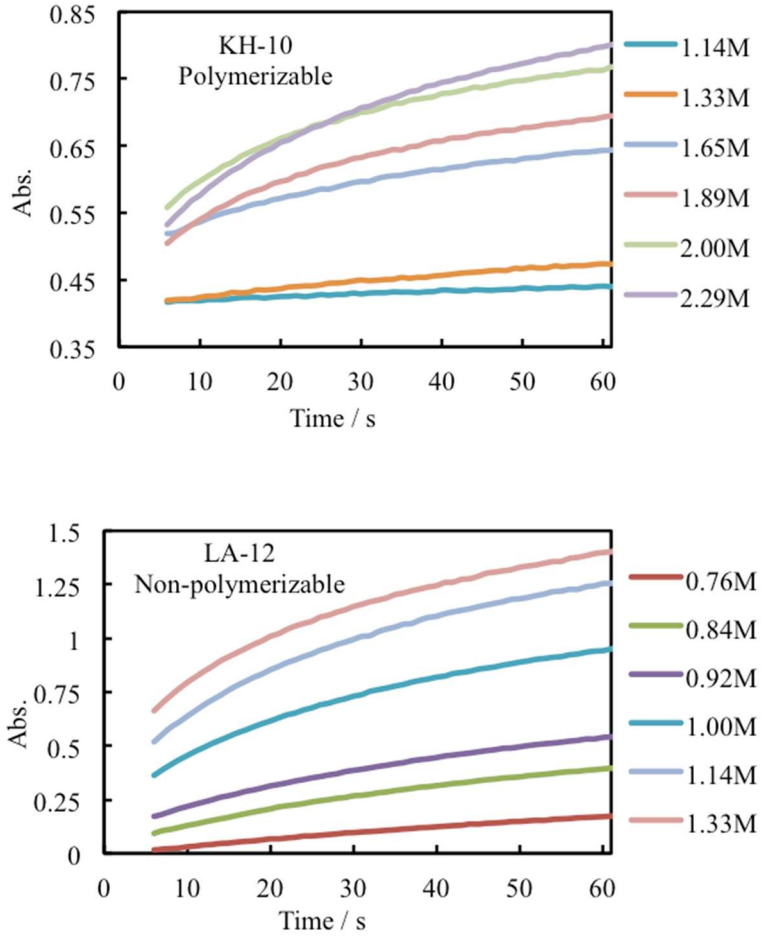

Figure 2-6. Changes of turbidity after different amounts of NaCl was added to latex. (Left: latex prepared with polymerizable surfactant KH-10; right: prepared with non-polymerizable LA-12)

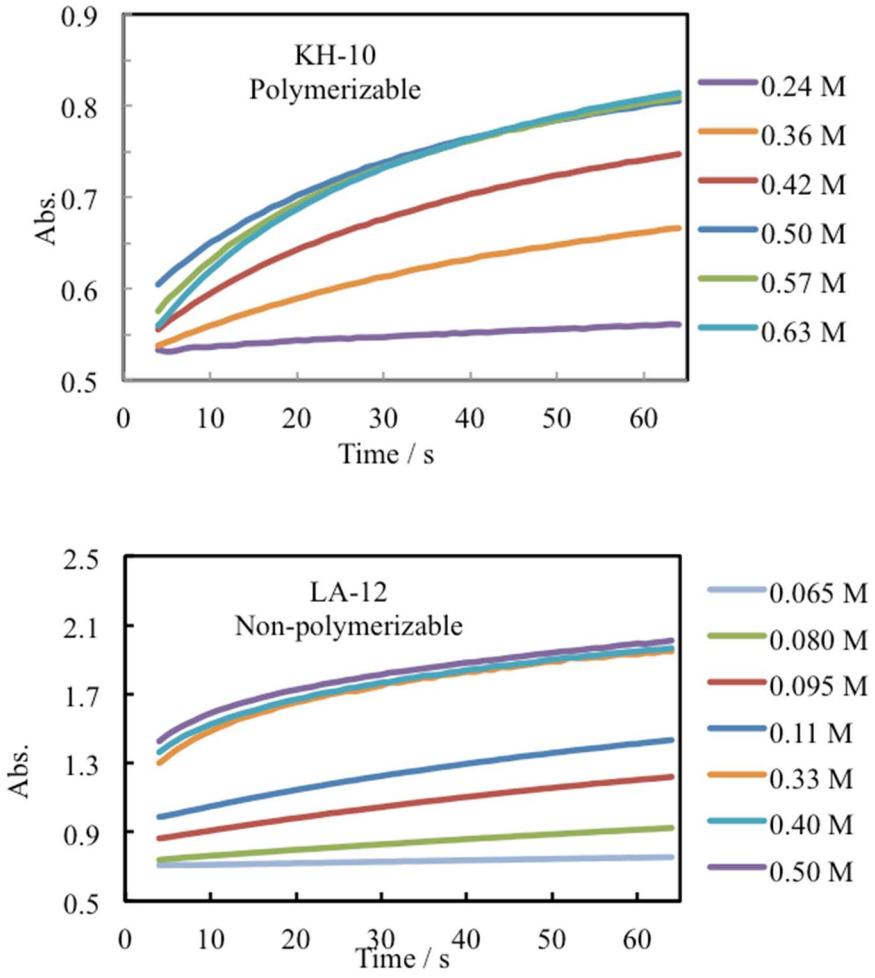

Figure 2-7: Changes of turbidity after different amounts of $CaCl_2$ was added to latex. (Left: latex prepared with polymerizable surfactant KH-10; right: prepared with non-polymerizable LA-12)

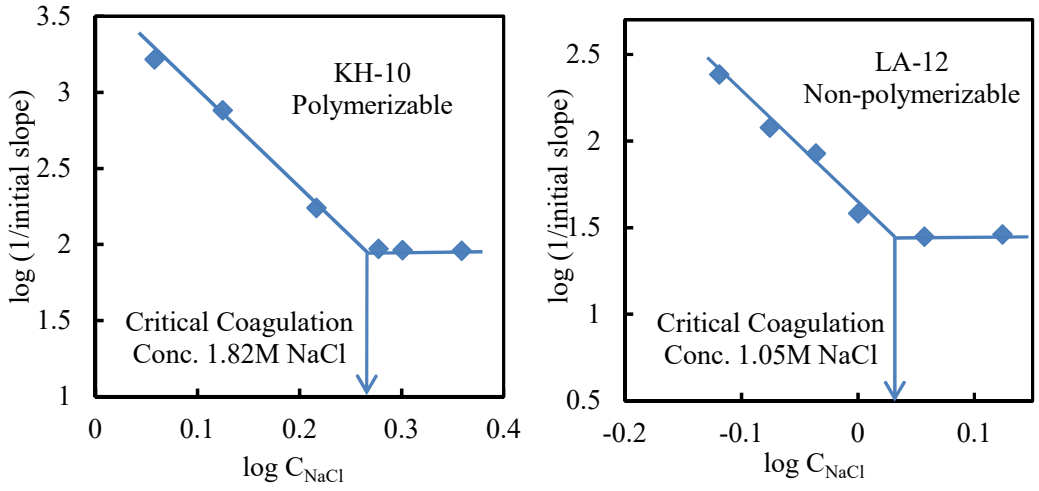

Figure 2-8. C.C.C of latexes against added NaCl. (Left: latex prepared with polymerizable KH-10 surfactant; right: latex prepared with non-polymerizable LA-12 surfactant).

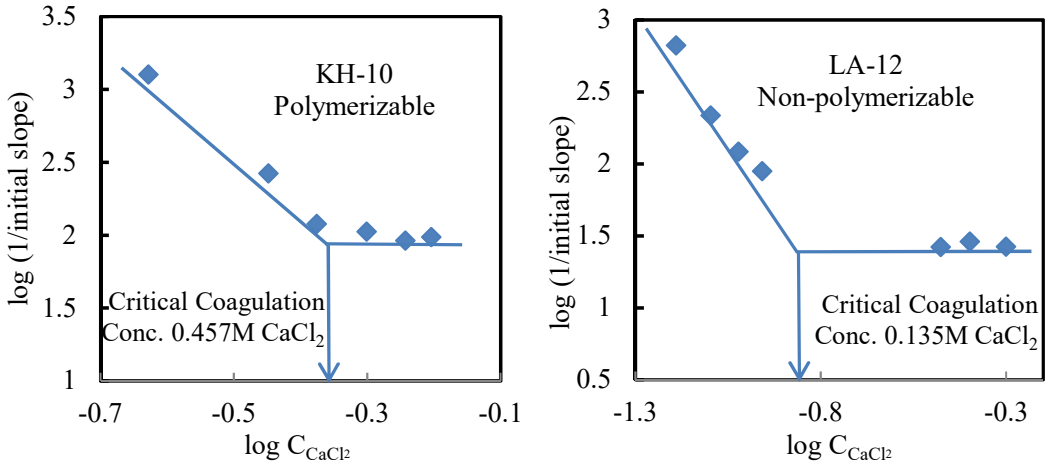

Figure 2-9: C.C.C of latexes against the addition of $CaCl_2$ (Left: latex prepared with polymerizable KH-10 surfactant; right: prepared with non-polymerizable LA-12 surfactant).

In Figures 2-6 and 2-7, the initial slopes of absorbance (i.e. optical density) versus time curves increased as electrolyte concentration increased until a critical slope was reached, after which further increase in electrolyte concentration did not affect the initial

slopes any more. The slopes of absorbance-time curves gradually decreased, indicating that the rate of coagulation decreased over time as particle number decreased due to coagulation over time.

In Figures 2-8 and 2-9, the stability curves were shown. Two fitted straight lines combined to form each stability curve according to DLVO model. The sloped line represented slow coagulation and the horizontal one represented repaid coagulation (stability factor W=1 in equation # 1). The concentration taken at the intersection of these two lines was read as C.C.C.

$$\text{Stability factor: } W = \frac{k_{rapid\ coagul.}}{k_{slow\ coagul.}} = \frac{\left.\frac{d(Absorbance)}{dt}\right|_{t=0,\ c\geq C.C.C.}}{\left.\frac{d(Absorbance)}{dt}\right|_{t=0,\ c}} \qquad (1)$$

From Figures 2-8 and 2-9 it was shown that with the latex prepared with KH-10 the C.C.C. against NaCl was 1.82 M while the C.C.C. for LA-12 was only 1.05 M. With polymerizable surfactant KH-10, the C.C.C. was 73% higher than the non-polymerizable LA-12 surfactant. Since KH-10 and LA-12 share a similar structure, this improvement should result from the incorporation of the polymerizable surfactant into the latex particles to achieve better colloidal stability. Also, with the KH-10 polymerizable surfactant, the C.C.C. of $CaCl_2$ was 0.457 M while latex prepared with LA-12 was only 0.135 M. Again, with the polymerizable KH-10 surfactant, the C.C.C. of $CaCl_2$ was 240% higher than the latex prepared with non-polymerizable LA-12 surfactant. This improvement was even much more prominent with divalent electrolyte $CaCl_2$. For KH-10, the ratio of C.C.C of divalent electrolyte $CaCl_2$ to monovalent NaCl was 0.25, while

for LA-12, this ratio was 0.13 within normal range obtained from similar studies [12]. The ratios of C.C.C. values for monovalent and divalent electrolytes did not follow the Schulze-Hardy inverse sixth power rule. Instead, they approximately followed an inverse second power rule as Wu's experimental results indicated [12]. Wu suspected that the restriction of a constant Stern potential might be the reason for the discrepancy. Polymerizable KH-10 surfactant exhibited great improvement towards latex stability against electrolyte addition, especially in the presence of multivalent electrolyte. In the following section possible mechanism accounting for this improvement will be investigated.

2.3.3. Batch Conventional Emulsion Polymerization System

2.3.3.1. Batch Emulsion Polymerization with Various Surfactant Concentrations

In previous miniemulsion polymerization study, experimental procedure, solids, buffer and initiator concentrations were all screened and set. Thus for the conventional emulsion polymerization study, the only important screening was for surfactant concentration. In 4 oz. reaction bottles, batch emulsion polymerization was carried out using the recipe given in Table 2-7, under various surfactant concentrations (given in Table 2-8) to choose a suitable surfactant concentration for further latex and film formation studies. After polymerization, percent coagulum, conversion and latex particle size and distribution were examined (Table 2-8). Deviation in the table is machine generated standard deviation σ of particle size distribution measured using the Nicomp Submicron Particle Sizer (Model 370). For example, if σ = 25 nm while the average diameter is 90 nm, then 68.3% of all the particle measured in the sample have diameters in the range of interval (90-25, 90+25) = (65, 115) nm.

Table 2-7. Recipe for finding suitable surfactant concentration.

Solids	BMA	Water	$NaHCO_3$	KPS
25%	20 g	60 g	0.05 g *	0.16 g **

* 10mM based on water

** 10 mM based on water

Table 2-8. Characterization results of PBMA latexes prepared using conventional emulsion polymerization.

Sample #	Surfactant	Surfactant conc.*	Conversion	Coagulant percentage**	Average particle diameter /nm***	Deviation /nm
A1	KH-10	15mM	>99%	0.44	90.7	24.4
A2		20mM		0.32	81.6	19.5
A3		25mM		0.35	67.1	20.0
A4		30mM		0.39	65.6	18.0
B1	LA-12	15mM		0.60	84.8	15.8
B2		20mM		0.52	81.2	19.1
B3		25mM		0.52	72.8	14.8
B4		30mM		0.49	80.1	21.7

* Concentration based on water

** $\text{Coagulant percentage} = \frac{\text{Dried polymer wt. in coagulant}}{\text{Total monomer wt. added for polymerization}}\%$

*** Light scattering intensity weighted particle size distribution

From results in Table 2-8, coagulant percentage varied with different surfactant concentration but not significant when it's higher than 20 mM; average particle size decreased with increasing surfactant concentration. Because 20 mM surfactant concentration brought a drop in coagulant amount, and the higher surfactant concentration did not cause further reduction in the % coagulum, but resulted in smaller particle size (which is not of interest in this particular study), 20 mM was chosen as surfactant concentration for further studies of latexes and films. For the two model latexes prepared with 20 mM surfactant concentration, A2 and B2, the surface tension of latex after polymerization was measured. It was 64.5 and 61.5 dyne/cm respectively for A2 and B2 and remained the same after 20X, 50X and 100X dilutions.

2.3.3.2. Latex Particle Sizing using Electron Microscopy

A model recipe for emulsion polymerization of *n*-butyl methacrylate (BMA) for study of the role of polymerizable surfactant in latex and film properties was established as given in Table 2-9.

Table 2-9. Recipe for study of polymerizable surfactant in conventional emulsion polymerization of BMA

Sample	Surfactant	Solids	BMA	Water	KPS	Buffer	Surfactant
1	KH-10	25%	40 g	120 g	10 mM* (0.2g)	10 mM (0.062g)	20 mM (1.88g)
2	LA-12	25%	40 g	120 g	10 mM (0.2g)	10 mM (0.062g)	20 mM (1.27g)

* Concentration based on water

Sample of poly(*n*-butyl methacrylate) latexes were used for particle size analysis using transmission electron microscope (TEM) (Figure 2-10). Because poly(*n*-butyl methacrylate) is low T_g polymer (~35°C), negative staining agent phosphotungstic acid was used for better electron conductance and image contrast.

To ensure TEM imaging was valid instead of false imaging of flat round shapes of melted latex particles, a shadowing technique combined with SEM imaging were employed. After the phosphotungstic acid-treated latex sample was imaged using TEM, sample grid was mounted onto a flat surface and shadowed with evaporated Au-Pd 60:40 wire at 21° shadowing angle for a theoretical 5 nm thickness. After shadowing, samples were imaged again using for the SEM to observe if there were shadowing of latex particles (Figure 2-11) and to roughly measure the particle size through the shadowing angle relation.

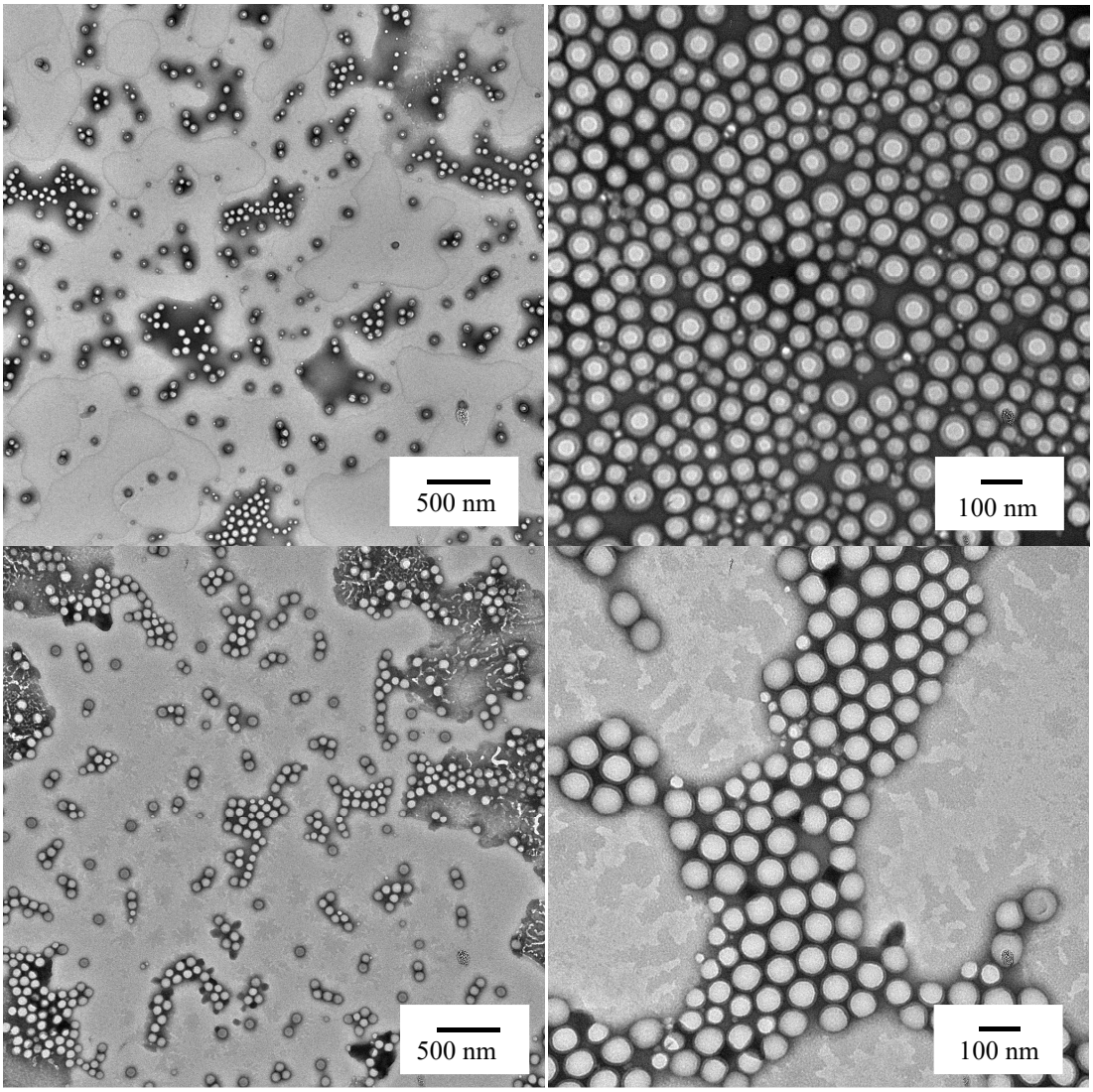

Figure 2-10. TEM images of dried stained latex. Top: sample 1 with KH-10; bottom: sample 2 with LA-12.

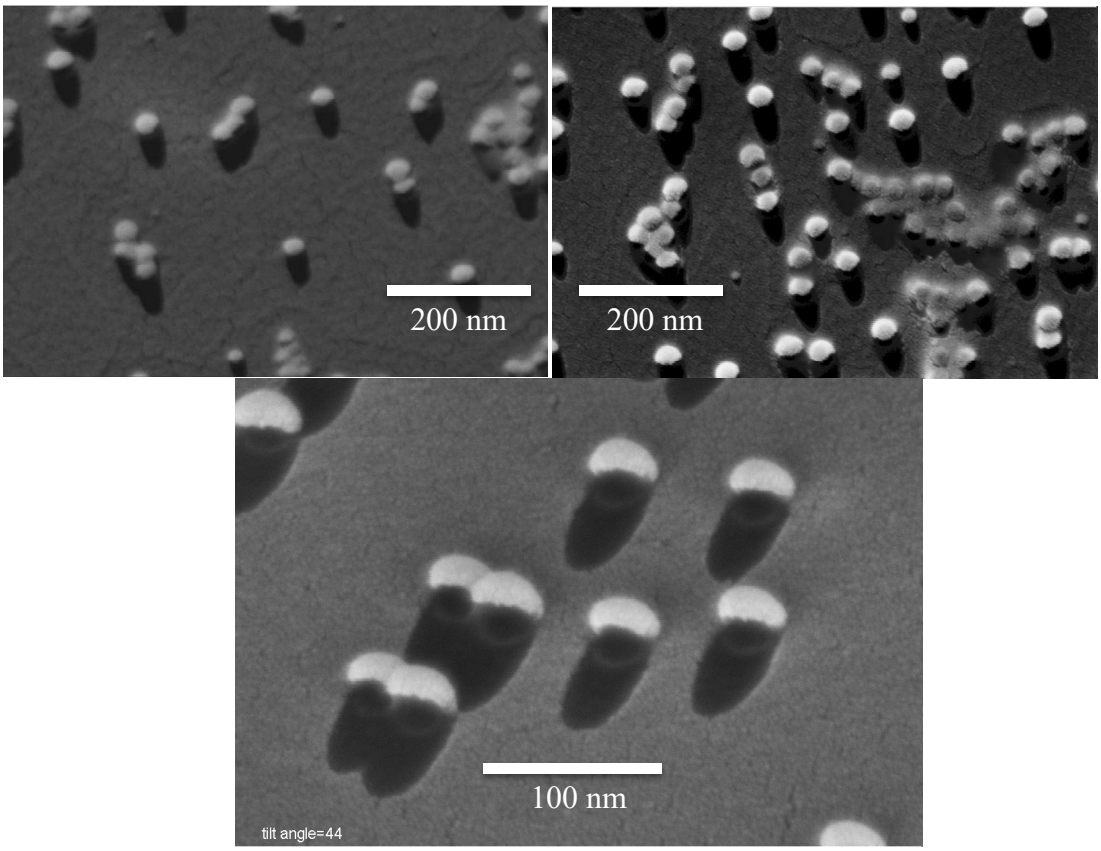

Figure 2-11: SEM images of PBMA latex particles shadowed by Pd-Au vapor after staining with phosphotngstic acid and imaging with TEM

After shadowing and SEM imaging (Figure 2-11), it was obvious that latex particles were not deformed by high voltage electron beam during TEM imaging. Thus the TEM imaging of samples with phosphotungstic acid treatment was effective for our poly (*n*-butyl methacrylate) latex samples. According to shadow length and shadowing angle, particle diameter can be estimated using equation: $D = \tan(\theta) * L$. Calculated average particle diameter from both TEM imaging method and SEM imaging of the shadow length was around 88 nm for both samples. Thus, we found that PBMA latex prepared using polymerizable surfactant KH-10 and non-polymerizable LA-12 both yielded similar latex particle diameter and size distribution. . This result is similar to what

previous studies have showed. [9, 10] From this part of particle imaging study, it was found polymerizable surfactant did not affect the latex particle size and size distribution to a noticeable extent, which means the benefits that polymerizable surfactants offered to latex stability and film properties (discussed in section 2.3.2.3) should be brought in through other microscopic mechanisms (e.g. particle surface modification) instead of change of particle size and size distribution. .

2.3.4. Study of Particle Surface Modification by Polymerizable Surfactants

To better understand how polymerizable/non-polymerizable surfactants modify particle surface thus affect latex and film properties, it is crucial to know how much surfactants incorporate into different phases/loci inside a latex (i.e. aqueous phase, inside polymer particles and on the surface of polymer particles) and how surfactants distribute/migrate inside latex films.

2.3.4.1. Study of Surfactant Incorporation Mechanism in Latexes

To quantify the surfactant amount incorporated into different phases in model latexes, the following technique was applied. A known amount of model latex (~20 g) was diluted and placed into a pressured stirred-filtration cell installed with 76 mm diameter 0.1micron pore size polycarbonate filter paper. Cell pressure was obtained by the height difference of the source of DI water and the cell. As DI water constantly flew into the cell, the eluent stream exiting from the cell carried salts, washed off surfactants, oligomers and possibility latex particles (only if they are small enough to pass through pores of the polycarbonate filter paper). All the eluent was collected until the conductance of fresh eluent equaled DI water. Then the “cleaned” latex and concentrated eluent were both obtained for further analysis. For the cleaned latex: mixed anionic and

cationic ion exchange resin of 5 wt.% based on cleaned latex was added into the latex followed by stirring for 2 hours. Then the used resin was filtered out and discarded. A new batch of resin was added and the same procedure was repeated until the conductance of ion-exchanged latex remained the same. After ion exchange, the weight and % solids of the cleaned latex were measured. After ion exchange, the ammonium sulfate end groups of the surfactant (located on the latex particle surface) were ion-exchanged into —SO_3H, which can be titrated and quantified by 0.02N NaOH titrant using an in-house conductometric titration unit. In this way, the amount of surfactant anchored on latex particle surfaces was calculated in the form of "mole surfactant on polymer particle surface per gram of pure polymer", which can be converted via the weight of pure polymer to obtain the total amount of surface-anchored surfactant in the original latex. For the concentrated eluent: volume of the eluent was firstly measured. Surface tension of the eluent was then measured and thus surfactant concentration in the aqueous phase was obtained through surface tension-surfactant concentration calibration curves obtained in previous study. Then the amount of surfactant that can be washed off from original latex (i.e. surfactant in aqueous phase and physically adsorbed on latex particles) was calculated. Amount of surfactant buried inside particles was then calculated by subtracting former two amounts from total surfactant amount. This method was derived from former students Lai and Braganza-Pugh's dissertations. [8, 9]

Table 2-10. Surfactant (S) distribution in model latexes

Sample	Total S /mmol	S in eluent *	S buried inside particles	S anchored on particle surface	Estimated area occupied by one surfactant molecule /nm^2 **
KH-10 latex 19.36 g	0.2866 (100%)	0.0652 (22.7%)	0.0318 (11.1%)	0.1896 (66.2%)	2.6
LA-12 latex 19.16 g	0.2846 (100%)	0.0882 (31.0%)	0.1364 (47.9%)	0.0600 (21.1%)	7.9

* Surfactant in aqueous phase of latex and physically adsorbed on latex particles
** Latex particle diameter was estimated as the average diameter obtained by TEM

From results in Table 2-10 we can see for polymerizable surfactant KH-10, there was less surfactant in forms that can be washed off by filtration technique—22.7% compared to 31.0% for non-polymerizable LA-12. For surfactant that was anchored on latex particle surface and buried inside latex particles (either physically trapped or chemically bound for polymerizable surfactant), KH-10 significantly reduced the amount of surfactant buried and increased the amount anchored on particle surface by 220% due to the reactivity of C=C double bond in surfactant molecule. The reason why more polymerizable surfactants were anchored on particle surface could be that polymerizable surfactant is neither favorable for homopolymerization nor competitive for copolymerization with monomer. Thus it tends to react at the end of polymerization when monomer concentration is low. In this way more polymerizable surfactant can be anchored at the surface of latex particles for particle surface modification rather than buried inside particles.

Area density of anchored surfactant molecules on latex particle surface can be estimated using the average particle diameter obtained by TEM. Since the amount of surfactant anchored on particle surface was much higher for KH-10 than LA-12, a denser

surfactant population on particle surface can be expected for KH-10. The area occupied by one polymerizable surfactant molecule was one third of the area occupied by non-polymerizable surfactant molecule. The estimated spacing between KH-10 molecules was 1.6 nm.

2.3.4.2. Study of Surfactant Distribution in Films

Besides surfactant distribution in latex system, quantitative study of surfactant distribution inside latex films was of interest, because by examining it and its evolution with time or other variables, one can better study the effect of surface modification by polymerizable surfactants on surfactant migration inside films. In this study an X-ray photoelectron spectroscopy method was tried for this purpose. Surfactant molecule has N and S elements which can be detected by XPS on film-air interface. Two films were cast from model latexes and one of them went through water immersion process. Films were cast for 16 hours at 45℃, then 24 hrs at 55℃. Water immersion test was under room temperature for 48 hours and film were dried at 55℃ after immersion. Sample films were carefully pressed onto conductive tape attached to a sample holder. Charge neutralization was invoked during the analysis.

Table 2-11.Apparent sample composition detected on latex sample film surface (%)

Sample	Surfactant	Immersion	C(1s)	O(1s)	N(1s)	S(2p)
1-1	KH-10	No	82	18	<0.01	<0.01
1-2	KH-10	Yes	84	16	<0.01	<0.01
2-1	LA-12	No	84	16	<0.01	<0.01
2-2	LA-12	Yes	85	15	<0.01	0.04

From Table 2-11, we can see that C and O were detected in all film samples. However, N element was beyond detection limit due to combination of its low

concentration and small atomic number. But interestingly we can see for the latex film prepared with non-polymerizable LA-12 surfactant that went through a water immersion process, the amount of S element increased noticeably on film surface. This can be attributed to enhanced surfactant migration to film-air interface during the water immersion process. For films prepared with polymerizable surfactant KH-10 similar phenomenon was not found. Thus it could be concluded that surfactant migration inside latex films can be suppressed to some extent by polymerizable KH-10 comparing to non-polymerizable LA-12, presumably due to more anchored surfactant molecules in the case of polymerizable surfactant than that of non-polymerizable surfactant. Suppressed surfactant migration is beneficial to maintain desired film properties, such as adhesion, hydrophobicity, gloss and uniformity.

2.3.4.3. Effect of Polymerizable Surfactant on T_g and Particle Coalescence Enthalpy

Table 2-12. Effect of removal of free surfactant on film glass transition temperature.

Sample	T_g, film cast from original latex	T_g, film cast from cleaned latex
KH-10 latex	34.1 °C	34.7 °C
LA-12 latex	34.0 °C	34.6 °C

Polymerizable surfactants, as means of particle surface modification, should not alter bulk composition and glass transition temperature to a noticeable extent. Thus glass transition temperature changes of films made from latexes before and after serum replacement were measured by DSC (Table 2-12). Films cast from cleaned latexes after removal of free surfactant in aqueous phase and physically adsorbed on latex particle surface exhibited slightly higher glass transition temperature (this might be induced by plasticization of films by surfactants, but instrumental error range should be borne in

mind). But it lacked of noticeable T_g differences between polymerizable and non-polymerizable surfactants. So we can conclude that neither polymerizable surfactant nor non-polymerizable surfactant under normal usage concentrations would vary bulk polymer's glass transition temperature. Thus polymerizable surfactants can be employed as a technique for latex particle surface modification without altering the bulk polymer properties.

As previous results of surfactant molecule spacing on latex particle surface indicated, latex prepared with polymerizable KH-10 rendered a denser surfactant population on particle surface thus smaller molecule spacing—around 1.6 nm, which was near the range of poly (ethylene oxide) crystalline spacing. One possible outcome would be small crystalline regions among latex particles and these regions might impede the process of particle coalescence during film formation. A technique employing DSC was used here to investigate this possible effect [13].

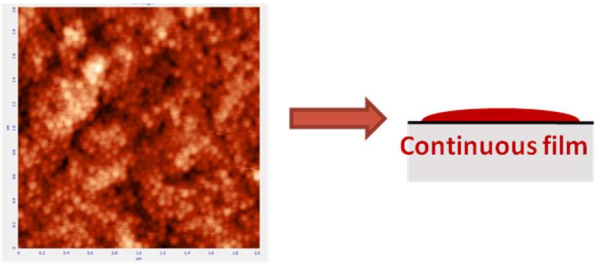

Figure 2-12: Latex particle coalescence from packed particles (left: AFM image of dried latex) to a coherent film above polymer T_g.

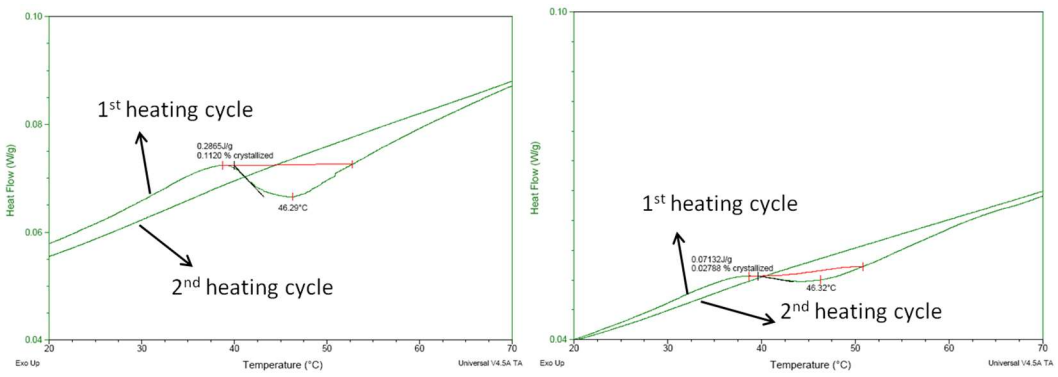

Figure 2-13: Particle coalescence process and its enthalpy change ΔH_c.

Particle coalescence enthalpy ΔH_c is a measurement of energy barrier for disappearance of latex particle boundaries. This process usually occurred near glass transition temperature. ΔH_c was measured by experimental design employing DSC. Quantification of ΔH_c needed to rule out changes due to glass transition. Thus annealed equal-weighted sample films were used as reference to rule out glass transition effect. Dried latex was heated from room temperature through T_g to 100°C. Then it was cooled under room temperature and heated again through T_g. The results given in Figure 2-13 show that the transition appeared during first heating cycle indicating the particle coalescence process which disappeared during second heating cycle. ΔH_c can be analyzed by built-in software from the transition curve during first heating cycle, and the results showed a ΔH_c of 0.2865 J/g for latex particles prepared with KH-10 while a ΔH_c of 0.07132 J/g for latex particles prepared with LA-12 we did find a 300% higher ΔH_c for latex prepared with KH-10 compared to LA-12. This difference should only be introduced by the effect of polymerizable surfactant used on particle surface modification, most possibly by the dense surfactant molecular spacing on latex particle surface. Polymerizable surfactant can render more regular aligned surfactant molecules

around latex particles in such a way that ethoxylate chains of surfactant molecules may form small crystalline regions to impede particle coalescence during film formation process, signified by an elevated ΔH_c.

2.4. Summary and Conclusions

Several HITENOL surfactants were characterized and used in miniemulsion and conventional emulsion polymerization of *n*-BMA. Latexes and films prepared with polymerizable surfactant KH-10 and its non-polymerizable control LA-12 were compared and contrasted in multiple aspects. Latexes prepared with KH-10 exhibited 240% higher stability against electrolyte addition, and resulted in films with suppressed water-sensitivity and surfactant migration. Surfactant incorporation into different loci in latex (including in aqueous phase, on latex particle surfaces and inside latex particles) was quantitatively studied. The mechanism accounting for those improvements was the increased amount of surfactant covalently bound on latex particle surfaces. It was found that 220% more surfactants were anchored on particle surfaces in latex prepared with polymerizable KH-10 than that with non-polymerizable LA-12. But this causes a 300% increase of particle coalescence enthalpy during film formation, potentially not beneficial to film formation processes that are sensitive to temperature and energy requirements.

2.5. References

[1] E. Ozdeger, E. D. Sudol, M. S. El-Aasser and A. Klein, J. Polym. Sci. Part A: Polym. Chem. 35 (1997), 3837.

[2] J. I. Amalvy, M. J. Unzue, H. A. S. Schoonbrood, J. M. Asua. Macromolecules, 31 (1998), 5631.

[3] D. Colombié, E. D. Sudol and M. S. El-Aasser, Macromolecules, 33 (2000), 7283.

[4] X. Wang, B. Boya, E. D. Sudol and M. S. El-Aasser, Macromolecules, 34 (2001), 8907.

[5] S. Krishnan, A. Klein, M. S. El-Aasser, E. D. Sudol, Macromolecules, 36 (2003), 3152.

[6] E. Aramendia, M. J. Barandiaran, J. C. de La Cal, J. Grade, T. Blease, J. M. Asua. J. Polym. Sci. Part A Polym. Chem., 42 (2004), 4202.

[7] C. Arnold, F. Thalmann, C. Marques, P. Marie, Y. Holl, J. Phys. Chem. B, 114 (2010), 9135.

[8] Z. Lai, Role of Reactive Surfactants in Emulsion Polymerization (Ph.D. diss.), 2004, Lehigh University

[9] S. N. Braganza-Pugh, Role of Reactive Surfactants in Miniemulsion Polymerization (Ph.D. diss.), (2010), Lehigh University

[10] H. Matahwa, J. B. Mcleary, R. D. Sanderson, J. Polym. Sci. Part A: Polym. Chem., (2005) 44,427

[11] Crespy, A. Musyanovych, K. Landfester, Colloid Polym. Sci., (2006) 284, 780

[12] W. C. Wu, Preparation and Surface Characterization of Latexes as Model Colloids (Ph.D. diss.), (1976), Lehigh University

[13] L. A. Cannon, R. A. Pethrick. Polymer (2002) 43, 6421.

CHAPTER 3

SYNTHESIS OF SILICA/PBA/PMMA MULTILAYER CORE-SHELL PARTICLES

3.1. Introduction

Epoxy resins are widely used as engineering plastics, structural adhesives, composite materials and microelectronic packaging materials. Epoxies are inherently brittle so they are often toughened for applications that require flaw tolerance and strength. Rubber-toughened epoxies are amongst the most widely studied toughening agents for epoxies. Reactive oligomers (liquid rubbers) can be mixed with epoxy resins and phase-separate to form micron scale rubber domains during epoxy curing process. Commonly used liquid rubbers include Carboxyl-terminated butadiene-acrylonitrile (CTBN) rubbers; ATBN (amino-terminated), ETBN (epoxy-terminated), VTBN (vinyl-terminated), etc. However, rubber-toughened epoxies often result in compromises in modulus and strength. These disadvantages might be overcome by adding inorganic fillers like silica nanoparticles, carbon nanotubes and nanoclay platelets. It is also important to note that liquid rubber phase separation during the epoxy curing process often generates a non-uniform rubber particle size distribution that depends on cure chemistry and cure conditions. The non-uniform particle size distribution can complicate studies on the relationship between particle size/morphology and toughening effect. Structured core-shell rubber particles have also been studied as toughening agents for epoxies and offer a tighter control of particle size that is not dependent on epoxy cure

chemistry and/or cure conditions. Recently, one study has suggested the use of a novel composite particle morphology might greatly contribute to toughening efficiency of these particles because of possible synergistic effect from silica core, rubber interlayer and epoxy-compatible outer layer. (Figure 3-1) [1]

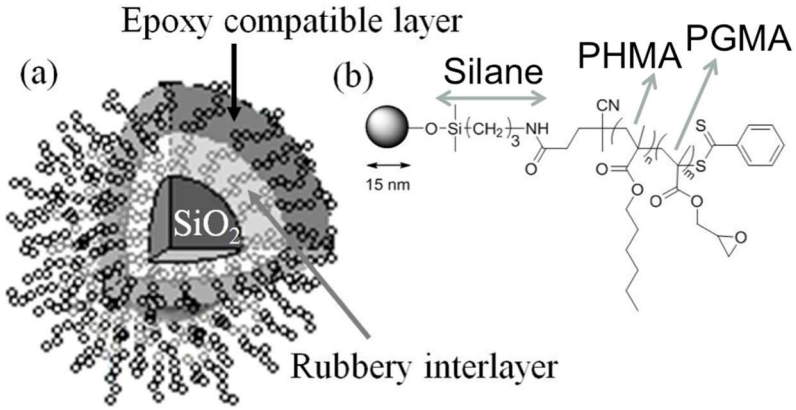

Figure 3-1. Novel multilayer composite particle morphology. Reprinted. [1]

According to this work, these particles were synthesized using a reversible addition fragmentation chain-transfer (RAFT) polymerization technique. [2] When these particles were used as toughening agents for epoxies a 300% improvement of toughness was observed without a compromise in modulus, however, neither multilayer particle morphology nor causality between particle morphology and improvement of toughness were confirmed. In this chapter, an emulsion polymerization process was utilized for synthesis of well-defined silica/PBA/PMMA multilayer particles resembling Figure 3-1. Later in Chapter 4 these particles would be compared with hybrid toughening agents having the same composition as multilayer particles to elucidate the contribution of structured particle morphology to toughening efficiency.

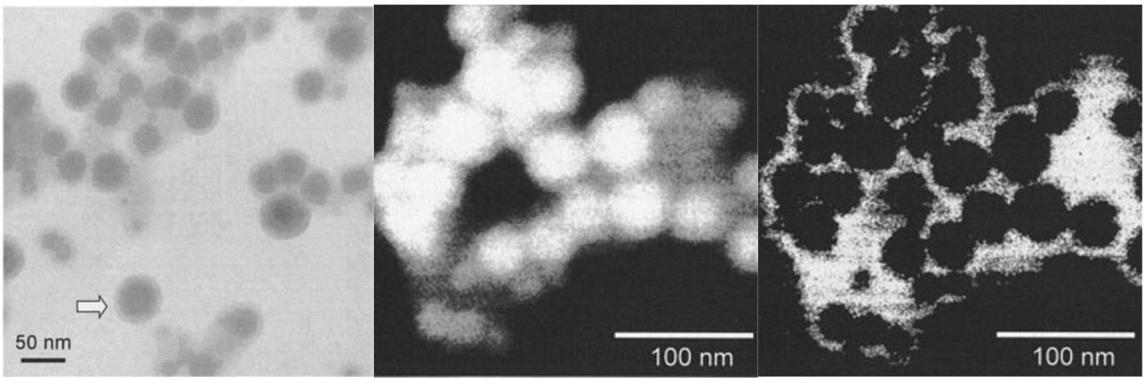

Figure 3-2. Composite silica/acrylics particles. Left and middle: TEM images; right: carbon map. Reprinted. [3]

The objective of this chapter is to encapsulate silica nanoparticles (avg. diam. 22 nm) with first PBA then PMMA to form silica/PBA/PMMA core-shell multilayer composite particles. As reviewed in Chapter 1, nanoparticles at this size scale are extremely hard to be encapsulated individually. They prefer to stay at interfaces and form raspberry-like structures. Mizutani et al. [3] has performed research relevant to the goal in this work. They used an acrylic monomer mixture to encapsulate silica nanoparticles of 20 ~ 30 nm diameter via emulsion polymerization. A core-shell morphology was somewhat observed from TEM images in Figure 3-2. Image on the right is a carbon map image, in which white areas indicate carbon-based polymer phase. However, as would be revealed later in this chapter, these images could be derived from latex consisting of polymer with a glass transition temperature (T_g) lower than room temperature and un-encapsulated silica nanoparticles. With a simple calculation using Fox equation (1), copolymer in Mizutani's work did have a low T_g around -14 °C.

$$\frac{1}{T_g} = \frac{w_1}{T_{g,1}} + \frac{w_2}{T_{g,2}} \quad (1)$$

3.2. Experimental

3.2.1. Materials

Colloidal silica dispersions Ludox TM-40 (ca. 22 nm diam.) and HS-40 (ca. 12 nm diam.) were purchased from Sigma-Aldrich. 3-methacryloxypropyl trimethoxysilane (MPTMS, Gelest) was used for silica treatment (see Figure 3-3 for molecular structure) . Surfactants used include octyl phenol ethoxylate (Triton X-100, Sigma-Aldrich), nonylphenol ethoxylate (ca. 7) (Tergitol NP-7, Sigma-Aldrich), polyethylene glycol (ca. 23) dodecyl ether (Brij-35, Alfar-Aesar), sodium dodecyl sulfate (SDS, electrophoresis grade, Kodak) and sodium dodecylbenzenesulfonate (SDBS, TGI). Anionic initiator potassium persulfate (KPS), cationic initiator 2,2-azobis(2-methylpropionamidine) (AIBA) and sodium bicarbonate were from Sigma-Aldrich. Monomers *n*-butyl methacrylate (BA), methyl methacrylate (MMA) and methacrylic acid (MAA), divinylbenzene (DVB) were from Acros and used as received. Phosphotungstic acid (PTA) from Fisher was used as a negative staining agent to prepare latex particles for TEM imaging.

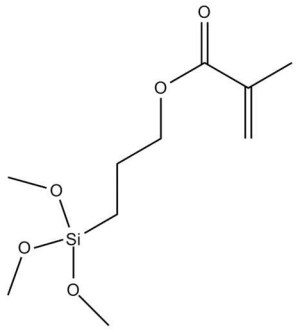

Figure 3-3. Molecular structure of MPTMS.

3.2.2. Polymerization Procedure and Characterization Techniques

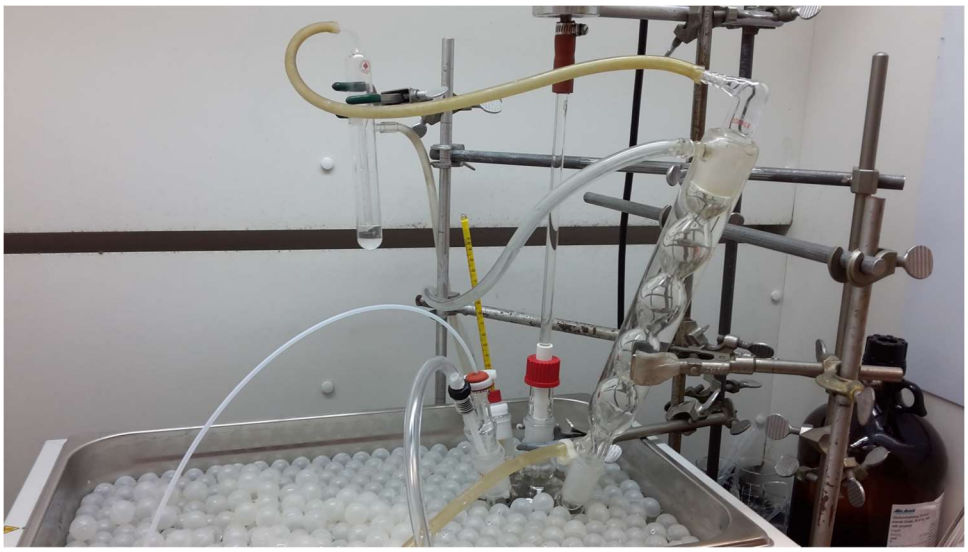

Figure 3-4. Setup for semi-batch emulsion polymerization.

Emulsion polymerization was carried out in batch and semi-batch processes in a setup shown in Figure 3-4. A four-necked glass reactor equipped with a reflux condenser, a half-moon shaped PTFE stirrer, a thermometer and nitrogen purge inlet with monomer feed inlet was used to carry out polymerization. Syringe pump (Harvard Apparatus) was used to feed monomer into reactor at set speeds. Fisher Automatic Tensiometer (6 cm Pt-Ir ring) was used to measure surface tension of latexes and aqueous solutions at 23±0.5°C. Dynamic light scattering (DLS, ALV-CGS) was used to measure latex particle size and size distribution. Transmission electron microscope (TEM, JEOL JEM-1200EX) was used to image dried latex particles for sizing purpose and morphology observation.

3.3. Results and Discussion

3.3.1. Toward Successful Encapsulation of Silica Nanoparticles

Encapsulation of inorganic nanoparticles or synthesis of hybrid nanoparticle/polymer nanocomposite particles were reported in several papers. [4-6] However, near one-to-one core-shell encapsulation of inorganic nanoparticles at a scale of 20 nm via emulsion polymerization and resulting inorganic core-polymer shell morphology were not achieved and evident in literature. Toward this goal, a journey of experimenting and re-searching was unfolded. At the beginning, nonionic surfactants were chosen as means of surface treatment of silica nanoparticles because of its simplicity and compatibility with emulsion polymerization process. [7] Polar hydroxyl group of nonionic surfactant molecule prefers to adsorb onto silica nanoparticle surface by forming hydrogen bond and thus hydrophobize the silica surface. Hydrophobized silica nanoparticles are stabilized by surfactants in aqueous phase for being encapsulated by polymers during emulsion polymerization. Table 3-1 is a recipe of two-stage emulsion polymerization. First stage is to coat silica nanoparticle with PBA and second stage is to further form an outer shell of PMMA on existing particles. Nonionic surfactant Triton X-100 was used to treat silica nanoparticle surfaces.

Table 3-1. Initial two-stage emulsion polymerization process.

	Ingredient	Amount/g	Procedure
Silica core	Ludox TM-40	1.99	Premix and pour into reactor. Stirring at 150 rpm under nitrogen purge.
1st stage PBA layer synthesis	Water	150.07	
	Triton X-100	0.33	
	$NaHCO_3$	0.1028	
	BA	10	
	KPS	0.1212	Add at 70 °C. React for 4 hrs
	Water	5.02	
2nd stage PMMA layer synthesis	Water	10	Premix and pour into reactor containing above latex
	SDS	0.1976	
	$NaHCO_3$	0.1172	
	MMA	20	
	KPS	0.3448	Add at 70 °C. React for 4 hrs
	Water	10.3	

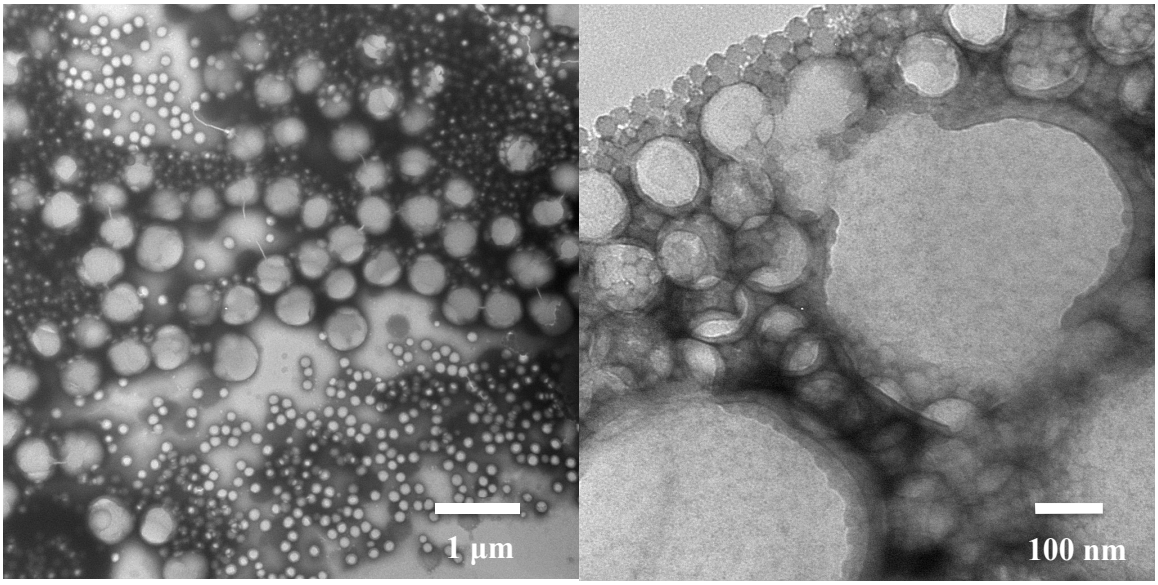

Figure 3-5. Latex prepared according to recipes in Table 3-1 (stained w. PTA).

Figure 3-5 is TEM image of latex particles synthesized according to recipe listed in Table 3-1. With the contrast between polymer and background created by negative staining agent PTA, bimodal latex particle size distribution and silica nanoparticles (avg. 22 nm diameter) not encapsulated are clearly seen throughout the imaged area. Two

distinct latex particle sizes are observed as ~100 nm and ~500 nm diameter. Bridging is clearly seen between some of large particles. Since PBA and PMMA do not exhibit an image contrast under TEM, based on experiences of author on PBA and PMMA latex synthesis, ~100 nm latex particles are most possibly PMMA particles generated in second stage of polymerization while ~500 nm latex particles are PBA/PMMA core-shell particles. To prove the assumption, that bimodal latex particles were formed because of two-stage polymerization process, a monomer combination of 130 g BA, 69 g MMA and 1 g methacrylic acid (MAA) was used in one-stage polymerization to encapsulate silica nanoparticles. (Table 3-2) This monomer combination and recipe was derived from a paper on encapsulating silica nanoparticles. [3] A method was claimed effective for encapsulation of 20 -30 nm diameter silica nanoparticles: use a nonionic surfactant to treat silica nanoparticles for encapsulation during emulsion polymerization at temperature above cloud point of the nonionic surfactant. Above cloud point, hydrophilic end of nonionic surfactant molecule loses its water affinity and tends to form hydrogen bond with surface silanols when pH < 7. In this way silica nanoparticles are rendered hydrophobicity and stabilized by surfactants in aqueous phase. This treatment route was experimented extensively in this work. Tergitol NP-7 was chosen to treat silica nanoparticles because it is a nonionic surfactant with a low cloud point (20 °C).

Table 3-2. One-stage polymerization process with a monomer mixture.

Layer	Ingredient	Amount/g	Procedure
Silica core	Ludox TM-40	425	Mix Tergitol, KPS and water. Drop in at 60°C. Raise to 70 °C
One-stage synthesis of BA-MMA-MAA shell	Water	55	
	Tergitol NP-7	3.41	
	KPS	0.592	
	1st stage monomer	5	Drop in and react for 1 h
	SDBS	6	Mix and drop into reactor
	KPS	0.711	
	Water	50	
	2nd stage monomer	195 g	Drop in and react for 12 h

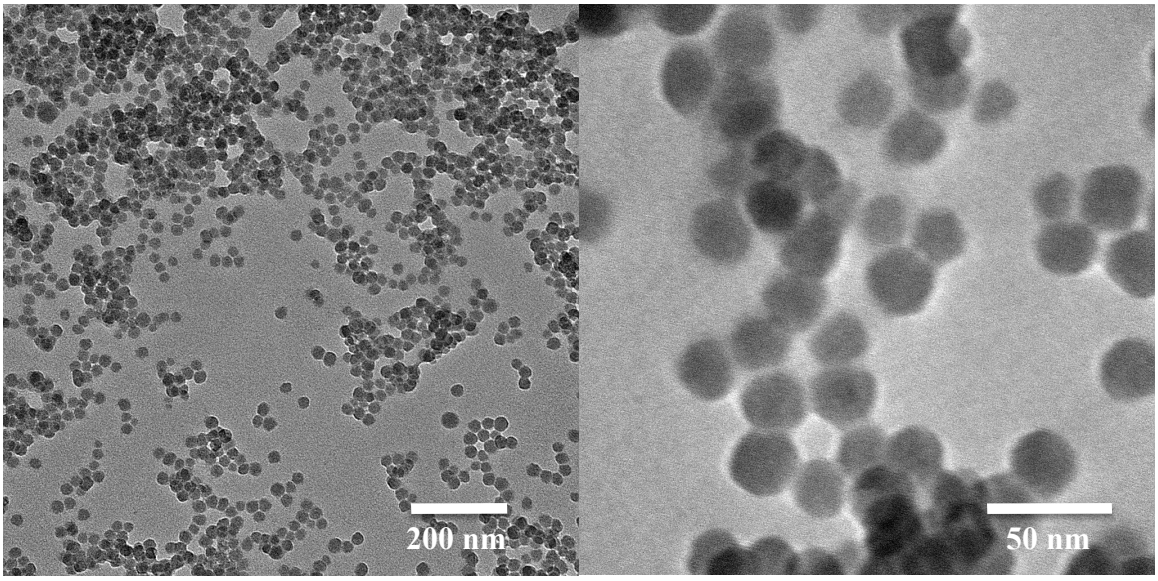

Figure 3-6. Unstained silica-BA-MMA-MAA latex prepared based on Table 3-2.

Figure 3-6 contains TEM images of latex synthesized from BA-MMA-MAA monomer mixture in the presence of silica nanoparticles. Imaged sample was diluted latex without any staining agent. Latex particles were not showing without contrast to the background. But the hazy outlines of dark silica particles and honeycomb-shaped

junctions among silica particles indicate polymer around them. Compared with the paper [3], in which TEM images were taken from samples without staining agent, it is not convincing that a real core-shell morphology was obtained either in the paper or in Figure 3-6.

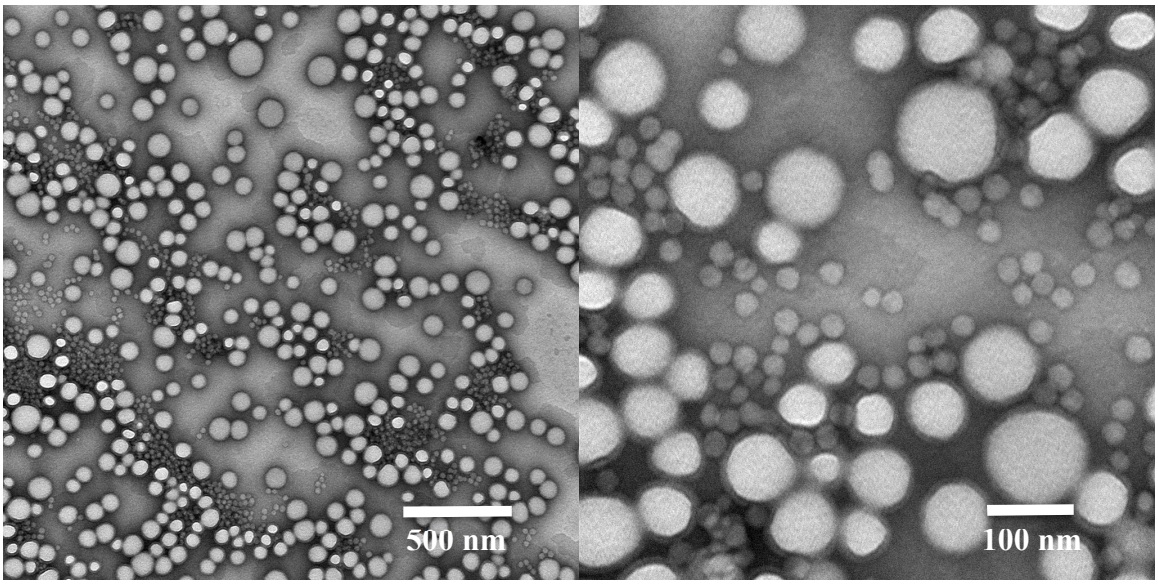

Figure 3-7. Stained silica-BA-MMA-MAA latex prepared based on Table 3-2.

Figure 3-7 contains TEM images from same sample as in Figure 3-6 but with a negative staining agent PTA. Like the conclusion drawn from Figure 3-6, silica nanoparticles were obviously not encapsulated by the copolymer. 50 – 100 nm latex particles were present without a bimodal distribution as in Figure 3-5, which proved the point that bimodal latex particles in Figure 3-5 were generated because of two-stage seeded polymerization process.

From results of above-mentions experiments, one phenomenon was observed as an indicator of unsuccessful encapsulation of silica nanoparticles. A ring of silica aggregates will appear on the inside wall of reactor at interface between latex mixture and

air. Formation mechanism is possibly surface coagulation. [8] If silica nanoparticles are encapsulated by polymer, this phenomenon should be minimized based on our understanding of latex systems. This served as a criterion for judging whether successful encapsulation was achieved because of its convenience over TEM imaging for every batch of synthesized latex.

A series of emulsion polymerization of only BA monomer in the presence of silica were conducted targeting encapsulation of silica nanoparticles. Monomer amount, initiator concentration, anionic surfactant type and concentration were systematically varied based on recipe listed in Table 3-3.

Table 3-3. Silica/PBA latex synthesis procedure based on Mizutani [3]

Layer	Ingredient	Amount/g	Procedure
Silica core	Ludox TM-40	85	Mix Tergitol, KPS and water. Drop in at 60°C. Raise to 70 °C
PBA layer synthesis	Water	28	
	Tergitol NP-7	1	
	KPS	0.12	
	1st stage BA	1	Drop in and react for 1 h
	SDBS	1.2	Mix and drop into reactor
	KPS	0.144	
	Water	10	
	2nd stage BA	19 g	Drop in and react for 4 h

Among these batches of latexes, one of them did not generate a ring of silica aggregates on the wall of reactor inside, which indicated possible encapsulation. Variations of recipe for this sample included: KPS amount was increased to 0.3 g; 2nd stage BA and water amount were doubled and 0.6 g divinylbenzene (DVB) was mixed with 2nd stage BA and dropped in for synthesizing crosslinked PBA. Resultant latex was

diluted as seed for PMMA shell synthesis. Recipe of seeded polymerization is listed in Table 3-4.

Table 3-4. PMMA layer synthesis using silica/PBA latex as seeds.

Layer	**Ingredient**	**Amount/g**	**Procedure**
Seed	Silica/PBA	44	Mix and raise to 70 °C
PMMA layer synthesis	Water	88	
	KPS	0.12	
	Water	15	
	MMA	15	Drop in and react for 5 h

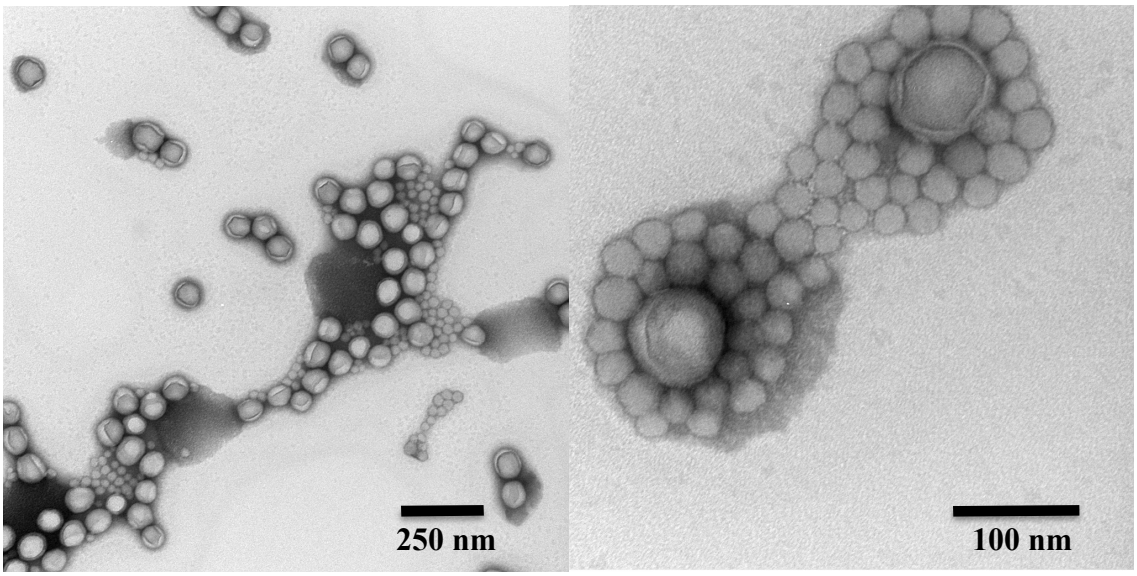

Figure 3-8. Latex prepared based on recipe in Table 3-4 (stained w. PTA).

Figure 3-8 is TEM images of resultant latex according to recipe listed in Table 3-4. Latex particles in the picture have a single modal size distribution even if the sample was synthesized in a two-stage emulsion polymerization process. Bimodal size distribution as in Figure 3-5 was successfully avoided. Reason for this was incomplete encapsulation of PBA particles by PMMA, which was observed for most of particles. Silica nanoparticles

were not encapsulated. But in the close-up image tiny latex particles around silica nanoparticles were observed. Affinity of these tiny polymer particles to silica nanoparticles might be the result of hydrophobized silica surface due to treatment by nonionic surfactant. Silica nanoparticles with polymer aggregates on their surface behave like latex particles [9] and do not easily aggregate upon surface coagulation. This might be the reason why this batch of latex did not show a silica ring of aggregates inside reactor.

From above experimental results, several thoughts emerged. Although it is very difficult to use BA alone for encapsulating silica or other inorganic nanoparticles because of its much lower water solubility than MMA, which is more commonly used for encapsulating inorganic nanoparticles [10], experiments were carried out in order to find ways to increase affinity of PBA polymer chains or tiny PBA particles to silica nanoparticles. Surface-initiated nitroxide-mediated polymerization (SI-NMP) is based on reversible activation and deactivation of growing polymer chains by a nitroxide radical. [11] This method can generate polymer brushes growing from particle surface and forming an encapsulating layer. But these NMP initiators are too expensive for general purposes. Use of a cationic initiator AIBA was reported to bring small PMMA particles and silica particles together by initiation of polymerization at silica surfaces. [12] Cationic group of this initiator forms ionic bond with surface silanol under basic pH. In this paper and similar studies larger size silica nanoparticles (> 60 nm diameter) were commonly used and that is very different from the system in this work (~ 20 nm diameter silica). Besides, PBA was not used in these studies as a coating polymer due to formerly mentioned reason. But “grow from” silica nanoparticles might be an interesting route to

experiment with. This new route involved treatment of silica by nonionic surfactant polyethylene glycol dodecyl ether (Brij-35) and MPTMS together and use of a cationic initiator AIBA. Treatment of silica nanoparticles was largely similar to steps used in Bourgeat-Lami's work. [13] Treatment of silica particles with silane to render surface hydrophobicity is a common act for silica encapsulation purposes. [13-16] After silica treatment, a large portion (around 4/5) of silane molecules remains unattached to silica surfaces and needs to be removed. In these studies larger silica particles were used (> 60 nm diameter). Larger silica particles will have more silane molecules attached on surfaces due to large surface area thus treated silica is easily centrifuged and re-dispersed to remove excess silane molecules. [13, 16, 17] For silica nanoparticles as small as 20 nm, this method is not viable because: fewer silane molecules attached to silica surface; sedimentation by centrifugation is very hard to achieve in aqueous phase; even if sedimentation happens, it is impossible to re-disperse silica nanoparticles completely afterwards. [18] Thus here instead of centrifugation, dialysis was used for removing unattached silane molecules with a dialysis tube of high cutoff molecular weight (MWCO=12,000). By controlling concentrations of free AIBA and free micelle-forming surfactants, free polymer particles might be avoided.

Table 3-5. Silica/PBA latex synthesis procedure with use of a cationic initiator

Layer	**Ingredient**	**Amount /g**	**Procedure**
Treatment of silica nanoparticles	Ludox	2.57	Dissolve surfactant, adjust pH to 9.8 before adding Ludox. Dropwise add silane+ethanol solution and mix for two days. Then dialyze against water for two days
	Brij-35	1.67 g	
	Water	197.5	
	MPTMS	0.17 g in 10 g ethanol	
PBA layer synthesis	Initiator AIBA	0.0228 g AIBA in 5.8 g water	Adjust pH to 9.8
	BA	6	Feed rate: 2 mL/h

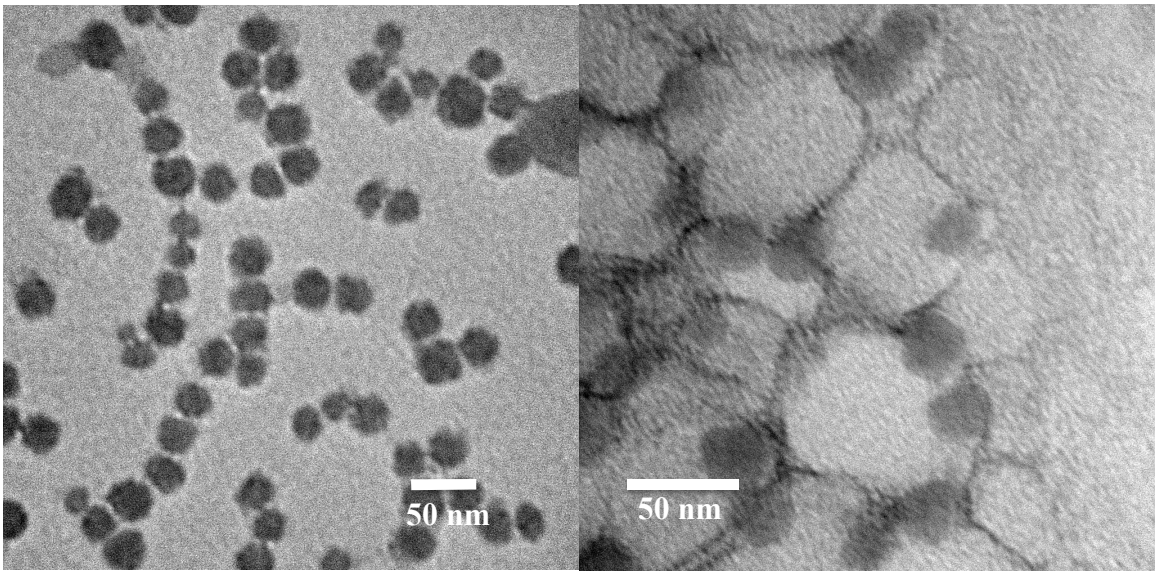

Figure 3-9. Latex prepared based on Table 3-5. Left: before staining; right: after staining.

Figure 3-9 is TEM images of latex synthesized according to Table 5. The image on left side is without negative staining agent PTA. Unlike the case in the article on synthesis of silica/PMMA nanocomposite particles using a cationic initiator [12], raspberry-like morphology with small polymer particles surrounding silica particle did not show in Figure 3-9, mainly because of much smaller size of silica nanoparticles used in our work. A strung-beads-like morphology of silica nanoparticles was found in the

image. Explanation of this phenomenon could be combination of surface-anchored cationic radicals. Cationic group of the initiator AIBA forms ionic bond with deprotonated silanol thus gets anchored on silica nanoparticle surface. After AIBA decomposes and generates radicals, once in touch during particle collision, surface-anchored radicals might combine and link silica nanoparticles together. In image on the right side, boundaries of PBA particles are seen and silica nanoparticles mostly reside on these boundaries. This could be also caused by radical combination between silica nanoparticles and growing chain ends on surface of polymer particles. Both images in Figure 3-9 indicate formation of silica aggregates and raspberry-like PBA core – silica shell morphology rather than silica encapsulated by PBA.

3.3.2. Synthesis of Silica/PBA/PMMA Multilayer Latex Particles Containing Single Silica Nanoparticle Cores

3.3.2.1. Rationale

Since it is not helping with silica encapsulation by using a cationic initiator for generating surface-anchored radicals, cationic initiator was dropped out of consideration. A water-soluble anionic initiator KPS should be continued for use. It is also clear that even if silica nanoparticle are treated with silane (MPTMS), the following attempts have not been successful in the literature and in this work so far:

The challenge is to encapsulate silica nanoparticles of ~20 nm diameter with a relatively hydrophobic monomer BA and avoid raspberry-like structure caused by partially hydrophobized silica surface—this is always the case when this treatment method is applied. The second challenge is to achieve a one-to-one silica encapsulation

with minimized multi-core particles or secondary polymer particles (polymer particles without any silica nanoparticles in them).

From previous experiences of unsuccessful encapsulation, several thoughts and ideas emerged as following:

(1) Silica nanoparticles (~20 nm) were rendered limited hydrophobicity after treatments, due to their tiny sizes.

(2) Partially hydrophobized silica nanoparticles had little affinity to the relatively hydrophobic monomer BA and its polymer PBA.

(3) Low affinity of treated silica nanoparticles to BA and PBA rendered separated silica nanoparticles and PBA particles, or raspberry-like structure with silica nanoparticles surrounding PBA particle.

(4) To ensure silica nanoparticles are the ONLY loci where growing PBA chains go to, surfactant micelles and monomer droplets should be absent in the latex system AT ALL TIMES. Above critical micelle concentration (CMC), surfactant molecules form micelles. Monomer-swelled micelles then become the main loci for radical polymerization in an emulsion. Monomer droplets can accommodate growing chains and particles thus form secondary polymer particles without silica nanoparticles. Thus surfactant concentration should be well controlled below CMC throughout polymerization process and monomer droplets should be eliminated by keeping monomer feed rate at an extremely low value to ensure monomer concentration is lower than its solubility limit in water. (Table 3-6)

(5) In emulsion polymerization, particle size decreases when surfactant concentration increases but within a limit. Likewise, particle number has an upper limit too. Actively growing particles cannot be as many as surfactant concentration allows. Typical particle number in emulsion polymerization is around 10^{18}/L scale. Looking back to previous literature and experiments, a proper silica number was not used. A proper silica number combined with controlled surfactant and monomer concentration might be the key to successful encapsulation of silica nanoparticles.

Table 3-6. Properties of BA and MMA

Monomer	Monomer density, g/cm^3	Polymer density, g/cm^3	Polymer T_g, °C	Monomer solubility in water, wt.% (20 °C)
BA	0.89	1.09	-54	0.2
MMA	0.94	1.20	120	1.5

3.3.2.2. Technique for Synthesis of Silica/PBA/PMMA Multilayer Latex Particles

A new set of experiments was designed. Amount of silica nanoparticles was chosen to match typical particle number in emulsion polymerization. Silica treatment and dialysis are the same as in Table 3-5. Dialysis removes unattached silane and excess surfactants until surfactant concentration is well below CMC. Monomer BA and MMA feed rates were chosen to be 2 and 4 mL/h in order to ensure no monomer droplets were present during polymerization. In this way, since monomers are completely dissolved in water, this process resembles dispersion polymerization.

Table 3-7. Developed process for silica/PBA/PMMA multilayer particle synthesis

Layer	Ingredients	Weight /g	Comment
Silica treatment and dialysis	Silica (Ludox TM-40)	5	Dissolve surfactant in water; adjust pH to 9.3 before adding silica. Add silane+ethanol solution dropwise and mix for 19 h. Then dialyze against DI water for 24 h.
	Surfactant (SDS)	0.4 g	
	Water	195	
	Silane (MPTMS)	0.6 g in 10 g ethanol	
PBA layer synthesis	Initiator (KPS)	0.1 g in 10 g water	Add in one dose before BA addition.
	BA	7.2 g	Feed rate = 2 mL/h
PMMA layer synthesis	Seed PBA latex	100 g	Latex after PBA layer synthesis
	Water	195.5 g	Premix and gradually add to seed PBA latex.
	SDS	Varies	
	Initiator (KPS)	0.1 g in 10 g water	Add in one dose before BA addition.
	MMA	8.4 g	Feed rate = 4 mL/h

Figure 3-10. Bottles containing PBA latexes without (left) and with (right) silica nanoparticles

Latexes in Figure 3-10 were prepared with same ingredients and via same process except one difference: image on the left in Figure 3-10 is latex prepared without treated silica nanoparticles. Judging from the latex appearance, latex in the left image with an opaque whitish color has a significantly larger particle size and broader size distribution than the right image, translucent bluish latex indicating much smaller particle size and

near-monodisperse size distribution. This distinct difference suggested treated silica nanoparticles actively interacted with polymerization process and affected particle nucleation and growth stages thus finally altered particle size and distribution. Dynamic light scattering (DLS) results suggested that latex in the left image had an average particle radius of 61 nm while latex in the right image of 32 nm. The average radius of silica nanoparticles in use was 11 nm. Calculated theoretical particle radius of silica/PBA core-shell particle is 21 nm assuming perfect one-to-one encapsulation of silica nanoparticles was achieved. (Footnote in Table 3-8) These results indicated latex in the right image should be close to encapsulation desired. This was proved by further TEM imaging analysis in Figure 3-11.

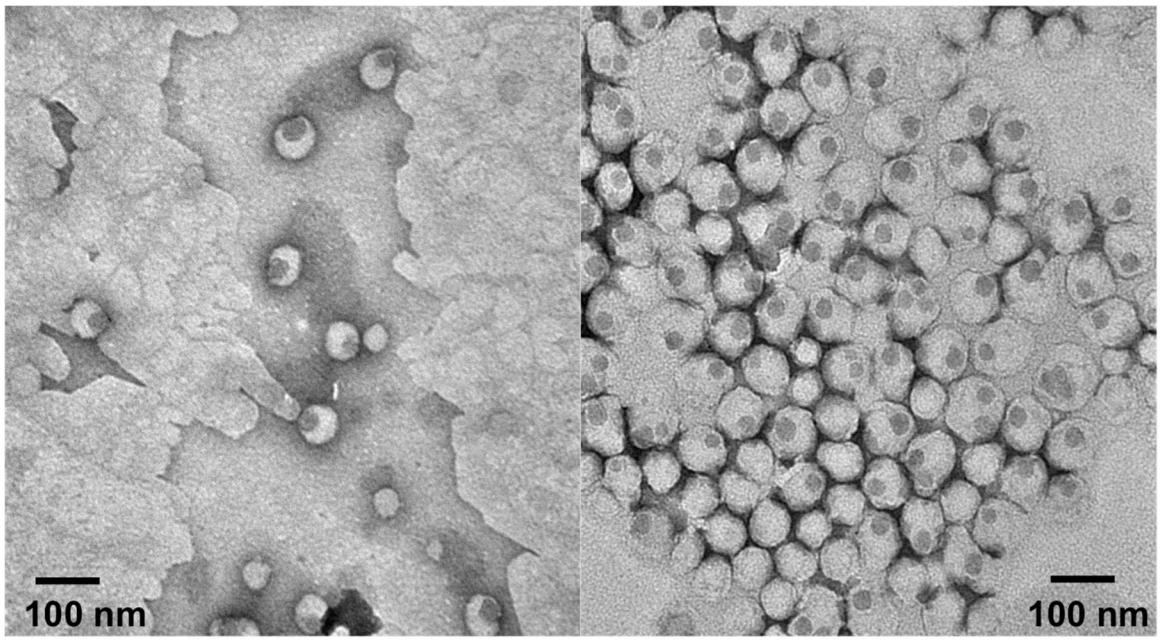

Figure 3-11. Latex particles with encapsulated silica nanoparticles. Left: Silica/PBA; right: silica/PBA/PMMA (both were stained w. PTA).

Left image in Figure 3-11 is latex obtained after PBA layer synthesis according to Table 3-7. Latex sample was negatively stained with PTA to protect PBA particles. Imaging revealed most of silica nanoparticles were coated with PBA layer. Right image in Figure 3-11 is latex obtained after PMMA layer synthesis on top of PBA layer. Two images are at the same length scale. It is obvious that particle size is larger in the right image and most latex particles contain single silica cores. Theoretically average particle radius in the right image should be 10 nm more than that in the left image and this is actually the case confirmed by both DLS and TEM. Thus these results indicate successful encapsulation of silica nanoparticles (22 nm diam.) with two layers of polymers.

Table 3-8 is repeatability of this developed technique (described in Table 3-7) for encapsulating silica nanoparticles. Two batches of latexes were prepared separately following the same recipe and procedures. Comparison between latex particle size and size distribution measured with DLS of 1L (one layer of PBA) and 2L (one layer of PBA and another layer of PMMA) latexes showed highly repeatable results.

Table 3-8. Repeatability of developed synthesis process described in Table 3-7

Name	Theoretical radius* /nm	Theoretical thickness of PMMA layer /nm	Radius (DLS) /nm	Deviation /nm	2nd order PDI**
Batch 1: 1L	20.2	-	32	±5	0.0894
Batch 1: 2L	31.0	10.8	42	±5	0.0406
Batch 2: 1L	19.8	-	32	±5	0.0939
Batch 2: 2L	29.7	9.9	43	±5	0.0433

*Theoretical radius—calculation assumptions: all latex particles are single-core and total particle number remains the same throughout the synthesis process as total number of silica nanoparticles; all monomer converts to coating polymer.

** Second-order polydisersity index is generated automatically from DLS data analysis with cumulant method [19]; a PDI close to 0 means close to monodisperse size distribution.

3.3.2.3. Effect of Process Parameters on Multilayer Particle Morphology

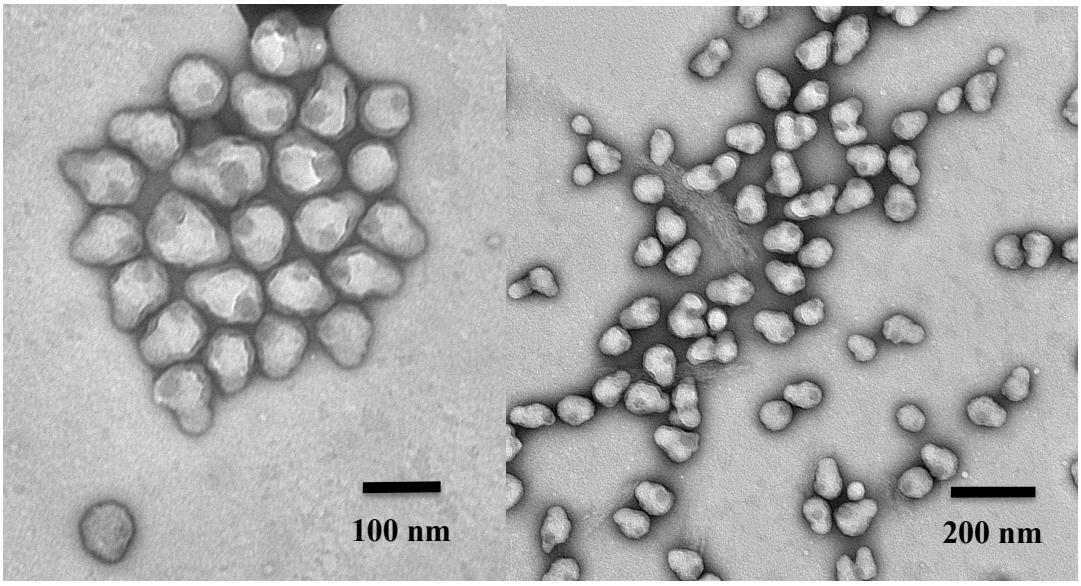

Figure 3-12. Silica/PBA/PMMA particles prepared without a dialysis step (stained w. PTA).

Using dialysis to remove silane molecules unattached to silica particle surfaces was an innovative method. In previous work in literature, centrifugation and re-dispersion were commonly used for larger silica nanoparticles while this is not viable for smaller silica nanoparticles. Effect and necessity of this dialysis step was investigated. Figure 3-12 is silica/PBA/PMMA latex prepared according to Table 3-7 but without dialysis step after silica treatment. Clearly encapsulation of silica nanoparticles was achieved but particle shape became irregular as if two or more particles stick together. This phenomenon has similarity to what was observed in Figure 3-9 when cationic initiator was used. Given that silane used here was MPTMS with a polymerizable site to be able to convert to a radical, unattached silane molecules might actively participate into

radical polymerization and cause particles to either grow non-uniformly or aggregate to tiny clusters.

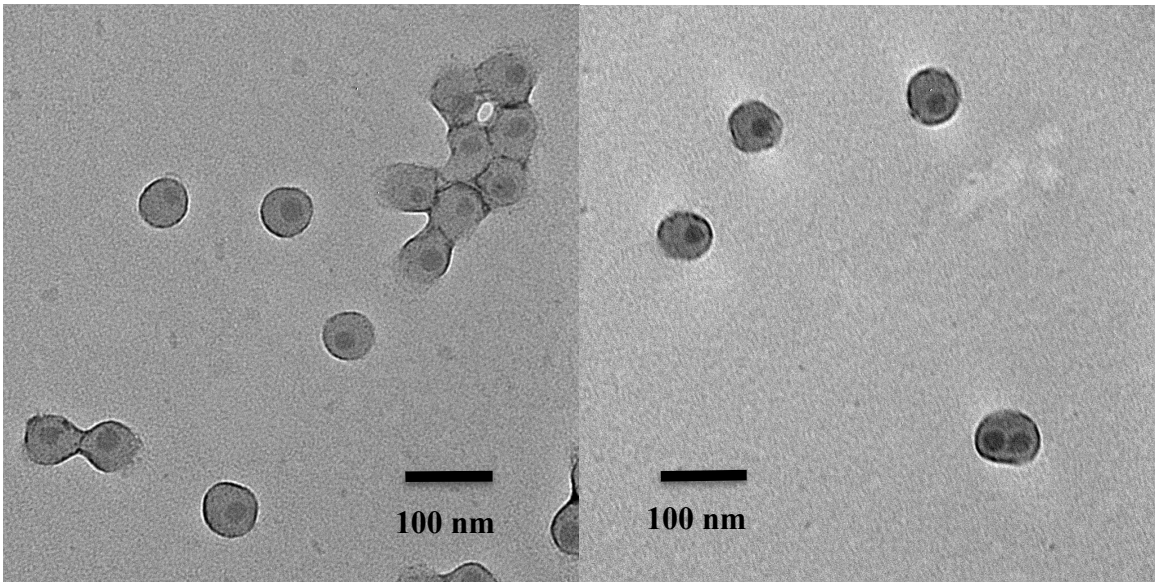

Figure 3-13. Silica/PBA/PMMA particles prepared with a dialysis step (stained w. PTA).

Latex in Figure 3-13 was prepared via the same process as latex in Figure 3-12 but with dialysis step after silica treatment. More spherical particle shape and more centered position of silica nanoparticles inside composite particles were observed. This proved necessity and effect of dialysis step for removing unattached silane molecules in aqueous phase.

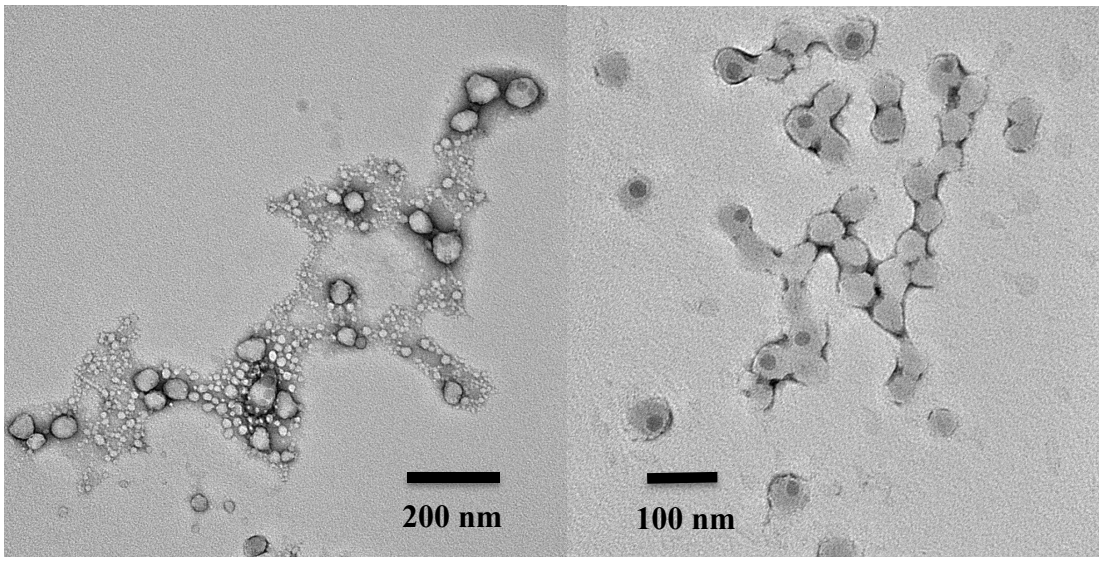

Figure 3-14. Silica/PBA/PMMA particles prepared at different MMA feed rates. Left: 12 mL/h; right: 4 mL/h (both were stained w. PTA)

In semi-batch polymerization process in Table 3-7, monomer feed rate is a critical factor contributing to successful encapsulation of silica nanoparticles. Feed rate of 2 mL/h for BA and 4 mL/h for MMA were chosen based on solubility of these two monomers in order to ensure that no monomer droplets are present any time during polymerization. Figure 3-14 is a comparison between latexes prepared at fast and slow MMA feed rates. In the left image, MMA feed rate was three times of that in right image. A bimodal particle size distribution was observed. Some of larger particles (50-80 nm) had silica nanoparticle cores inside of them. Besides, 10-20 nm unwanted free polymer particles are present. Compared with latex prepared at low MMA feed rate, these tiny particles might be the result of fast MMA feed rate, which promoted pure PMMA particle nucleation and growth. Contrary to this, under monomer-starved condition, the probability of seed particles (silica/PBA core-shell particles) to serve as main loci for MMA polymerization was higher.

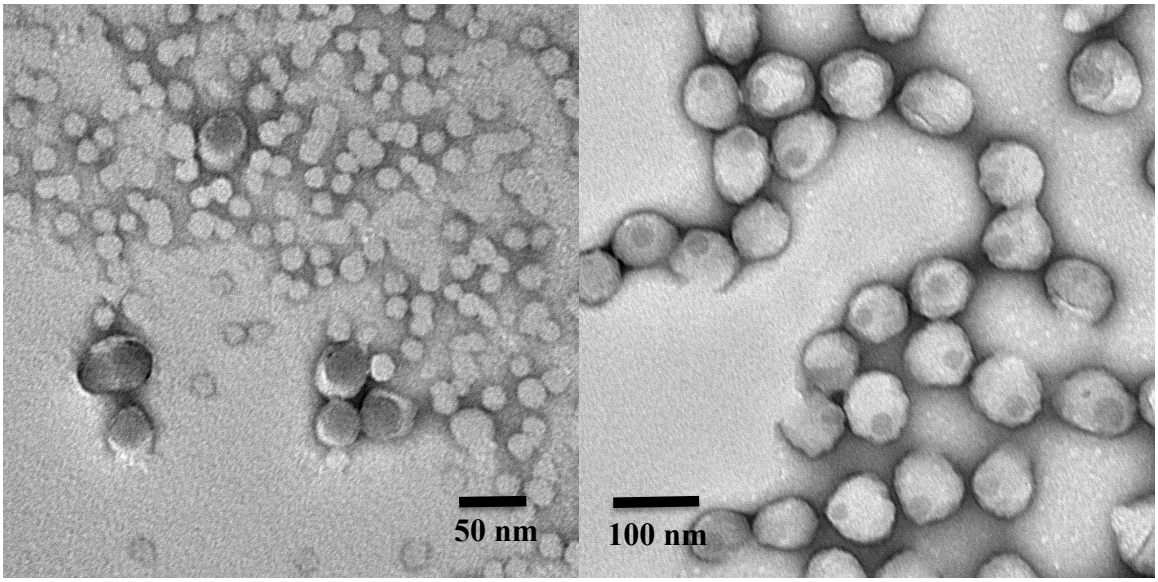

Figure 3-15. Silica/PBA/PMMA multilayer particles prepared at different surfactant concentration during PBA layer synthesis. Left: above CMC. Right: below CMC

Surfactant concentration plays an equally important role in encapsulating silica nanoparticles as monomer feed rate discussed before. Left image in Figure 3-15 is latex prepared according to Table 3-7 but at a surfactant concentration above CMC during PBA layer synthesis step. Few silica nanoparticles were encapsulated by a thin layer of polymer and most of polymers formed single modal sized particles of ~10 nm diameter. Right image is latex prepared at a surfactant concentration below CMC and in a specific range. Silica nanoparticles are encapsulated and no free polymer particles present. Reason for this difference is, when surfactant concentration is above CMC during polymerization process, large amount of surfactant micelles were generated and became the main loci for polymer particle nucleation and growth rather than desired silica nanoparticles being seeds for seeded polymerization. Surfactant concentration must be carefully controlled both in PBA and PMMA layer synthesis. On one hand, for PBA layer

synthesis, surfactant concentration is controlled during dialysis process because surfactant can be continuously removed during dialysis until a desired concentration is reached. On the other hand, too long a dialysis time can remove too much surfactant concentration thus destabilize the silica colloidal dispersion. Surfactant concentration has to be well controlled during PMMA layer synthesis too.

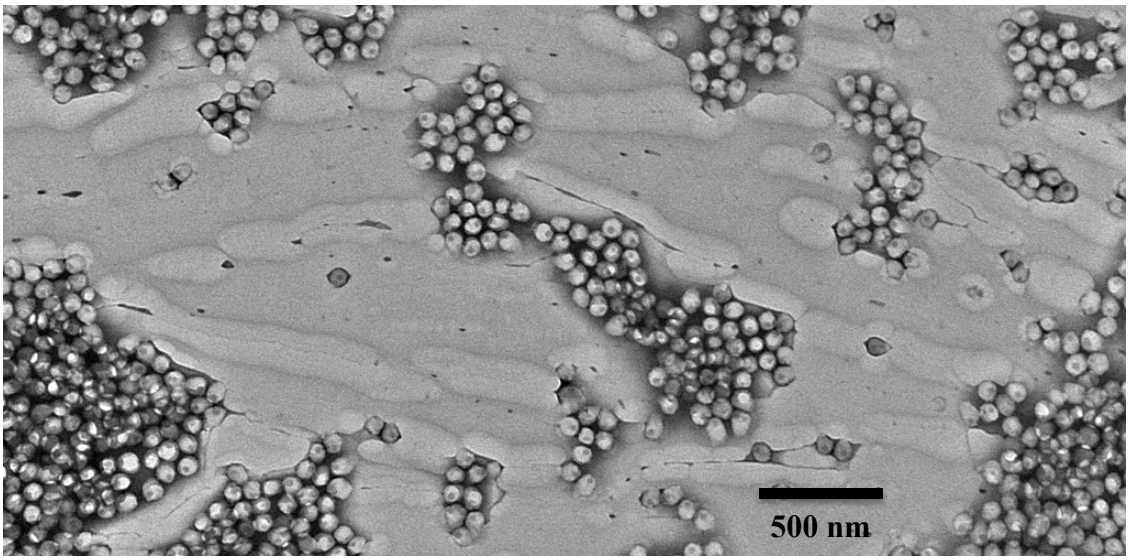

Figure 3-16. Silica/PBA/PMMA multilayer particles (stained w. PTA).

After a series of parameter optimization, a practically one-to-one and centered encapsulation of silica nanoparticles by two layers of polymers was achieved with minimized multi-core particles and free polymer particles (Figure 3-16). By eliminating multi-core particles and free polymer particles, the average particle size approached calculated theoretical particle size of perfect core-shell composite particles, with a difference of only ~7 nm between these two as listed in Table 3-9.

Table 3-9. Silica/PBA/PMMA multilayer particles with least free polymer and multicore particles

Sample	R(DLS) /nm	Deviation /nm	PDI	Theoretical R /nm	R(DLS)-R(Theor.)
1L	35	±3	0.0221	28	7
2L	45	±5	0.0493	38	7

3.3.2.4. Encapsulation of 12 nm Silica Nanoparticles Using Developed Technique

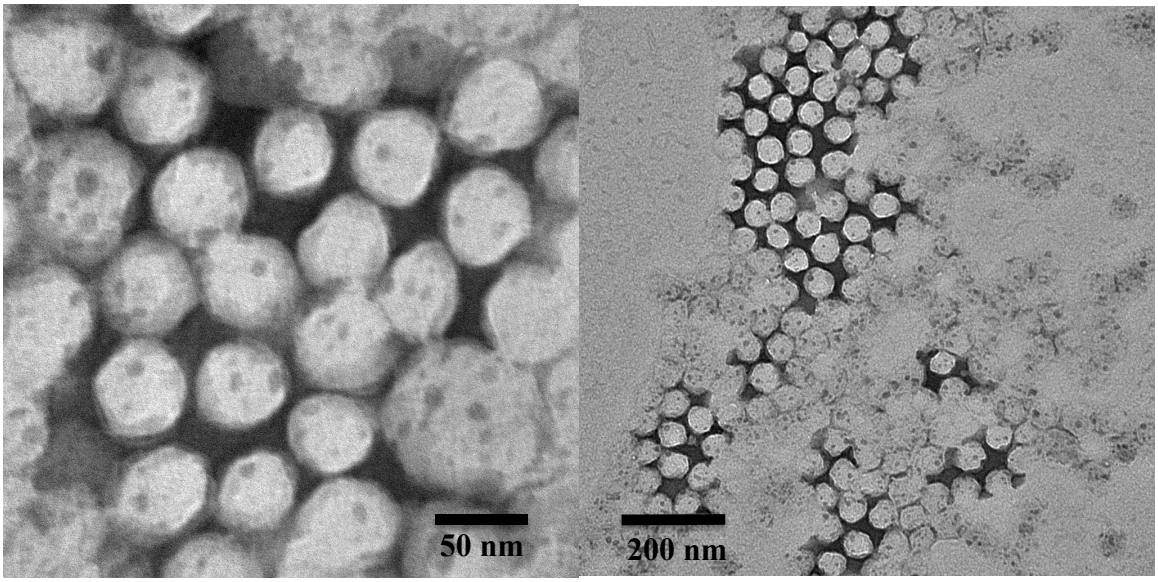

Figure 3-17. Silica/PBA/PMMA particles prepared with 12 nm silica nanoparticles (stained w. PTA)

Out of scientific curiosity, this developed technique for encapsulating silica nanoparticles was applied to even smaller sized silica—Ludox HS-40 colloidal silica nanoparticles of an average particle diameter of 12 nm. Recipe in Table 3-7 was adjusted proportionally according to larger surface area of smaller particle size. Figure 3-17 gives the images of resulted latexes. Clearly even for nanoparticles of such a small diameter, raspberry-like structure with silica particles surrounding a polymer core was successfully avoided with this technique. Several silica nanoparticles were encapsulated together into

one composite particle. Composite particle diameter ranged from around 60 to 80 nm similar to previous results, which resulted from a same combination of ingredients and process parameters like surfactant concentration, monomer feed rate and total amount of monomers, etc.

3.4. Summary and Conclusions

A novel synthesis technique of emulsion polymerization was developed and invented for encapsulating silica nanoparticles (avg. diam. 22 nm) with PBA and PMMA and synthesizing silica/PBA/PMMA multilayer core-shell composite particles with single silica cores (avg. diam. ~80 nm). This synthesis process is robust and highly repeatable. It can be utilized to encapsulate even smaller silica nanoparticles (avg. diam. 12 nm). To achieve a one-to-one encapsulation without either multi-core particles or free polymer particles without silica cores, several steps and parameters are essential to ensure silica nanoparticles are the main loci for polymer deposition during emulsion polymerization. We proved and demonstrated the necessity and effect of these factors, including silica surface treatment, dialysis after treatment, process type of emulsion polymerization, surfactant concentration and monomer feed rate. After optimization of these factors, a practically one-to-one encapsulation was achieved. Resulted particle size approximated theoretical particle size calculated based on perfect one-to-one encapsulation. Synthesized inorganic-organic multilayer composite particles would be utilized as toughening agents for diglycidyl ether of bisphenol A (DGEBA) in Chapter 4.

3.5. References

[1] J. Gao, J. Li, S. Zhao, B. C. Benicewicz, H. Hillborg and L. S. Schadler. Polymer, 54 (2013), 3961.

[2] C. Z. Li, J. W. Han, C. Y. Ryu, B. C. Benicewicz. Macromolecules, 39 (2006), 3175.

[3] T. Mizutani, K. Arai, M. Miyamoto, Y. Kimura. J. Applied Polym. Sci., 99 (2006), 659.

[4] I. Sondi, T. H. Fedynyshyn, R. Sinta, E. Matijević. Langmuir, 16 (2000), 9031.

[5] D. –M. Qi, Y. –Z. Bao, Z. –X. Weng, Z. –M. Huang Polymer, 47 (2006), 4622.

[6] M. M. Rahim-Abadi, A. R. Mahdavian, A. Gharieh, H. Salehi-Mobarakeh. Prog. in Organic Coatings, 88 (2015), 310.

[7] M. Z. Rong, M. Q. Zhang and W. H. Ruan. Mater. Sci. and Technol., 22 (2006), 787.

[8] W. Heller. in Colloidal Dispersions and Micellar Behavior. American Chemical Society, Chapter 3, 1975, pp. 40-63

[9] J. -L. Luna-Xavier, A. Guyot and E. Bourgeat-Lami. Polym. Int., 53 (2004), 609.

[10] E. Bourgeat-Lami, G. A. Farzi, L. David, J.-L. Putaux and T. F. L. McKenna. Langmuir, 28 (2012), 6021.

[11] R. Barbey, L. Lavanant, D. Paripovic, N. Schüwer, C. Sugnaux, S. Tugulu, and H. -A. Klok. Chem. Rev., 109 (2009), 5437.

[12] J-L Luna-Xavier, A. Guyot, and E. Bourgeat-Lami, J. Colloid and Interface Sci., 250 (2002), 82.

[13] E. Bourgeat-Lami, N. N. Herrera, J. -L. Putaux. Macromol. Symp., 229 (2005), 32.

[14] G. Chang, L. He, W. Zheng, A. Pan, J. Liu, Y. Li and R. Cao. J. Colloid and Interface Sci., 396 (2013), 129.

[15] E. Bourgeat-Lami, N. N. Herrera, J-L Putaux, Macromol. Symp., 248 (2007), 213.

[16] R. Hashemi-Nasab and S. M. Mirabedini. Prog. in Organic Coatings, 76 (2013), 1016.

[17] K. Zhang, H. Chen and X. Chen. Macromol. Mater. Eng., 288 (2003), 380.

[18] E. Bourgeat-Lami, P. Espiard and A. Guyot. Polymer, 36 (1995), 4385.

[19] B. J. Frisken. Applied Optics, 40 (2001), 4087.

CHAPTER 4

SILICA/PBA/PMMA MULTILAYER PARTICLES AS EPOXY TOUGHENING AGENTS

4.1. Introduction

Epoxies are widely used in industry and everyday life. They are often toughened to reduce inherent brittleness. Many types of inorganic and organic materials are utilized as epoxy toughening agents such as silica nanoparticles, clay nanoplatelets, carbon nanofibers, liquid rubbers (reactive oligomers), block copolymers, structured core-shell rubber particles, etc. Combinations of toughening agents of high and low modulus are often studied because they provide possible synergistic toughening effects without compromising modulus. For example, silica nanoparticles and micron-sized glass spheres combined with rubber particles were used to make toughened hybrid epoxy nanocomposites. [1-3] It was found that micron-sized glass spheres enhanced toughening effect by crack pinning and crack-tip shielding mechanisms for hybrid epoxy composites than rubber-toughened epoxy. Also these glass spheres might provide enhancement to rubber cavitation and shear deformation of rubber-toughened epoxy. [4] Synergistic toughening effect was also found when low fraction (1.6-3.2 vol.%) of silica nanoparticles were added into rubber-toughened epoxy, but toughening mechanism from which synergistic toughening effect derived from was not clear. [5] For rubber-toughened epoxy, rubber particle size/morphology and distribution largely depend on curing chemistry and process. Importantly, particle size/morphology and distribution greatly

affect toughening efficiency. This incurs complexity to studies on hybrid epoxy composites toughened by inorganic particles and rubbers simultaneously. In order to eliminate effect of rubber phase separation during curing process, structured core-shell rubber particles with rigid thermoplastic shell were proposed and studied. [6-8] It was found not only did these particles have consistent size and size distribution that contributed to comparable results, but also their epoxy-compatible shell enhanced particle dispersion and blend morphology inside epoxy matrix. In this chapter, commercial core-shell rubber particles with a styrene-butadiene core and acrylic shell was used together with silica nanoparticles to make toughened hybrid epoxy nanocomposites, which were compared to epoxy toughened by silica/PBA/PMMA multilayer core-shell particles synthesized in Chapter 3. Difference of toughening effect and mechanism between hybrid epoxy nanocomposites and multilayer-particles-toughened epoxy was investigated in order to elucidate whether a synergistic effect due to encapsulated silica nanoparticles exist as claimed in Gao's work. [9]

4.2. Experimental

In this chapter, previously synthesized silica/PBA/PMMA multilayer core-shell composite particles were freeze-dried and used as epoxy toughening agents. Nanocomposites of epoxy toughened by mixed silica nanoparticles and core-shell rubber particles were compared with epoxy toughened by multilayer particles to elucidate whether a synergistic toughening effect existed for structured multilayer particles. Mechanical tests were performed to measure fracture toughness and compressive strength of toughened epoxy. Several imaging techniques were used to observe particle blend

morphology in epoxy matrix, fracture surface morphology and birefringence from shear yielding.

4.2.1. Materials

Model epoxy resin is diglycidyl ether of bisphenol A (DGEBA, D.E.R. 331) was from Dow Chemical Company. It has an epoxy equivalent weight of 187 g/eq. Specific gravity at 25°C is 1.16. A lightly cross-linked epoxy was desired in this study because it was more "toughenable". Thus piperidine (Sigma-Aldrich) was chosen as a curing agent. Poisson's ratio of model epoxy system is 0.39. Curing reaction of epoxy and piperidine was illustrated in Chapter 1.

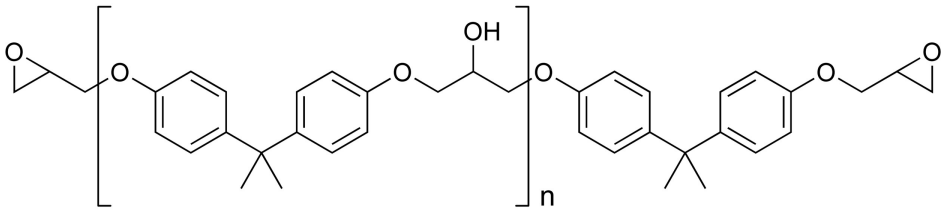

Diglycidyl ether bisphenol A (DGEBA)

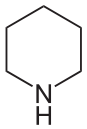

Piperidine

Figure 4-1. Chemical structures of DGEBA and piperidine. n = 0.1 for DER 331 resin

Two commercial toughening agents were used in this work for comparison with synthesized multilayer particles: 40 wt.% silica nanoparticles (ca. 22 nm diam.) dispersed in bisphenol A resin (Nanopox A-410, Evonik) and 25 wt.% styrene-butadiene core-shell rubber (CSR) particles (ca. 100 nm diam.) dispersed in bisphenol A resin (Kane Ace MX-

120, Kaneka Americas). They were labeled as silica and CSR respectively in this chapter. Previously synthesized multilayer particles in this work had a core of silica nanoparticle (ca. 22 nm diam.) encapsulated by a middle layer of 10 nm thick PBA and an outer layer of 10 nm thick PMMA. These particles were freeze-dried and utilized as epoxy toughening agents. Dispersing aid Solsperse 53095 (a phosphate ester, Lubrizol) was used to improve dispersion of multilayer particles in epoxy resin. Modifier content was expressed by volume fraction (vol.%) or phr (parts-per-hundred resin) and they are practically interchangeable for multilayer particles in this work because of their composition.

4.2.2. Processing

Toughening agents were added to DGEBA resin at a certain volume fraction. Mixture was stirred at 300 rpm under vacuum at 80°C for 4 hours. Then piperidine was added to the mixture at a ratio of 5 parts-per-hundred-parts (phr) of epoxy resin. Resulting mixture was stirred for 10 minutes under vacuum. After mixing, mixture was poured into a Teflon-coated steel mold preheated at 160°C. The filled mold was placed in air-circulated oven for 6 hours of curing process at 160°C. After curing, the mold stayed in the oven to gradually cool to room temperature overnight. Resulting toughened epoxy plaques were machined into single-edge-notched three-point bend (SEN-3PB) specimens for three-point flexural test per ASTM D5045 and into small prisms for compressive test per ASTM D695.

4.2.3. Mechanical Testing

Screw-driven universal testing machines (Instron 5500, 5567) were used to perform three-point flexural test and compressive test respectively. For three-point

flexural test, a sawed notch was created on the specimen with jeweler's saw and then a natural crack was created with liquid-nitrogen-chilled razor blades per ASTM D5045. Notched specimens were tested at a crosshead speed of 1 mm/min and load-displacement curves were obtained. Fracture toughness (conditional stress intensity factor) K_Q was calculated from those curves. Prism specimens (12 mm × 6mm × 6 mm) were used in compressive test at a crosshead speed of 1 mm/min per ASTM D695. Load-displacement curves were obtained and compressive yield strength σ_{cy} was calculated.

4.2.4. Morphology

Cured epoxy samples were sent to University of Massachusetts Medical School for microtome and staining with OsO_4. Microtomed samples were ~100 nm thick and imaged under transmission electron microscope (TEM, JEOL JEM-1200EX) to observe particle morphology and blend morphology. Fracture surfaces of 3PB specimens were sputter-coated with Iridium and imaged under scanning electron microscope (SEM, Hitachi S-4300 SE/N) to observe slow and fast crack propagation regions. Fractured specimens were ground and polished to obtain 80~100 nm thick cross sections in the middle of specimens. These thin sections were imaged to observe damage zone and birefringence near crack front from shear yielding under transmission optical microscope (TOM, Olympus BH-2).

4.3. Results and Discussion

Only one type of structured silica/PBA/PMMA multilayer particles were designed and synthesized (from multiple batches) for applications in this chapter. Silica nanoparticles (ca. 22 nm diam.) were encapsulated firstly with PBA then with PMMA to form a ~10 nm thick PBA interlayer and a ~10 nm thick PMMA outer shell.

Conceptually a much thicker PBA interlayer might better contribute to toughening efficiency of final multilayer particles because larger rubber domains undergo cavitation more prominently in stress field thus induce more shear deformation and plastic void growth. However, thicker PBA layer means silica content in the multilayer particle goes progressively smaller to the extent that it is negligible as listed in Table 4-1.

Table 4-1. Calculated silica content in multilayer particles of different PBA layer thickness

PBA interlayer thickness /nm	PMMA shell thickness /nm	Silica core diameter /nm	vol.% of silica core in a multilayer particle	vol.% of silica at various vol.% of toughening agent (multilayer particles) in epoxy composite		
				2.5%	5%	7.5%
10	10	22	3.4	0.085	0.17	0.255
20	10	22	2	0.05	0.1	0.15
30	10	22	1	0.025	0.05	0.075
40	10	22	0.6	0.015	0.03	0.045

4.3.1. Blend Morphology

Blend morphology of particles inside epoxy matrix after curing process was imaged using TEM (Figures 4-2 to 4-5). Cured epoxy composites were microtomed and stained with OsO_4 for better contrast. PBA interlayer and PMMA outer shell are not distinguishable because neither of the two can be stained by OsO_4. Thus dispersion of multilayer particles was observed indirectly from dispersion of silica nanoparticle cores (black) in these images. Different gray scale of epoxy matrix background was due to different sample thickness and staining condition.

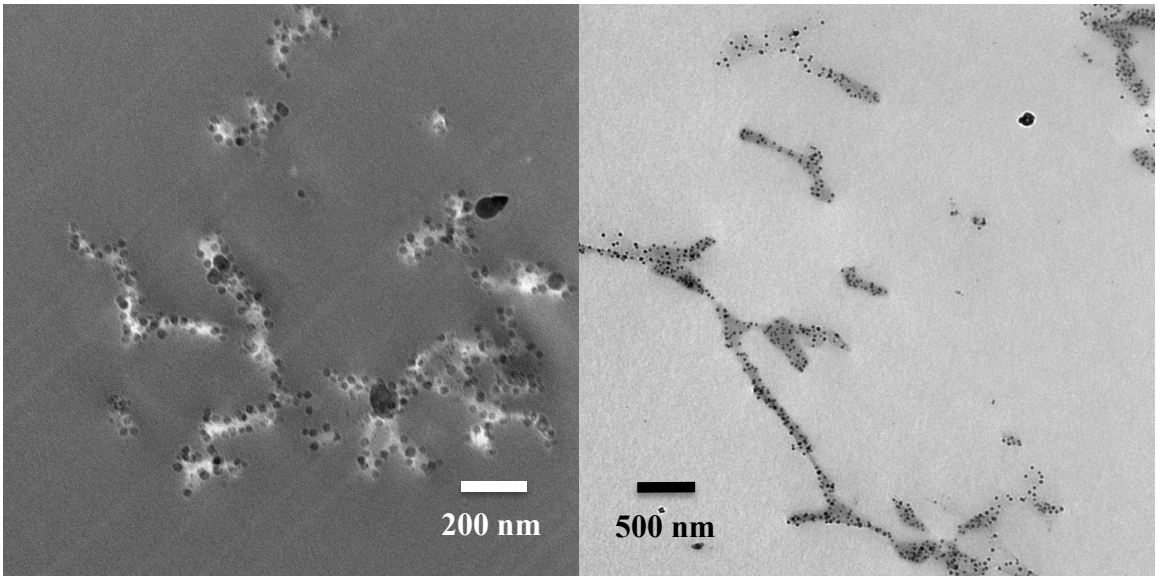

Figure 4-2. TEM images of microtomed epoxy composites. Left: 2.5 vol.% multilayer particles; right: 2.5 vol.% multilayer particles w. 0.5 wt.% Solsperse 53095.

Figure 4-2 contains TEM images of epoxy composite toughened by 2.5 vol.% synthesized multilayer particles with and without a polymeric dispersant, which is commonly utilized for dispersing organic and inorganic nanoparticles in hydrophobic phase. Black silica nanoparticles are uniformly segregated because of indiscernible polymer layers around them. It is obvious that multilayer particles formed small clusters inside epoxy matrix. From comparisons among epoxy toughened by different volume fraction of multilayer particles (Figures 4-2 and 4-3), it was observed that cluster size and shape had no obvious variance. Besides, addition of a dispersant during process of mixing epoxy resin and freeze-dried particles did not improve the dispersion of multilayer particles inside epoxy matrix (image on the right). From these observations a conclusion was drawn that these small clusters were most possibly formed during freeze process before lyophilizing (freeze-drying under vacuum). During freezing of latexes, ice crystals form and result in interstices between them, where higher pressure, higher

electrolyte concentration and higher collision frequency work together to destabilize latexes and form aggregates of latex particles. [10]

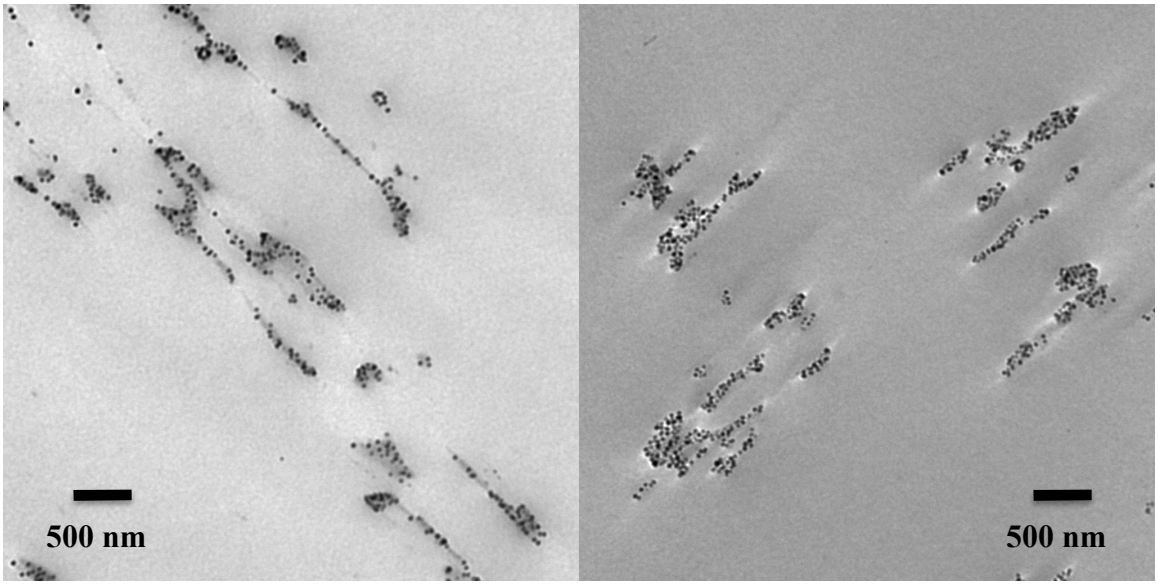

Figure 4-3. TEM images of microtomed epoxy composites. Left: 5 vol.% multilayer particles; right: 7.5 vol.% multilayer particles

Figure 4-3 contains TEM images of epoxy composite toughened by 5 vol.% (left) and 7.5 vol.% (right) of synthesized multilayer particles. Dispersion of particles and cluster morphology shared similarity with that of 2.5 vol.% in Figure 4-2, affirming the aforementioned speculation that these clusters were formed prior to mixing process. Images in Figure 4-3 were from thin sections of epoxy composites possibly inside stress field thus clusters of particles were stretched and orientated in direction of stress during fracturing.

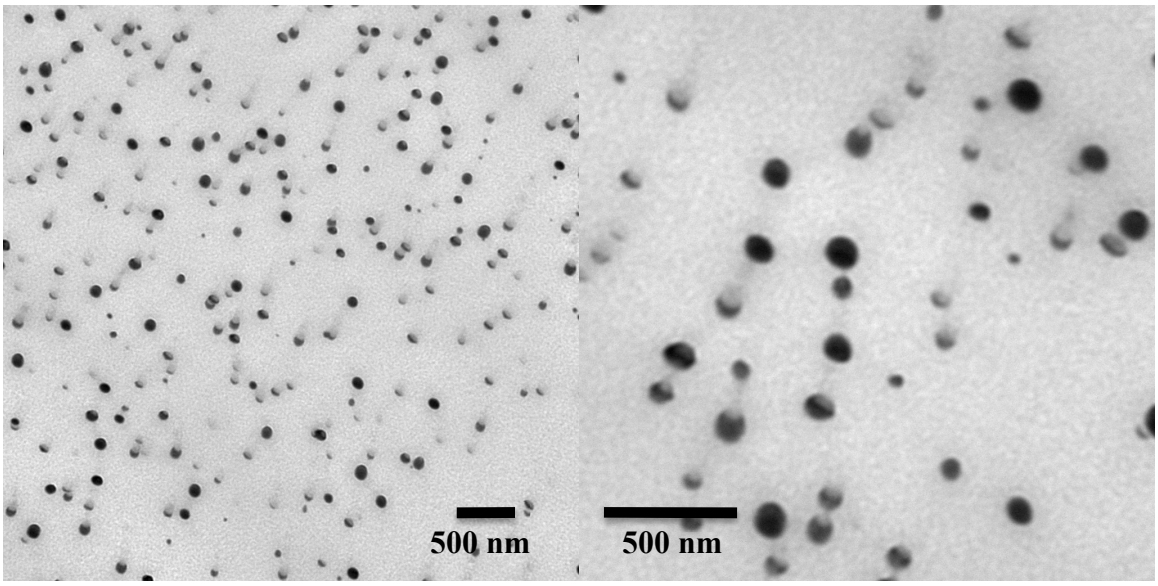

Figure 4-4. TEM images of microtomed epoxy composites. 5 vol.% CSR

Figure 4-4 contains images of epoxy toughened by 5 vol.% styrene-butadiene core – acrylic shell rubber particles (CSR) of ~100 nm diameter at different magnifications. These rubber particles had unsaturated sites in polymer chains thus they can be stained by OsO_4 and show black color. Light grey traces around rubber particles were due to pullout of particles during cryogenic ultra-microtoming process. These rubber particles were in an epoxy concentrate and well dispersed before use so they remained uniformly dispersed in the cured epoxy composites.

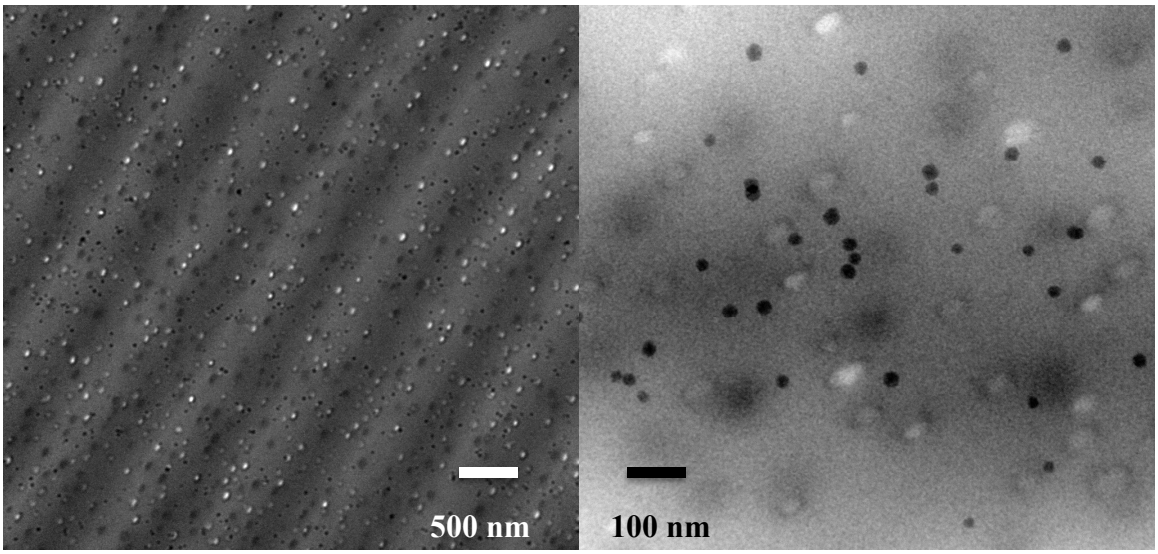

Figure 4-5. TEM images of microtomed epoxy composites. 5 vol.% hybrid toughening agents including CSR and silica at same composition as multilayer particles

Figure 4-5 contains images of epoxy toughened by 5 vol.% hybrid toughening agents comprising 93.8 wt.% CSR and 6.2 wt.% of silica nanoparticles of ~22 nm diameter at different magnifications. Ratio of rubber particles to silica nanoparticles was determined according to composition of synthesized multilayer particles so that a comparison between structured multilayer particles and mixed hybrids can be made. These silica nanoparticles were in an epoxy concentrate and well-dispersed before use so they remained uniformly dispersed inside cured epoxy composites. Stained dark rubber particles and light traces of particle pullout were seen in these images as well as black silica nanoparticles. These particles were all uniformly dispersed inside epoxy matrix.

4.3.2. Mechanical Properties

4.3.2.1. Experimental Fracture Toughness and Yield Strength

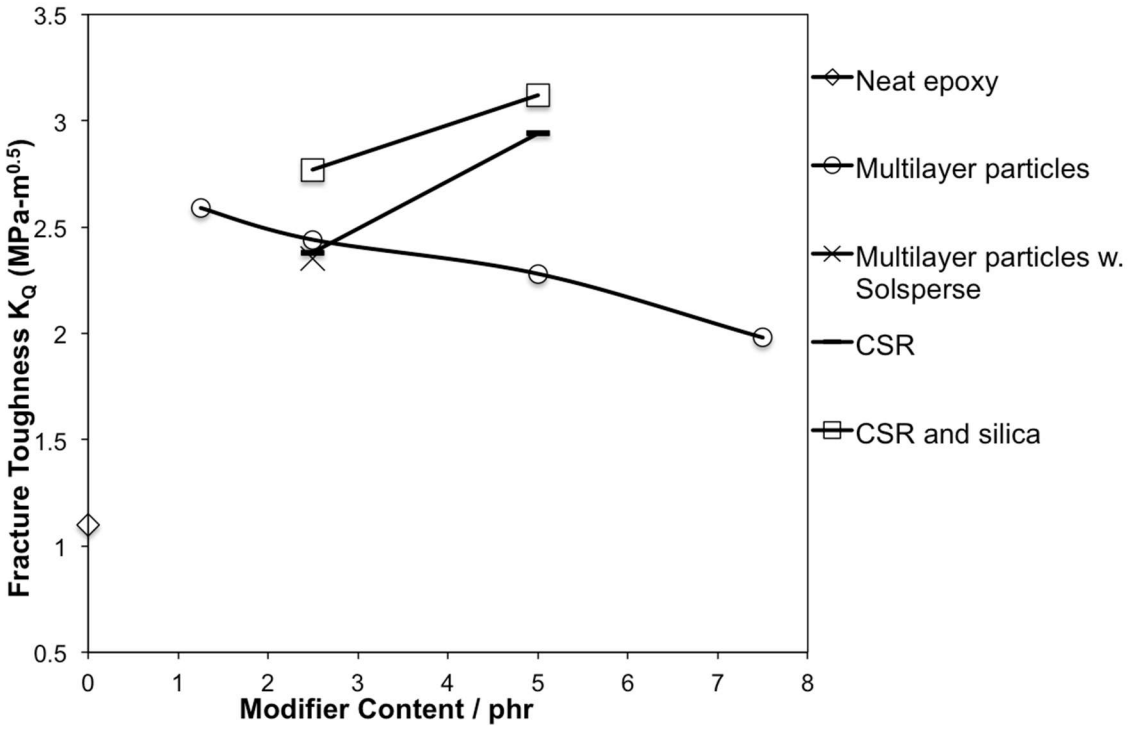

Figure 4-6. Effect of modifier content on fracture toughness K_Q for toughened epoxy

Figure 4-6 is a chart of conditional fracture toughness (K_Q: mode I stress intensity factor under plane-strain conditions) of several toughened epoxy systems calculated according to procedures described in detail in ASTM D5045. [11, 12] Fracture toughness of neat epoxy is around 1.1 MPa-m$^{0.5}$ while epoxy toughened by synthesized multilayer particles had fracture toughness as high as 2.59 MPa-m$^{0.5}$ at only 1.25 vol.% of multilayer particles. At same volume fraction of toughening agents, this high value of fracture toughness exceeded all the toughening agents previously studied in the same model epoxy system. [5,7, 13-16] However, as the volume fraction of multilayer particles

increases, fracture toughness steadily decreases (at a rate of ~0.1 MPa-$m^{0.5}$/vol.%), a trend opposite to typical behavior of common toughening agents. This trend was not discovered in a previous study of very similar toughened epoxy system [7] because an unvarying 10 vol.% of toughening agents was used throughout the study. This novel phenomenon might be explained based on blend/dispersion morphology of multilayer particles in epoxy matrix. These particles formed small clusters able to be stretched and orientated under stress instead of being uniformly and individually distributed. And the segregation distance between neighboring clusters became shorter as volume fraction of multilayer particles increased. Previous studies pointed out potential improvement of fracture toughness by cluster formation. [17-28] In some of them it was claimed that mechanism of toughness improvement was because of bridging effect from small clusters acting like big particles. [17-21] In others it was claimed that improvement was from cooperative deformation of inter-connected rubber clusters (a percolation concept). [22-28] However, neither of these explanations might be applied to findings in this work. If cluster formation improved toughness by acting like big rubber particles, according to common trends, increase of volume fraction of these big particles should increase fracture toughness. If cluster formation improved toughness by acting like inter-connected rubber clusters, increase of volume fraction of clusters should enhance this inter-connection and thus increase fracture toughness. A possible explanation is, as volume fraction of particles increased, segregation of clusters became closer and inter-connection of clusters became enhanced, increasing the possibility that crack propagated along pathways formed by low-modulus inter-connected clusters.

In Figure 4-6 and 4-7, epoxy toughened by 2.5 vol.% of multilayer particles with a polymeric dispersant Solsperse did not show a noticeable difference from that without the dispersant regarding to both fracture toughness and compressive yield strength.

In Figure 4-6, both CSR-toughened epoxy and hybrid-toughened epoxy showed increased fracture toughness as modifier content increased. Epoxy toughened by hybrid toughening agents comprising CSR and silica nanoparticles showed higher fracture toughness than CSR-toughened epoxy. Considering the very low content of actual silica in the system (ca. 0.085 vol.% and 0.17 vol.% for 2.5 and 5 modifier phr respectively), higher fracture toughness of hybrid-toughened system might be from synergistic effect from combination of two types of toughening agents.

Table 4-2. Epoxy systems toughened by various toughening agents

Inorganic toughening agent		**Organic toughening agent**		**K_Q /MPa-m$^{0.5}$**	**Ref.**
Type	**Vol.%**	**Type**	**Vol.%**		
-	-	SBR core - PMMA shell CSR (100 nm diam.)	10	2.69 ± 0.02	[32]
Silica nanoparticles (20 nm diam.)	0.8	-	-	1.5 ± 0.1	[33]
Silica nanoparticles (20 nm diam.)	3.2	CTBN	3.7	2.76 ± 0.25	[34]
Silica nanoparticles (23 nm diam.)	2.5	-	-	1.72	[14]
-	-	SBR CSR (100 nm diam.)	5	2.4	[15]
Silica nanoparticles (25 nm diam.)	2.5	-	-	1.65 ± 0.03	[16]
Synthesized multilayer particles			**Vol.%**	**K_Q**	This work
			1.21	2.59 ± 0.34	
			2.42	2.44 ± 0.15	
			4.84	2.28 ± 0.21	
			7.27	1.98 ± 0.02	

In Table 4-2, fracture toughness results of epoxy toughened by multilayer particles were compared with similar piperidine-cured epoxy systems in literature. Various toughening agents were used in these studies including silica nanoparticles, core-

shell rubber particles and hybrids containing silica and rubber phase. Synthesized multilayer particles in this work contain only 1.5 vol.% of silica nanoparticles thus the silica content in cured epoxy is extremely low. The major contribution of toughness should be from organic phase and blend morphology of multilayer particles. Comparison with epoxy toughened by silica nanoparticles alone suggests a superior toughening efficiency of multilayer particles. Epoxy toughened by up to 2.5 vol.% of silica nanoparticles has a fracture toughness range of 1.5~1.8, lower than toughness of epoxy toughened by 7.27 vol.% of multilayer particles, which gave the lowest toughness among epoxy toughened by multilayer particles in this study. In Table 4-2, epoxy systems toughened by organic particles show much higher toughness than those by silica alone. At 5 vol.% of SBR CSR (100 nm diam.) [15], K_Q is slightly higher than 4.84 vol.% of multilayer particles. For epoxy toughened by 10 vol.% of SBR core - PMMA shell CSR (100 nm diam.) [32] or a hybrid toughening agent containing 3.2 vol.% silica nanoparticles and 3.7 vol.% CTBN [34], K_Q was higher than epoxy toughened by 1.21 vol.% of multilayer particles, which gave the highest toughness for multilayer- particle-toughened epoxy studied in this work.

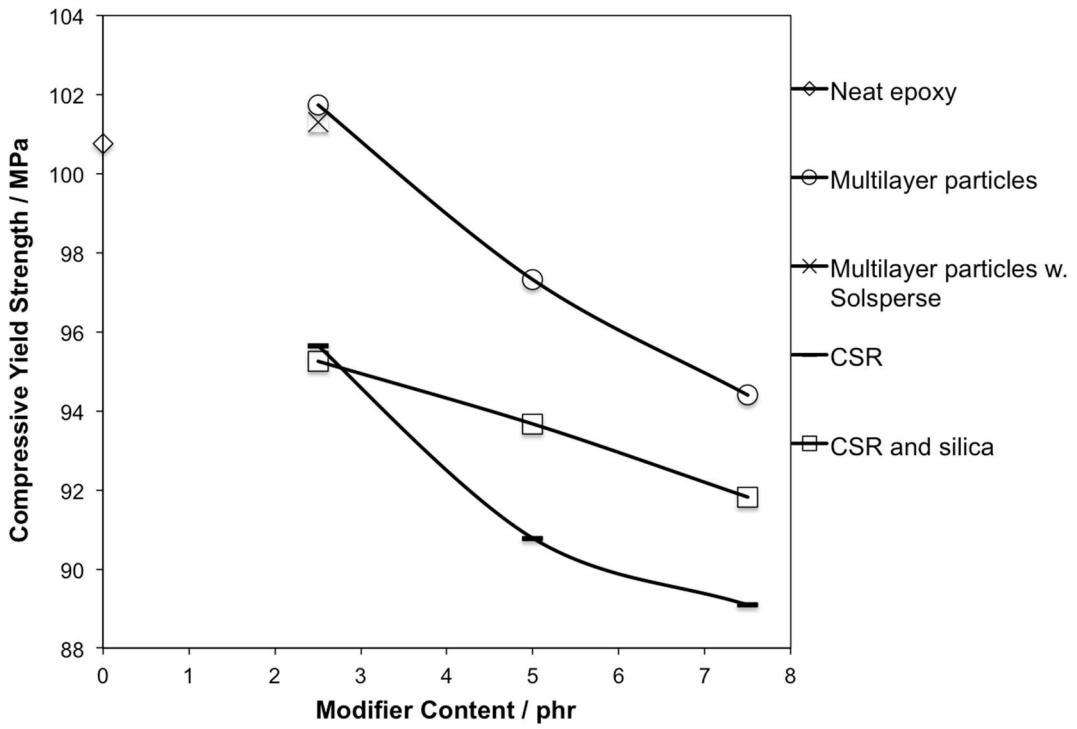

Figure 4-7. Effect of modifier content on compressive yield strength σ_{cy} for different toughened epoxy

In Figure 4-7, compressive yield strength σ_{cy} steadily decreased as modifier content increased, in accordance with the increasing rubber content in toughened epoxy. Hybrid-toughened epoxy had higher compressive yield strength than CSR-toughened epoxy when modifier content was higher than 3 phr possibly because of lower absolute rubber content in hybrid system. From comparison between epoxy toughened by multilayer particles and by hybrid toughening agents (CSR and silica) with the same rubber and silica contents, the former showed a heightened compressive yield strength and modulus. When modifier content was lower than 3 phr, σ_{cy} was even slightly higher for multilayer-particle-toughened epoxy than that of neat epoxy. This could be attributed

to special particle size/morphology and blend morphology of multilayer particles inside epoxy matrix.

4.3.2.2. Comparison Between Experimental Results and Predicted Fracture Toughness

Fracture energy G_{Ic} is the energy dissipated during fracture per unit area of newly created fracture surface at critical condition. It is a central property in fracture mechanics as a measurement of toughness of material. In principle, G_{Ic} can be obtained from experimental results through following relationship:

$$G_{Ic} = \frac{(1-\nu^2)K_{Ic}{}^2}{E} \tag{1}$$

where ν is Poisson's ratio of cured epoxy, taken to be 0.39. K_{Ic} is stress intensity factor and E is Young's modulus. Young's modulus was not measured in this study. But results from study of a similar CSR-toughened epoxy system [15] can be used for calculation of G_{Ic}. In that study, a linear relationship between E and modifier content was found where E ≈ 3.375 GPa at 0 modifier content and E ≈ 3 GPa at 7.5 phr of modifier content. Calculated G_{Ic} is listed in Table 4-2.

Overall fracture energy contribution from various toughening mechanisms Ψ includes ΔG_s and ΔG_v, contributions of rubber particle shear and void growth respectively in this study, as is found in Section 4.3.3 and 4.3.4 that shear banding and matrix void growth are toughening mechanisms. Thus ΔG_s and ΔG_v are calculated using Huang and Kinloch's prediction model. [29, 30]

$$\Psi = \Delta G_s + \Delta G_v \tag{2}$$

$$\Delta G_s = 0.5\left(1+\frac{\mu_m}{\sqrt{3}}\right)^2\left[\left(\frac{4\pi}{3V_f}\right)^{1/3} - \frac{54}{35}\right]V_f\sigma_{yc}\gamma_f r_{yu}{K_{vm}}^2 \tag{3}$$

$$\Delta G_v = \left(1+\frac{\mu_m}{\sqrt{3}}\right)^2 (V_{fv} - V_{fr})\sigma_{yt} r_{yu}{K_{vm}}^2 \tag{4}$$

$$\sigma_{yt} = \sigma_{yc}\left(\frac{\sqrt{3}-\mu_m}{\sqrt{3}+\mu_m}\right) \tag{5}$$

where each parameter and its value is listed in Table 4-3. V_f is taken to be volume fraction of multilayer particles since silica nanoparticles in multilayer particles only contributes less than 1% of particle volume.

Table 4-3. Parameters in Huang and Kinloch model [29]

Parameter	Meaning	Value
μ_m	von Mises pressure coeff. for shear yielding	0.2 [29]
V_f	Volume fraction of rubber particles	Varies
σ_{yc}	Compressive yield stress of cured unmodified epoxy	100.76 MPa (measured)
σ_{yt}	Tensile yield stress of cured unmodified epoxy	-
γ_f	Shear fracture strain of cured unmodified epoxy	0.71 [29]
r_{yu}	Radius of plastic zone of cured unmodified epoxy	7.7 μm [16]
K_{vm}	Maximum stress concentration factor of the von Mises stress in the matrix	2.22 [30]

Volume fraction, fracture toughness and compressive yield strength are listed in Table 4-4. G_{Ic} was calculated from experimental results. At 1.25 phr of modifier content, fracture energy G_{Ic} has a high value of 1.717 kJ-m^{-2} and continues to decrease as modifier content increases. ΔG_s, contribution of fracture energy from rubber particle shear banding was calculated using Huang and Kinloch model (equation 3). Shear banding contributes to fracture toughness and ΔG_s increases as modifier content increases. But it only counts for a small fraction in total fracture energy (less than 25%).

Table 4-4. Measured and predicted fracture toughness of epoxy toughened by different volume fraction of multilayer particles

Modifier content /phr	Modifier vol.%	K_Q /MPa-m$^{0.5}$	σ_{cy} /MPa	G_{Ic}* /kJ-m^{-2}	ΔG_s** /kJ-m^{-2}	ΔG_v /kJ-m^{-2}	V_{fv}-V_{fr} vol.%
0	0	1.16 ± 0.35	100.8 ± 2.0	0.255	-	-	-
1.25	1.21	2.59 ± 0.34	100.6 ± 0.9	1.717	0.112	1.35	28
2.5	2.42	2.44 ± 0.15	101.7 ± 0.6	1.553	0.165	1.13	24
5	4.84	2.28 ± 0.21	97.3 ± 1.1	1.410	0.236	0.92	19
7.5	7.27	1.98 ± 0.02	94.4 ± 1.1	1.108	0.285	0.57	12

*Calculated from experimental results using equation (1)
**Predicted using Huang and Kinloch model [29]

Calculation of ΔG_v, contribution of fracture energy from plastic void growth, requires experimental measurements of volume fraction of voids. In this study these measurements were not performed. However, by examining fracture surface under SEM in section 4.3.4, we found void growth was not prominent on fracture surface and it was sporadic. Because of these difficulties, ΔG_v was not calculated from equation (4). Instead, an estimation of void growth $V_{fv} - V_{fr}$ was calculated from equation (4) by assuming $\Delta G_v = G_{Ic} - 0.255 - \Delta G_s$ according to Huang and Kinloch model, with 0.255 being fracture energy of neat epoxy. ΔG_v and $V_{fv} - V_{fr}$ are listed in Table 4-4. From the results, we found that if our system can be well predicted by Huang and Kinloch model,

void growth should be as high as 12 – 28 vol.%. But this phenomenon of high void growth was not proven in this study. A possible explanation is, besides shear banding and some extent of void growth, there might be another major contributing toughening mechanism in multilayer-particle-toughened epoxy in this work due to its unique micro-clustering blend morphology.

4.3.3. Subsurface Damage Zone Analysis

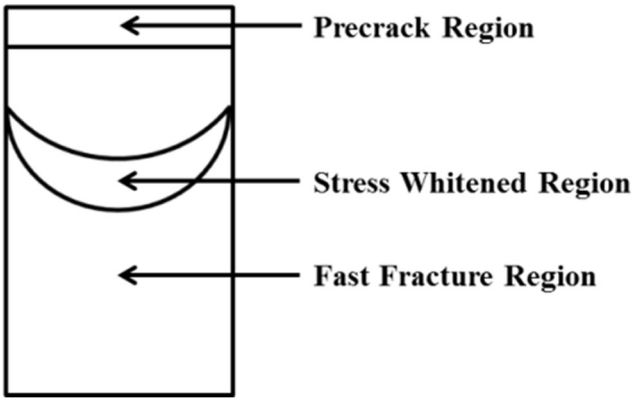

Figure 4-8. Fracture surface on SEN-3PB specimen. Reprinted. [15]

Figure 4-8 is a sketch of different regions on fracture surface of single-edge-notched specimen after three-point flexural test. Pre-crack was formed by sawing and the crack front was from formation of a small natural crack. After flexural test, a stress-whitened region (slow crack propagation region) followed by a fast fracture region can be distinctly observed. Usually major contributing toughening mechanisms happen inside the stress-whiten region, i.e. slow fracture region. These regions were examined under TOM and SEM to infer toughening mechanisms.

4.3.3.1. Observation of Damage Zone

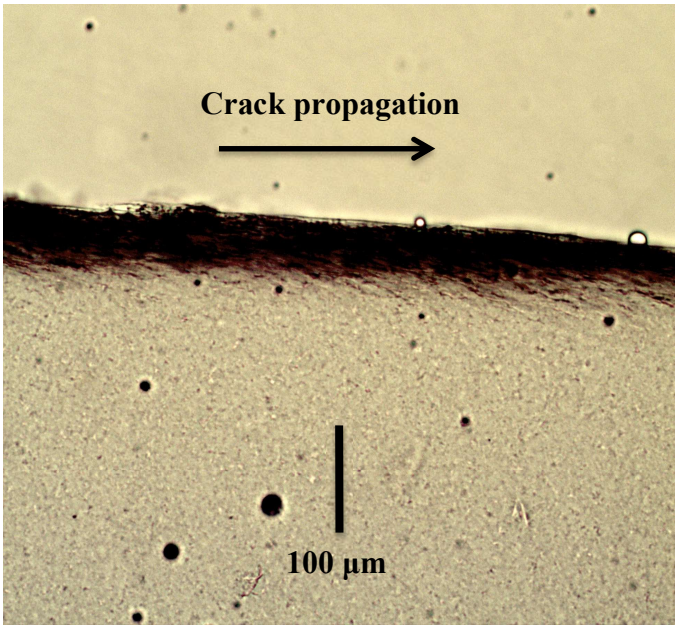

Figure 4-9. Bright field TOM image of shear deformation in epoxy toughened by 2.5 vol.% multilayer particles

Figure 4-9 is a TOM image of fracture front in stress-whitened region of a ~90 µm thin cross-section perpendicular to fracture surface. Dark-colored damage zone suggested shear deformation of the matrix. Faint dark streaks approximately 45° to the crack propagation direction might be shear bands. In the image the damage zone size is around 50 µm deep. Compared to previous rubber-toughened and silica nanoparticles toughened epoxy [14, 15], multilayer particles toughened epoxy exhibited a much deeper damage zone at a modifier volume fraction of only 2.5%. This might account for its superior toughening efficiency at 1.25-2.5 vol.%.

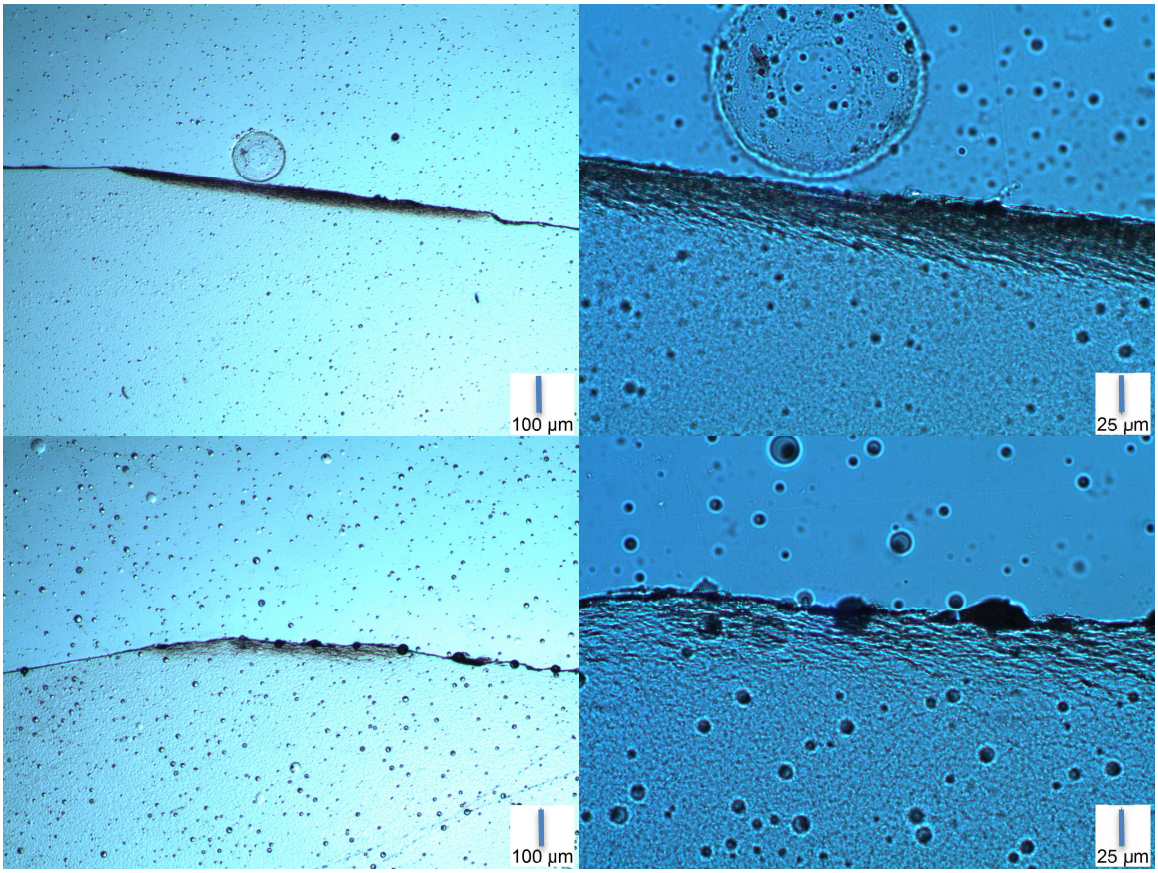

Figure 4-10. TOM images under cross polarizer of shear deformation in epoxy toughened by 2.5 phr (top) and 5 phr (bottom) of multilayer particles

Figure 4-10 contains TOM images under cross polarizer depicting shear bands inside damage zone of epoxy toughened by 2.5 and 5 phr of multilayer particles. For epoxy toughened by 1.25 phr multilayer particles, no shear bands were found under TOM. Both 2.5 and 5 phr cases exhibit similar damage zone size around 50 µm. For 2.5 phr case, damage zone length is 1.1 mm while for 5 phr damage zone length is 0.8 mm. Both damage intensity and damage zone length are greater for 2.5 phr case. This trend is in accordance with the fact that measured fracture toughness is higher for 2.5 phr case than 5 phr.

4.3.3.2. Comparison between Experimental Results and Predicted Damage Zone Size

Damage zone size can be predicted with Irwin theory as in equation (6) [31] or Huang and Kinloch model as in equation (7) [29].

$$r_y = \frac{K_{Ic}^{\ 2}}{6\pi\sigma_y^{\ 2}} \tag{6}$$

$$r_y = K_{vm}^{\ 2}\left(1+\frac{\mu_m}{\sqrt{3}}\right)^2 r_{yu} \tag{7}$$

where r_y is damage zone radius and σ_y is tensile yield stress taken to be 0.7 times measured compressive yield stress. Other parameters are listed in Table 4-3.

Table 4-5. Predicted and measured damage zone sizes

Modifier content /phr	avg. K_Q /MPa-$m^{0.5}$	avg. σ_{cy} /MPa	σ_y /MPa	r_y /μm (Irwin)	r_y /μm (Huang&Kinloch)	r_y /μm (measured)
2.5	2.44	101.7	71.2	62.3	47.2	50
5	2.28	97.3	68.1	59.5	47.2	50

From Table 4-5, a good agreement between damage zone sizes predicted using Huang and Kinloch model and measured value is found. Irwin theory gives overestimation of damage zone size probably because of high fracture toughness resulted from a combination of toughening mechanisms.

4.3.4. Observation of Fracture Surface

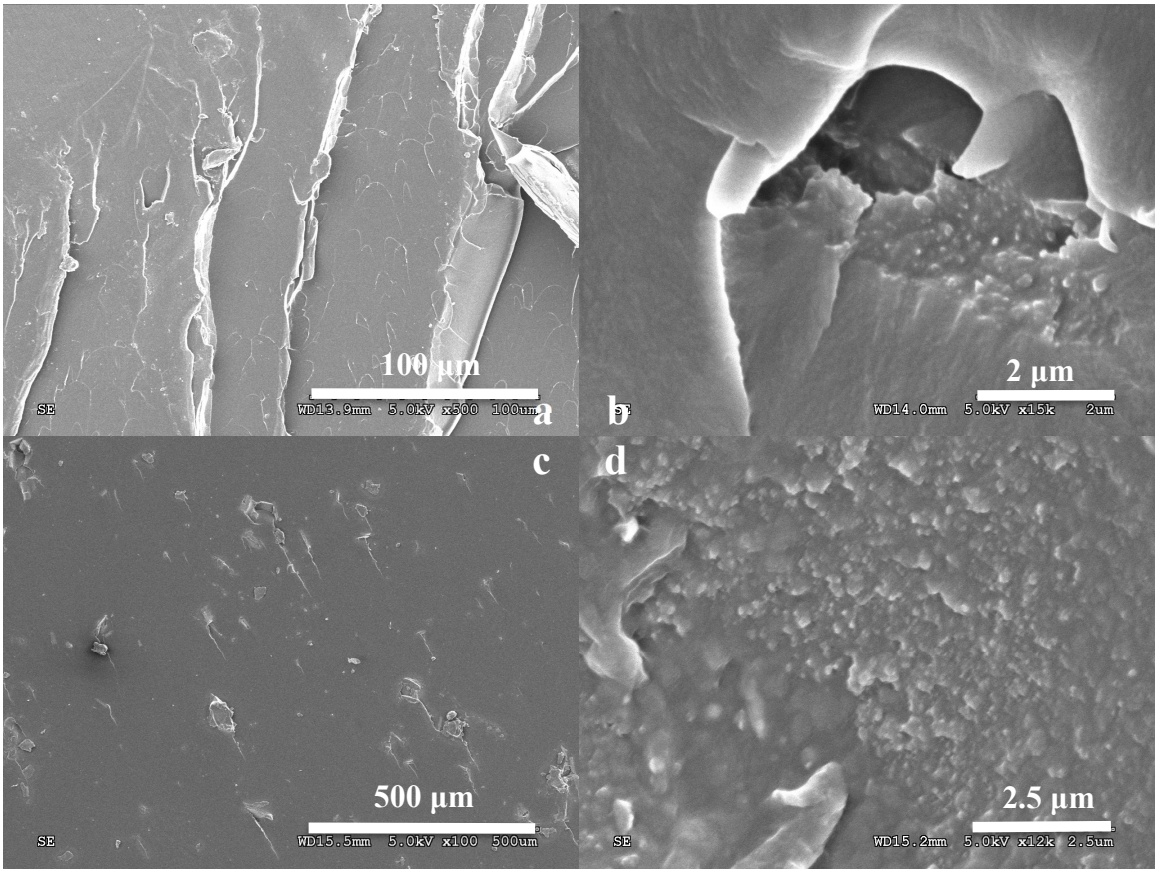

Figure 4-11. SEM images of fracture surface on epoxy toughened by 1.25 vol.% multilayer particles. a, b: stress-whitened region; c, d: fast fracture region.

Figure 4-11 contains SEM images of fracture surface of epoxy toughened by 1.25 vol.% multilayer particles. Image “a” showed little ductile tearing in stress-whitened region. Image “b” showed a major matrix void formed around clusters of multilayer particles. This kind of voids was seen only in the stress-whitened region. Cavitation of rubber phase inside multilayer particles was unseen. From these observations matrix void growth initiated near clusters of particles was considered the major contributing toughening mechanism. In fast fracture region, matrix voids were rarely seen. But fracture surface showed particle clustering.

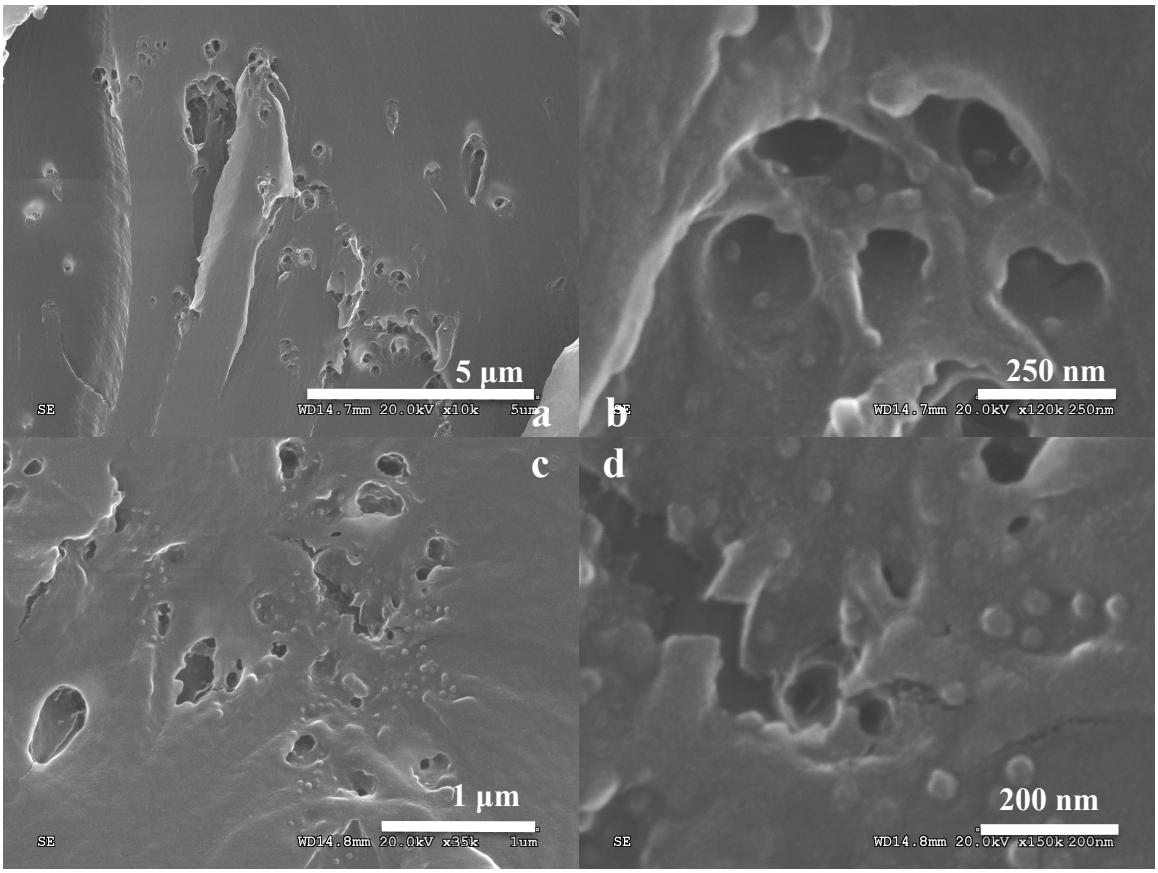

Figure 4-12. SEM images of fracture surface on epoxy toughened by 2.5 vol.% multilayer particles. a, b: stress-whitened region; c, d: fast fracture region.

Figure 4-12 contains SEM images of fracture surface of epoxy toughened by 2.5 vol.% multilayer particles. With a higher volume fraction of multilayer particles, matrix voids still showed but with a small size and patterned appearance compared to Figure 4-11. This difference might account for decrease of fracture toughness with higher volume fraction of particles. Particles did not cavitate or debond from the matrix. In fast fracture region, clusters of particles were seen without internal cavitation or debonding (as expected).

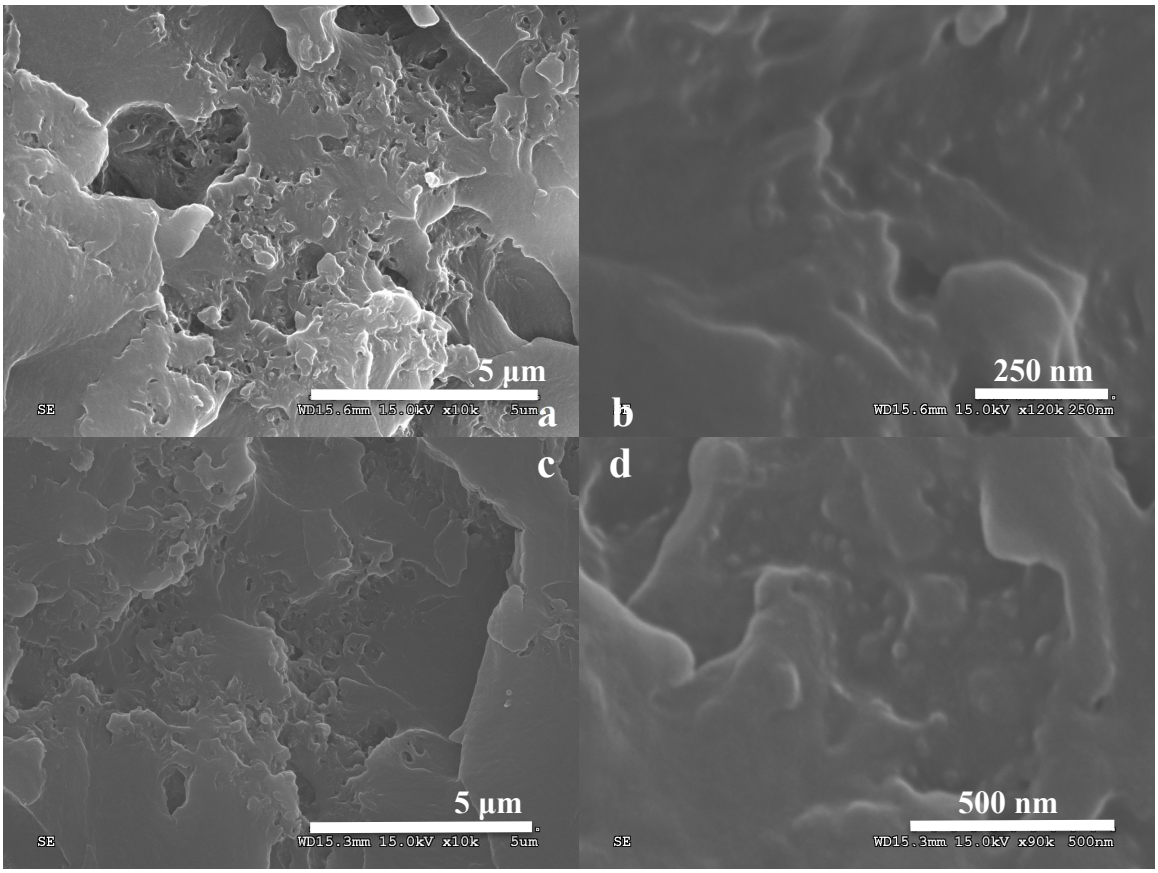

Figure 4-13. SEM images of fracture surface on epoxy toughened by 5 vol.% multilayer particles. a, b: stress-whitened region; c, d: fast fracture region.

Figure 4-13 contains SEM images of fracture surface of epoxy toughened by 5 vol.% multilayer particles. In stress-whitened region, more matrix ductile tearing was found while matrix voids around multilayer particles were not significant compared to Figure 4-11 and 4-12. Apparently matrix ductility had a limited contribution to fracture toughness compared to matrix void growth. Thus fracture toughness decreased for epoxy toughened by 5 vol.% multilayer particles due to decreased matrix void growth.

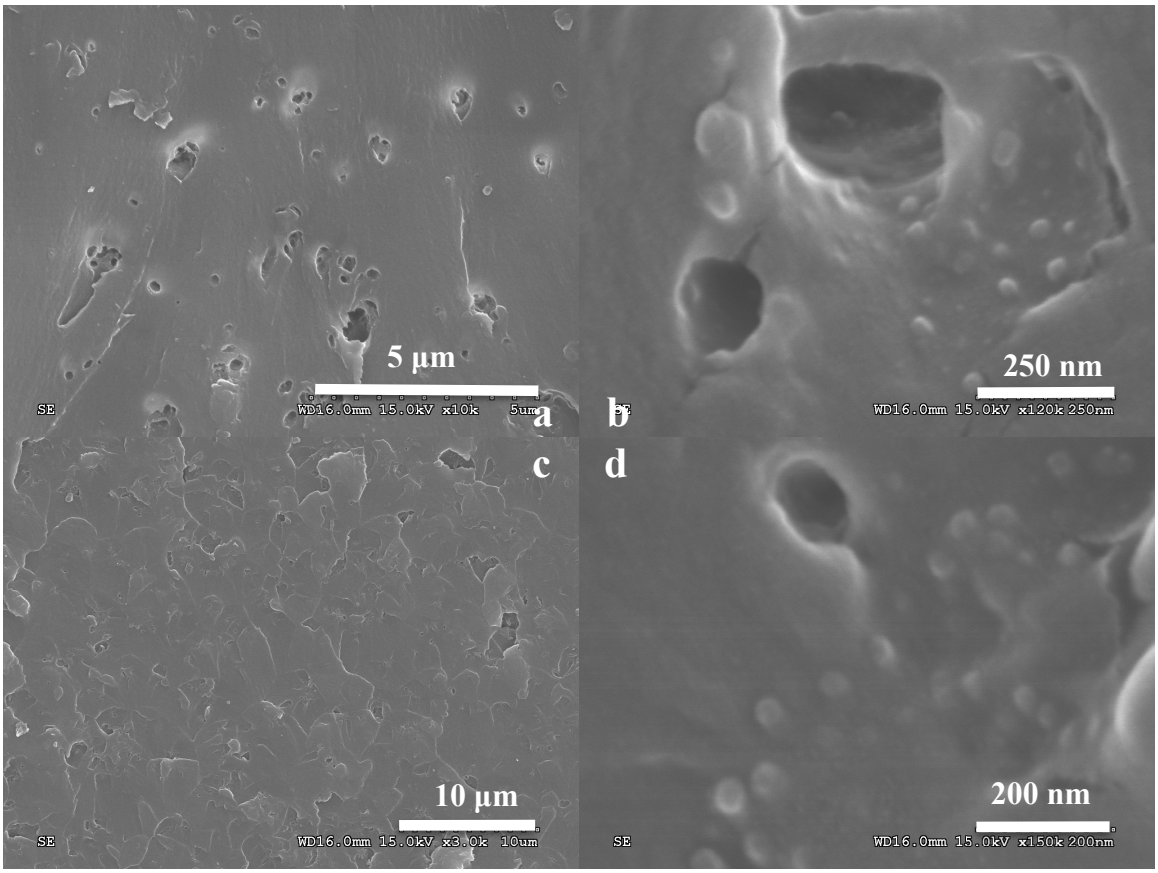

Figure 4-14. SEM images of fracture surface on epoxy toughened by 2.5 vol.% multilayer particles w. 0.5 wt.% Solsperse 53095. a, b: stress-whitened region; c, d: fast fracture region.

Figure 4-14 contains SEM images of fracture surface of epoxy toughened by 2.5 vol.% multilayer particles with addition of a dispersing aid for better dispersion of multilayer particles in epoxy. Compared to Figure 4-12, not much difference regarding matrix tearing and voids was observed. This is in accordance with mechanical test results indicating both fracture toughness and compressive yield strength did not show a noticeable difference between toughened epoxy with and without the dispersing aid.

4.4. Summary and Conclusions

Epoxy was toughened by three types of toughening agents: synthesized multilayer particles, CSR and a hybrid containing CSR and silica nanoparticles. Blend morphology was distinct for multilayer particles, which formed small clusters throughout the matrix with its size unvaried between different volume fractions of particles. For CSR and silica nanoparticles, they were well dispersed inside epoxy matrix regardless of volume fraction in this work. Because of this cluster-formation mechanism and distinct blend morphology, differences in mechanical properties and fracture morphology between epoxy toughened by multilayer particles and by hybrid toughening agents may not be explained by structure of multilayer particle only. Unlike common trends seen in epoxy toughened by CSR and hybrid toughening agents, fracture toughness (K_Q) of epoxy toughened by multilayer particles exhibited a trend that K_Q first peaked at 1.25 vol.% then decreased with increasing particle volume fraction. TOM and SEM images of fracture surfaces and subsurface revealed that shear banding and matrix void growth might account for superior toughening efficiency of multilayer particles at low volume fractions but they became less prominent as volume fraction of particles increased.

4.5. References

[1] A. J. Kinloch, D. L. Maxwell and R. J. Young. J of Mater. Sci., 20 (1985), 4169.

[2] H. R. Azimi, R. A. Pearson and R. W. Hertzberg. Polymer Eng. and Sci., 36 (1996), 18, 2352.

[3] A. J. Kinloch, J. H. Lee, A. C. Taylor, S. Sprenger, C. Eger and D. Egan. J. Adhes., 79 (2003), 867.

[4] J. Lee and A. F. Yee. Polym. Eng. and Sci., 40 (2000), 12, 2457.

[5] Y. Liang. The Toughening Mechanisms in Epoxy-Silica Nanocomposites and Hybrid Epoxy-Silica-Rubber Nanocomposites (Ph.D. diss.), 2008, Lehigh University

[6] H. -J. Sue, E. I. Garcia-Meitin, D. M. Pickelman and P. C. Yang. Toughened Plastics I — Science and Engineering. Adv. Chem. Ser., 233, Amer. Chem. Soc., Washington, D.C., (1993), 259

[7] J. Y. Qian. The Development of Core-Shell Latex Particles as Toughening Agents for Epoxies (Ph.D. diss.), 1994, Lehigh University

[8] J. Chen, A.J. Kinloch and S. Sprenger, A.C. Taylor. Polymer, 54 (2013), 4276.

[9] J. Gao, J. Li, S. Zhao, B. C. Benicewicz, H. Hillborg and L. S. Schadler. Polymer, 54 (2013), 396.

[10] D. C. Blackley. Polymer Latices - Science and Technology, 2nd ed., vol. 1, Chapman & Hall, (1997).

[11] J. E. Srawley. Int. J. Fracture Mechanics, 12 (1976), 475.

[12] O. L. Towers. “Stress Intensity Factors, Compliances and Elastic n_e Factors for Six Test Geometries,” The Welding Institute, 1981.

[13] R. Bagheri. Rubber-Toughened Epoxies: Role of Characteristics of Particle and Particle/Matrix Interface (Ph.D. Diss.), 1995, Lehigh University

[14] P. Dittanet. Fracture Behavior of Silica Nanoparticle Filled Epoxy Resin (Ph.D. diss.), 2011, Lehigh University

[15] L. N. Bacigalupo. Fracture Behavior of Nano-Scale Rubber-Modified Epoxies (Ph.D. Diss.), 2013, Lehigh University

[16] B. S. Patel. Toughening Mechanisms in Silica-Filled Epoxy Nanocomposites (Ph.D. Diss.), 2016, Lehigh University

[17] P.A. Mataga. Acta Metali, 37 (1989), 3349.

[18] B.G. Min, J.H. Hodgkin and Z.H. Stachurski. J. Appl. Polym. Sci., 50 (1993), 1065.

[19] T. Iijima, S. Miura, W Fukuda and M. Tomoi. Eur. Polym. J., 29 (1993), 1103.

[20] A. Murakami, D. Saunders, K. Ooishi and T. Yoshiki. J. Adhesion, 39 (1992), 227.

[21] K. Yamanaka and T. Inoue. Polymer, 30 (1989), 662.

[22] J. A. Cecere and J. E. McGrath. Polym. Preps., 27 (1986), 299.

[23] S. Wu. J. Appl. Polym Sci., 35, 549 (1988).

[24] S. Wu. Polym. Eng. Sci., 30 (1990), 753.

[25] W.Y. Hsu and S. Wu. Polym. Eng. Sci., 33 (1993), 293.

[26] A. Margolina and S. Wu. Polymer, 29 (1988), 2170.

[27] S. Wu and A. Margolina. Polymer, 31 (1990), 972.

[28] K Yamanaka, Y. Takagi and T. Inoue. Polymer, 60 (1989), 1839.

[29] Y. Huang, A. J. Kinloch. J Mater. Sci., 27 (1992), 2763.

[30] Y. Huang, A. J. Kinloch. J Mater. Sci., 27 (1992), 2753.

[31] G. R. Irwin. Sagamore Research Conference Proceedings, 4 (1961), 63.

[32] J. Y. Qian, R. A. Pearson, V. L. Dimonie, M. S. El-Aasser. J Appl. Polym. Sci., 58 (1995), 439.

[33] Y. L. Liang, R. A. Pearson. Polymer, 50 (2009), 4895.

[34] Y. L. Liang, R. A. Pearson. Polymer, 51 (2010), 4880.

CHAPTER 5

CONCLUSIONS AND RECOMMENDATIONS ABOUT FUTURE RESEARCH

5.1 Conclusions

This dissertation research focuses on two projects. In Chapter 2, the main goal is to elucidate how and why polymerizable surfactant HITENOL KH-10 improved PBMA latex stability and film properties. In Chapter 3 and 4, silica/PBA/PMMA nanoparticles of a novel multilayer core-shell structure were synthesized and utilized as toughening agents in a model epoxy to evaluate their toughening effect and elucidate the toughening mechanisms.

In Chapter 2, a polymerizable surfactant KH-10 was compared and contrasted with its non-polymerizable surfactant control LA-12 in multiple aspects. They both have very low CMCs, 0.24 mM and 0.17 mM respectively. In miniemulsion polymerization system, compared with LA-12, latexes prepared with KH-10 exhibited 240% higher stability against $CaCl_2$ addition, and resulted in films with suppressed water-sensitivity and surfactant migration. Latexes prepared with KH-10 or LA-12 exhibited similar particle size and size distribution in conventional emulsion polymerization system. However, major difference was found in surfactant incorporation into different loci in latex (including in aqueous phase, on latex particle surfaces and inside latex particles) for KH-10 and LA-12. 66% of KH-10 was anchored on latex particles surfaces compared with only 21% for LA-12, which accounts for improvement of latex and film properties.

But increase of surface-anchored surfactants causes 300% increase of particle coalescence enthalpy during film formation, increasing energy barrier for dried particles to heal and form a coherent film.

Chapter 3 focuses on development of a synthesis technique for encapsulating silica nanoparticles (avg. diam. 22 nm) with PBA and PMMA layers and synthesizing silica/PBA/PMMA multilayer core-shell composite particles (avg. diam. ~80 nm) with single silica cores. This developed synthesis process is robust and repeatable. To achieve a one-to-one encapsulation without either multi-core particles or free polymer particles without silica cores, several steps and control parameters are essential to ensure silica nanoparticles are the main loci for polymer deposition during emulsion polymerization. We proved and demonstrated the necessity and effect of these factors, including silica surface treatment, dialysis after treatment, process type of emulsion polymerization, surfactant concentration and monomer feed rate. After optimization of these factors, a practically one-to-one encapsulation was achieved. Resulted particle size approximated theoretical particle size calculated based on perfect one-to-one encapsulation. Synthesized multilayer composite particles were utilized as epoxy toughening agents in Chapter 4.

In Chapter 4, epoxy (DGEBA) was toughened by three types of toughening agents: synthesized multilayer particles, Poly(styrene-butadiene) core-shell rubber particles (CSR) and a hybrid containing CSR and silica nanoparticles. Multilayer particles formed small clusters throughout the matrix with their size roughly unvaried between epoxy toughened by different volume fractions of particles (from 1.25% to 7.5%). CSR and silica nanoparticles were well dispersed inside epoxy matrix without

cluster formation regardless of different volume fraction. Because of cluster-formation mechanism and distinct blend morphology for multilayer particles inside epoxy, differences in mechanical properties and fracture morphology between epoxy toughened by multilayer particles and by hybrid toughening agents may not be explained solely by multilayer structure. Unlike common trends seen in epoxy toughened by CSR and hybrid toughening agents, fracture toughness (K_Q) of epoxy toughened by multilayer particles exhibited a trend that K_Q first peaked at 1.25 vol.% (compared to neat epoxy) then decreased with increasing particle volume fraction. At low vol.%, multilayer particles exhibited a superior toughening efficiency compared to other toughening agents studied in similar systems previously. TOM and SEM images of fracture surfaces and subsurface revealed that shear banding and matrix void growth might account for toughening efficiency of multilayer particles but they became less prominent as volume fraction of particles increased.

5.2 Recommendations

5.2.1 Polymerizable surfactant in latex and film

Improvement of latex and film properties by use of polymerizable surfactants has been relatively well studied in literature. Surfactant incorporation mechanism that accounts for the improvement was elucidated in this dissertation research—use of polymerizable surfactant significantly increased amount of surface-anchored surfactant. Next interesting research topic would be: what accounts for the incorporation mechanism for a particular polymerizable surfactant? The answer might be its particular molecular structure and reactivity ratio to monomer. For a good polymerizable surfactant, its

reactivity ratio should satisfy below relation so that it would incorporate mostly onto particle surfaces instead of being buried inside particles:

$$r_2 << 1 << r_1$$

where r_2 is reactivity ratio of polymerizable surfactant and r_1 is reactivity ratio of monomer.

In future research, several polymerizable surfactants of well-controlled chemical properties and purity might be investigated for their reactivity ratios and incorporation mechanisms in a single monomer system. A correlation between reactivity ratios as well as rate of monomer addition in a semi-batch polymerization process and incorporation mechanism might be found and thus explain functioning of polymerizable surfactants fundamentally.

Small-angle neutron scattering (SANS) technique might be very useful to study surfactant distribution at film-air interface or inside films. Combined with proper temperature and humidity control, a model of surfactant migration might be established based on SANS data.

5.2.2 Multilayer core-shell particles for toughening epoxy

It is very interesting to compare toughening effect and mechanism between structured multilayer core-shell particles and mixed hybrid toughening agents of the same composition with multilayer particles. In this research multilayer particles formed micro-clusters while hybrid toughening agents dispersed uniformly in epoxy matrix. In order to confidently attribute differences in toughening effect and mechanism to solely multilayer structure, dispersion and blend morphology of modifiers inside epoxy matrix should be kept the same—uniform distribution of single particles being the most straightforward to

achieve and control. Incorporation of epoxy-miscible groups onto particle surfaces and improvement of particle extraction (from aqueous latexes) and mixing processes might yield desired particle distribution in epoxy matrix. If this target was achieved but superior toughening efficiency of multilayer particles was lost, micro-clustered particles instead of multilayer structure might be the underlying reason for high toughening efficiency of multilayer particles. If uniform distribution of multilayer particles was achieved and they exhibited a higher toughening efficiency, further study of modifier/matrix interface area and area of interfaces inside multilayer particles should be conducted, because the nature of multilayer particles compared with hybrid toughening agents is transformation of certain particle/matrix interface area into area of interfaces inside multilayer particles. Both interface area and nature of interfaces are different between multilayer particles and hybrid toughening agents. Studies focusing on these issues might uncover the underlying functioning mechanism of multilayer particles as toughening agents.

In order to achieve a uniform distribution of synthesized multilayer particles, instead of freeze-drying, solvent extraction method might be promising. A particle-compatible solvent like methyl ethyl ketone (MEK) may be used to exchange aqueous phase in the latex and form particle dispersion in MEK. This colloidal stable dispersion can be added into epoxy resin to maintain uniform distribution of latex particles. Then after solvent removing under heating and vacuum, a uniform distribution of particles in epoxy resin can be obtained. Curing process and chemistry should also be carefully monitored to maintain the uniform distribution.

Last but not least, results in this study indicate weak adhesion at PMMA/matrix interface because particle debonding and matrix void growth happened mostly around

clusters of multilayer particles. In future work, polar groups can be introduced into shell polymer composition during emulsion polymerization (e.g. copolymerization with acrylonitrile monomers) in order to enhance adhesion between particle shell and epoxy matrix. With enhanced particle/matrix interface, next weak interface would be interface between rubber layer and glassy shell, which might be more effective loci for energy dissipation via interface separation and rubber cavitation.

Vita

Yuanyuan Wang was born on Sep. 18th, 1986 in Qinghai, China, to Yanhong Wang and Ping Zhang. She enrolled in Tsinghua University, Beijing, China in 2004 and earned her Bachelor and Master of Science in 2008 and 2011 respectively. She enrolled in Lehigh University in August 2011 to pursue a Ph.D. degree in Chemical Engineering, which she proudly earned in May 2017.

Professional Experiences

Dissertation Research May 2012—May 2017

Comprehensively investigated and elucidated aspects of PBMA latex particle modification and resulting latex/film property improvement by using polymerizable surfactant, which is promising to mitigate surfactant migration—a critical issue in waterborne coatings and adhesives.

- Established a quantifying system to investigate the incorporation mechanism of polymerizable surfactant into latex particles and found 220% more surfactant molecules were anchored on particle surface with use of polymerizable KH-10 than its non-polymerizable control
- Evaluated not only the positive effects of modification by polymerizable surfactant but also potential trade-offs in aspects of electrochemical, physical and thermodynamic properties of latex and film.

Invented a method to synthesize multilayered core-shell latex nanoparticles with single silica cores via emulsion polymerization. These particles then served as innovative toughening agent for epoxy, which is often toughened for use as underfill material for electronic packaging.

- Developed an uncomplicated process to synthesize silica nanoparticle encapsulated core-shell acrylic latex particles with diameter as small as 70 nm and demonstrated necessity of every step in this process.

- Evaluated synthesized particles as epoxy toughening agents and found a superior toughening efficiency—110% increase in toughness of modified epoxy at only 2.5 vol.% modifier content. Toughening mechanism was investigated.

Side Projects June 2015—January 2017

Optimization of process parameters for Selective Laser Sintering on a new Sintratec 3D printer

- With a printer of low laser power (2 W), optimized printing parameters for PA-11, PA-12 and PA-12/silica nanocomposite powders. Printed parts had tensile properties comparable to injection-molded ones and better than manufacturer-provided data.

Fabrication of silica-polymer hybrid particles for Selective Laser Sintering

- Developed a novel dissolution-precipitation technique to fabricate nanosilica-filled PEKK and PA12 powders

Master Degree Thesis Research March 2009—June 2011

- Established an evaluating system for catalysts for dimethyl ether low temperature catalytic combustion including reactor and gas chromatography for analyzing composition of exhaust gas
- Designed and evaluated a series of γ-Al_2O_3 supported palladium-platinum catalysts and lowered combustion temperature of dimethyl ether by 225°C with one of prepared catalysts

Bachelor Degree Thesis Research August 2007—June 2008

- Learned experimental skills of catalyst preparation, characterization and evaluation
- With senior students, designed and used a palladium membrane reactor for dimethyl ether steam reforming

Undergraduate Research Training March 2007—August 2007

- Analyzed thermodynamics of biodiesel synthesis process employing Benson Group Increment Theory

Other Experiences

Teaching Assistant

- CHE031 Material & Energy Balances of Chemical Processes
- MAT486 Polymer Nanocomposites
- MAT492 Adhesion and Adhesives Technology

Honors and Awards

- 2016 Excellence in Polymer Science & Engineering Award, Society of Plastics Engineers, Lehigh Valley Section
- 2014 Fellowship of Dept. Chemical Engineering, Lehigh University
- 2010 Scholarship for outstanding organizers of graduate student activities, Tsinghua University
- 2006 Scholarship for outstanding organizers of undergraduate student activities, Tsinghua University

Presentations

Y. Wang (presentation), R. A. Pearson. Polyamide-12/Silica Nanocomposite Powders for Selective Laser Sintering. American Chemical Society National Meeting, Philadelphia, PA, August 21, 2016

Y. Wang (presentation and poster), E. S. Daniels, A. Klein, M. S. El-Aasser. Polymerizable Surfactants in Emulsion Polymerization and Latex Film Formation. Emulsion Polymers Institute Annual Review Meeting, Bethlehem, PA, May 7, 2014

Y. Wang (poster), E. S. Daniels, A. Klein, M. S. El-Aasser. Role of Polymerizable Surfactants in Miniemulsion Polymerization and the Resulting Latex Film Properties. International Polymer Colloids Group (IPCG) Research Conference, Shanghai, China, June 25, 2013

Publications

Y. Wang, C. M. DiNapoli, G. A. Tofig, R. W. Cunningham, R. A. Pearson. Selective laser sintering processing behavior of polyamide powders. The Plastics Technology Conference (ANTEC), Anaheim, 2017

C. Fang, **Y. Wang**, Z. Lin, E. S. Daniels, A. Klein. Partitioning of Monobutyl Itaconate and β-Carboxyethyl Acrylate between Organic and Water Phases. J. Applied Polymer Science, 131(19), 2014

Y. Wang, H. Xu, D. Feng, J. Wang. Catalytic Activity of Low-loading Pd and Pt Supported Catalysts for Combustion of Dimethyl Ether. Chinese Journal of Process Engineering, 11(1), 148-152, 2011

D. Feng, **Y. Wang**, D. Wang, J. Wang. Steam Reforming of Dimethyl Ether over CuO-ZnO-Al_2O_3-ZrO_2+ZSM-5: A Kinetic Study. Chemical Engineering Journal, 146(3), 477-485, 2009

D. Feng, **Y. Wang**, D. Wang, J. Wang. Pd-Ag-Au-Ni Membrane Reactor for Methoxymethane Steam Reforming. J. Chemical and Engineering Data, 54(9), 2444-2451, 2009